

Contents

Contents	i
1 The Nonlinear Surface Susceptibility	1
1.1 Length Gauge	2
1.2 Time-dependent Perturbation Theory	6
1.3 Layered Current Density	9
1.4 Microscopic surface susceptibility	12
1.5 Conclusions	14
2 Surface Second-Harmonic Generation Yield	15
2.1 The three layer model for the SSHG yield	16
2.1.1 Multiple SHG reflections	19
2.1.2 Multiple reflections for the linear field	20
2.1.3 Deriving the SSHG yield	21
2.2 \mathcal{R}_{iF} for different polarization cases	23
2.2.1 \mathcal{R}_{pP} (<i>p</i> -in, <i>P</i> -out)	25
2.2.2 \mathcal{R}_{sP} (<i>s</i> -in, <i>P</i> -out)	26
2.2.3 \mathcal{R}_{pS} (<i>p</i> -in, <i>S</i> -out)	26
2.2.4 \mathcal{R}_{sS} (<i>s</i> -in, <i>S</i> -out)	27
2.3 Some scenarios of interest	28
2.3.1 The 3-layer model without multiple reflections	28
2.3.2 The two layer, or Fresnel (2-layer-fresnel) model	29
2.3.3 The 2-layer-bulk model: evaluating $\mathcal{P}(2\omega)$ and $\mathbf{E}(\omega)$ in the bulk	29
2.3.4 The 2-layer-vacuum model: evaluating $\mathcal{P}(2\omega)$ and $\mathbf{E}(\omega)$ in the vacuum	29
2.3.5 The 3-layer-hybrid model: evaluating $\mathcal{P}(2\omega)$ in ℓ and $\mathbf{E}(\omega)$ in the bulk	30
2.4 About coding the SSHG yield	30
3 Results	32
3.1 Results for the Si(001)(2×1) surface	33
3.1.1 Calculating χ^{xxx}	34
3.1.2 Overview of the calculated \mathcal{R} spectra	39
3.2 Results for the Si(111)(1×1):H surface	40
3.2.1 Calculating χ^{xxx}	42
3.2.2 Comparing the theoretical \mathcal{R} to experiment	44
4 Final Remarks	55

4.1	Conclusions	55
4.2	Future Work	56
A	Useful derivations for the nonlinear surface susceptibility	57
A.1	\mathbf{r}_e and \mathbf{r}_i	57
B	Derived expressions for the SHG yield	60
B.1	Some useful expressions	60
B.1.1	2ω terms	61
B.1.2	1ω terms	62
B.1.3	Nonzero components of $\chi(-2\omega; \omega, \omega)$	63
B.2	\mathcal{R}_{pP}	64
B.2.1	For the (111) surface	65
B.2.2	For the (110) surface	68
B.2.3	For the (001) surface	69
B.3	\mathcal{R}_{ps}	70
B.3.1	For the (111) surface	71
B.3.2	For the (110) surface	71
B.3.3	For the (001) surface	72
B.4	\mathcal{R}_{sP}	72
B.4.1	For the (111) surface	73
B.4.2	For the (110) surface	74
B.4.3	For the (001) surface	74
B.5	\mathcal{R}_{ss}	75
B.5.1	For the (111) surface	75
B.5.2	For the (110) surface	76
B.5.3	For the (001) surface	76
C	Deriving the SSHG yield without multiple reflections	77
C.1	Three layer model for SSHG radiation	77
C.1.1	SSHG Yield	80
D	Some limiting cases of interest	83
D.1	The two layer model	83
D.2	Taking $\mathcal{P}(2\omega)$ and the fundamental fields in the bulk	84
D.3	Taking $\mathcal{P}(2\omega)$ and the fundamental fields in the vacuum	86
D.4	Taking $\mathcal{P}(2\omega)$ in ℓ and the fundamental fields in the bulk	88
E	The two layer model for SHG radiation from Sipe, Moss, and van Driel	91
E.1	\mathcal{R}_{pP}	92
E.2	\mathcal{R}_{ps}	94
E.3	\mathcal{R}_{sP}	95
E.4	Summary	96
Bibliography		97

Chapter 1

The Nonlinear Surface Susceptibility

chap:chi2

Outline

1.1	Length Gauge	2
1.2	Time-dependent Perturbation Theory	6
1.3	Layered Current Density	9
1.4	Microscopic surface susceptibility	12
1.5	Conclusions	14

In this section I will outline the general procedure to obtain the surface susceptibility tensor for SHG. We start with the nonlinear polarization \mathbf{P} written as

$$P_a(2\omega) = \chi^{abc}(-2\omega; \omega, \omega)E^b(\omega)E^c(\omega) + \chi^{abcd}(-2\omega; \omega, \omega)E^b(\omega)\nabla^c E^d(\omega) + \dots, \quad (1.1) \quad \text{mshg}$$

where $\chi^{abc}(-2\omega; \omega, \omega)$ and $\chi^{abcd}(-2\omega; \omega, \omega)$ correspond to the dipolar and quadrupolar susceptibilities. For ease of notation, I will drop the $(-2\omega; \omega, \omega)$ argument from this point on. The sum continues with higher multipolar terms. If we consider a semi-infinite system with a centrosymmetric bulk, we can separate the terms into two contributions from symmetry considerations alone. The first from the surface of the system, and the second from the bulk of the system. We take

$$P^a(\mathbf{r}) = \chi^{abc}E^b(\mathbf{r})E^c(\mathbf{r}) + \chi^{abcd}E^b(\mathbf{r})\frac{\partial}{\partial \mathbf{r}_c}E^d(\mathbf{r}) + \dots, \quad (1.2) \quad \text{mshg2}$$

as the polarization with respect to the original coordinate system, and

$$P_a(-\mathbf{r}) = \chi^{abc}E^b(-\mathbf{r})E^c(-\mathbf{r}) + \chi^{abcd}E^b(-\mathbf{r})\frac{\partial}{\partial(-\mathbf{r}_c)}E^d(-\mathbf{r}) + \dots, \quad (1.3) \quad \text{mshg3}$$

as the polarization in the coordinate system where inversion is taken, i.e. $\mathbf{r} \rightarrow -\mathbf{r}$. Note that we have kept the same susceptibility tensors as they must be invariant under $\mathbf{r} \rightarrow -\mathbf{r}$ since the system is centrosymmetric. Recalling that $\mathbf{P}(\mathbf{r})$ and $\mathbf{E}(\mathbf{r})$ are polar vectors [1], we have that Eq. (1.3)

reduces to

$$\begin{aligned} -P^a(\mathbf{r}) &= \chi^{abc}(-E^b(\mathbf{r}))(-E^c(\mathbf{r})) + \chi^{abcd}(-E^b(\mathbf{r}))\left(-\frac{\partial}{\partial \mathbf{r}_c}\right)(-E^d(\mathbf{r})) + \dots, \\ P^a(\mathbf{r}) &= -\chi^{abc}E^b(\mathbf{r})E^c(\mathbf{r}) + \chi^{abcd}E^b(\mathbf{r})\frac{\partial}{\partial \mathbf{r}_c}E^d(\mathbf{r}) + \dots, \end{aligned} \quad (1.4) \quad \boxed{\text{mshg4}}$$

that when compared with Eq. (1.2)^{mshg2} leads to the conclusion that

$$\chi^{abc} = 0 \quad (1.5) \quad \boxed{\text{sshg}}$$

for a centrosymmetric bulk.

If we move to the surface of the semi-infinite system, our assumption of centrosymmetry breaks down and there is no restriction on χ^{abc} . We conclude that the leading term of the polarization in a surface region is given by

$$\int P^a(\mathbf{R}, z) dz \approx lP^a \equiv P_{\text{surface}}^a \equiv \chi_S^{abc}E^bE^c, \quad (1.6) \quad \boxed{\text{sshgp1}}$$

where l is the surface region from which the dipolar signal of \mathbf{P} is different from zero (see Fig. 1.1), and $\mathbf{P}_{\text{surface}} \equiv l\mathbf{P}$ is the surface SH polarization. Then, from Eq. (1.1)^{f_{system}}^{mshg} we obtain that

$$\chi_S^{abc} = l\chi^{abc} \quad (1.7) \quad \boxed{\text{sshgp2}}$$

is the SH surface susceptibility. On the other hand,

$$P_{\text{bulk}}^a(\mathbf{r}) = \chi^{abcd}E^b(\mathbf{r})\nabla^cE^d(\mathbf{r}), \quad (1.8) \quad \boxed{\text{sshgp3}}$$

gives the bulk polarization. We immediately recognize that the surface polarization is of dipolar order while the bulk polarization is of quadrupolar order. The surface χ_S^{abc} , and bulk χ^{abcd} , susceptibility tensor ranks are three and four, respectively. We will only concentrate on SSHG in this work, even though bulk-generated SH is also a very important optical phenomenon. I will also exclude other interesting surface SH phenomena like, electric field induced second-harmonic (EFISH), which would be represented by a surface susceptibility tensor of quadrupolar origin. As I mentioned in Chapter ^{chap:intro}??, in centrosymmetric systems for which the quadrupolar bulk response is much smaller than the dipolar surface response, SH is a very capable and powerful optical surface probe ^{downerSTA01}[2].

In the following sections of this chapter, we will review the theoretical approach to derive the expressions for the surface susceptibility tensor χ_S^{abc} .

1.1 Length Gauge

longi

We follow the article by Aversa and Sipe ^{aversaPRB95}[3] to calculate the optical properties of a given system within the longitudinal gauge. More recent derivations can also be found in Refs. ^{sipePRB00}[4] and ^{ambrechtPSSB00}[5]. We assume the long-wavelength approximation which implies a position independent electric field, $\mathbf{E}(t)$. The Hamiltonian in the length gauge approximation is given by

$$\hat{H} = \hat{H}_0^\Sigma - e\hat{\mathbf{r}} \cdot \mathbf{E}, \quad (1.9) \quad \boxed{\text{ache}}$$

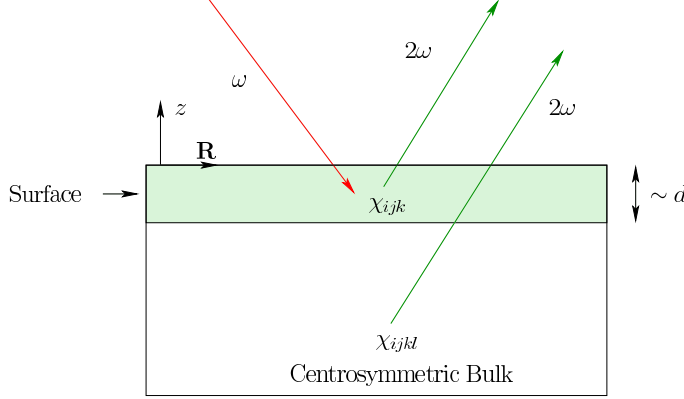


Figure 1.1: Sketch of a semi-infinite system with a centrosymmetric bulk. The surface region is of width $\sim l$. The incoming photon of frequency ω is represented by a downward red arrow, whereas both the surface and bulk created second-harmonic photons of frequency 2ω are represented by upward green arrows. The red color suggests an incoming infrared photon with a green second-harmonic photon. The dipolar (χ^{abc}), and quadrupolar (χ^{abcd}) susceptibility tensors are shown in the regions where they are nonzero. The z -axis is perpendicular to the surface and \mathbf{R} is parallel to it.

`fsystem`

with

$$\hat{H}_0^\Sigma = \hat{H}_0^{\text{LDA}} + \mathcal{S}(\mathbf{r}, \mathbf{p}), \quad (1.10) \quad [\text{ache.1}]$$

as the unperturbed Hamiltonian. The LDA Hamiltonian can be expressed as follows,

$$\begin{aligned} \hat{H}_0^{\text{LDA}} &= \frac{\hat{p}^2}{2m_e} + \hat{V}^{\text{ps}}, \\ \hat{V}^{\text{ps}} &= \hat{V}^l(\hat{\mathbf{r}}) + \hat{V}^{\text{nl}}, \end{aligned} \quad (1.11) \quad [\text{ache.2}]$$

where $\hat{V}^l(\hat{\mathbf{r}})$ and \hat{V}^{nl} are the local and the nonlocal parts of the crystal pseudopotential \hat{V}^{ps} . For the latter, we have that

$$V^{\text{nl}}(\mathbf{r}, \mathbf{r}') \equiv \langle \mathbf{r} | \hat{V}^{\text{nl}} | \mathbf{r}' \rangle \neq 0 \quad \text{for } \mathbf{r} \neq \mathbf{r}', \quad (1.12) \quad [\text{ache.3n}]$$

where $V^{\text{nl}}(\mathbf{r}, \mathbf{r}')$ is a function of \mathbf{r} and \mathbf{r}' representing the nonlocal contribution of the pseudopotential. The Schrödinger equation reads

$$\left(\frac{-\hbar^2}{2m_e} \nabla^2 + \hat{V}^l(\mathbf{r}) \right) \psi_{n\mathbf{k}}(\mathbf{r}) + \int \hat{V}^{\text{nl}}(\mathbf{r}, \mathbf{r}') \psi_{n\mathbf{k}}(\mathbf{r}') d\mathbf{r}' = E_i \psi_{n\mathbf{k}}(\mathbf{r}), \quad (1.13) \quad [\text{ache.4}]$$

where $\psi_{n\mathbf{k}}(\mathbf{r}) = \langle \mathbf{r} | n\mathbf{k} \rangle = e^{i\mathbf{k}\cdot\mathbf{r}} u_{n\mathbf{k}}(\mathbf{r})$, are the real space representations of the Bloch states $|n\mathbf{k}\rangle$ labeled by the band index n and the crystal momentum \mathbf{k} , and $u_{n\mathbf{k}}(\mathbf{r})$ is cell periodic. m_e is the bare mass of the electron. The nonlocal scissors operator is given by

$$\mathcal{S}(\mathbf{r}, \mathbf{p}) = \hbar \Delta \sum_n \int (1 - f_n(\mathbf{k})) |n\mathbf{k}'\rangle \langle n\mathbf{k}'| d^3 k', \quad (1.14) \quad [\text{chon.0}]$$

where $f_n(\mathbf{k})$ is the occupation number that is independent of \mathbf{k} for $T = 0$ K, and is $f_n = 1$ for filled bands and $f_n = 0$ for unoccupied bands. For semiconductors the filled bands correspond to valence bands ($n = v$), and unoccupied bands correspond to conduction bands ($n = c$). We have that

$$\begin{aligned} H_0^{\text{LDA}}|\mathbf{n}\mathbf{k}\rangle &= \hbar\omega_n^{\text{LDA}}(\mathbf{k})|\mathbf{n}\mathbf{k}\rangle \\ H_0^{\Sigma}|\mathbf{n}\mathbf{k}\rangle &= \hbar\omega_n^{\Sigma}(\mathbf{k})|\mathbf{n}\mathbf{k}\rangle, \end{aligned} \quad (1.15) \quad [\text{chon.1}]$$

where

$$\hbar\omega_n^{\Sigma}(\mathbf{k}) = \hbar\omega_n^{\text{LDA}}(\mathbf{k}) + \hbar\Delta(1 - f_n), \quad (1.16) \quad [\text{chon.78}]$$

is the scissored energy. Here, $\hbar\Delta$ is the value by which the conduction bands are rigidly (\mathbf{k} -independent) shifted upwards in energy, also known as the scissors shift. Δ could be taken to be \mathbf{k} dependent, but for most calculations (like the ones presented here), a rigid shift is sufficient. We can take $\hbar\Delta = E_g - E_g^{\text{LDA}}$ where E_g is the experimental or GW band gap taken at the Γ point, i.e. $\mathbf{k} = 0$. We used the fact that $|\mathbf{n}\mathbf{k}\rangle^{\text{LDA}} \approx |\mathbf{n}\mathbf{k}\rangle^{\Sigma}$, thus negating the need to label the Bloch states with the LDA or Σ superscripts. The matrix elements of \mathbf{r} are split between the *intraband* (\mathbf{r}_i) and *interband* (\mathbf{r}_e) parts, where $\mathbf{r} = \mathbf{r}_i + \mathbf{r}_e$ [5, 6, 3] and

$$\langle \mathbf{n}\mathbf{k} | \hat{\mathbf{r}}_i | m\mathbf{k}' \rangle = \delta_{nm} [\delta(\mathbf{k} - \mathbf{k}') \xi_{nn}(\mathbf{k}) + i \nabla_{\mathbf{k}} \delta(\mathbf{k} - \mathbf{k}')], \quad (1.17) \quad [\text{rnminn}]$$

$$\langle \mathbf{n}\mathbf{k} | \hat{\mathbf{r}}_e | m\mathbf{k}' \rangle = (1 - \delta_{nm}) \delta(\mathbf{k} - \mathbf{k}') \xi_{nm}(\mathbf{k}), \quad (1.18) \quad [\text{rnmenn}]$$

with

$$\xi_{nm}(\mathbf{k}) \equiv i \frac{(2\pi)^3}{\Omega} \int_{\Omega} u_{n\mathbf{k}}^*(\mathbf{r}) \nabla_{\mathbf{k}} u_{m\mathbf{k}}(\mathbf{r}) d\mathbf{r}, \quad (1.19) \quad [\text{zetann}]$$

where Ω is the unit cell volume. The interband part, \mathbf{r}_e , can be obtained as follows. We start by introducing the velocity operator

$$\hat{\mathbf{v}}^{\Sigma} = \frac{1}{i\hbar} [\hat{\mathbf{r}}, \hat{H}_0^{\Sigma}], \quad (1.20) \quad [\text{vop}]$$

and calculating its matrix elements

$$i\hbar \langle \mathbf{n}\mathbf{k} | \mathbf{v}^{\Sigma} | m\mathbf{k} \rangle = \langle \mathbf{n}\mathbf{k} | [\hat{\mathbf{r}}, \hat{H}_0^{\Sigma}] | m\mathbf{k} \rangle = \langle \mathbf{n}\mathbf{k} | \hat{\mathbf{r}} \hat{H}_0^{\Sigma} - \hat{H}_0^{\Sigma} \hat{\mathbf{r}} | m\mathbf{k} \rangle = (\hbar\omega_m^{\Sigma}(\mathbf{k}) - \hbar\omega_n^{\Sigma}(\mathbf{k})) \langle \mathbf{n}\mathbf{k} | \hat{\mathbf{r}} | m\mathbf{k} \rangle. \quad (1.21) \quad [\text{conhrnm}]$$

Defining $\omega_{nm}^{\Sigma}(\mathbf{k}) = \omega_n^{\Sigma}(\mathbf{k}) - \omega_m^{\Sigma}(\mathbf{k})$, we get

$$\mathbf{r}_{nm}(\mathbf{k}) = \frac{\mathbf{v}_{nm}^{\Sigma}(\mathbf{k})}{i\omega_{nm}^{\Sigma}(\mathbf{k})} \quad n \notin D_m, \quad (1.22) \quad [\text{pmnrnm}]$$

which can be identified as $\mathbf{r}_{nm} = (1 - \delta_{nm}) \xi_{nm} \rightarrow \mathbf{r}_{nm}$. Here, D_m are all the possible degenerate m -states. When \mathbf{r}_i appears in commutators we use [3]

$$\langle \mathbf{n}\mathbf{k} | [\hat{\mathbf{r}}_i, \hat{\mathcal{O}}] | m\mathbf{k}' \rangle = i\delta(\mathbf{k} - \mathbf{k}') (\mathcal{O}_{nm})_{;\mathbf{k}}, \quad (1.23) \quad [\text{conmri3n}]$$

with

$$(\mathcal{O}_{nm})_{;\mathbf{k}} = \nabla_{\mathbf{k}} \mathcal{O}_{nm}(\mathbf{k}) - i\mathcal{O}_{nm}(\mathbf{k}) (\xi_{nn}(\mathbf{k}) - \xi_{mm}(\mathbf{k})), \quad (1.24) \quad [\text{gendevnn}]$$

where “; \mathbf{k} ” denotes the generalized derivative (see Appendix A.1).

As can be seen from Eq. (1.10) and (1.11), both \mathcal{S} and \hat{V}^{nl} are nonlocal potentials. Their contribution in the calculation of the optical response has to be considered in order to get reliable results [7]. We proceed as follows: from Eqs. (1.20), (1.10) and (1.11) we find

$$\begin{aligned}\hat{\mathbf{v}}^\Sigma &= \frac{\hat{\mathbf{p}}}{m_e} + \frac{1}{i\hbar} \left[\hat{\mathbf{r}}, \hat{V}^{\text{nl}}(\mathbf{r}, \mathbf{r}') \right] + \frac{1}{i\hbar} \left[\hat{\mathbf{r}}, \hat{\mathcal{S}}(\mathbf{r}, \mathbf{p}) \right] \\ &\equiv \hat{\mathbf{v}} + \hat{\mathbf{v}}^{\text{nl}} + \hat{\mathbf{v}}^{\mathcal{S}} = \hat{\mathbf{v}}^{\text{LDA}} + \hat{\mathbf{v}}^{\mathcal{S}},\end{aligned}\quad (1.25) \quad [\text{vop2}]$$

where we have defined

$$\begin{aligned}\hat{\mathbf{v}} &= \frac{\hat{\mathbf{p}}}{m_e} \\ \hat{\mathbf{v}}^{\text{nl}} &= \frac{1}{i\hbar} \left[\hat{\mathbf{r}}, \hat{V}^{\text{nl}} \right] \\ \hat{\mathbf{v}}^{\mathcal{S}} &= \frac{1}{i\hbar} \left[\hat{\mathbf{r}}, \hat{\mathcal{S}}(\mathbf{r}, \mathbf{p}) \right] \\ \hat{\mathbf{v}}^{\text{LDA}} &= \hat{\mathbf{v}} + \hat{\mathbf{v}}^{\text{nl}}\end{aligned}\quad (1.26) \quad [\text{conhr}]$$

with $\hat{\mathbf{p}} = -i\hbar\nabla$ the momentum operator. Using Eq. (1.14), we obtain that the matrix elements of $\hat{\mathbf{v}}^{\mathcal{S}}$ are given by

$$\mathbf{v}_{nm}^{\mathcal{S}} = i\Delta f_{mn} \mathbf{r}_{nm}, \quad (1.27) \quad [\text{chon.2}]$$

with $f_{nm} = f_n - f_m$, where we see that $\mathbf{v}_{nn}^{\mathcal{S}} = 0$, then

$$\begin{aligned}\mathbf{v}_{nm}^\Sigma &= \mathbf{v}_{nm}^{\text{LDA}} + i\Delta f_{mn} \mathbf{r}_{nm} \\ &= \mathbf{v}_{nm}^{\text{LDA}} + i\Delta f_{mn} \frac{\mathbf{v}_{nm}^\Sigma(\mathbf{k})}{i\omega_{nm}^\Sigma(\mathbf{k})} \\ \mathbf{v}_{nm}^\Sigma \frac{\omega_{nm}^\Sigma - \Delta f_{mn}}{\omega_{nm}^\Sigma} &= \mathbf{v}_{nm}^{\text{LDA}} \\ \mathbf{v}_{nm}^\Sigma \frac{\omega_{nm}^{\text{LDA}}}{\omega_{nm}^\Sigma} &= \mathbf{v}_{nm}^{\text{LDA}} \\ \frac{\mathbf{v}_{nm}^\Sigma}{\omega_{nm}^\Sigma} &= \frac{\mathbf{v}_{nm}^{\text{LDA}}}{\omega_{nm}^{\text{LDA}}},\end{aligned}\quad (1.28) \quad [\text{chon.8}]$$

since $\omega_{nm}^\Sigma - \Delta f_{mn} = \omega_{nm}^{\text{LDA}}$. Therefore,

$$\mathbf{v}_{nm}^\Sigma(\mathbf{k}) = \frac{\omega_{nm}^\Sigma}{\omega_{nm}^{\text{LDA}}} \mathbf{v}_{nm}^{\text{LDA}}(\mathbf{k}) = \left(1 + \frac{\Delta}{\omega_c(\mathbf{k}) - \omega_v(\mathbf{k})} \right) \mathbf{v}_{nm}^{\text{LDA}}(\mathbf{k}) \quad n \notin D_m \quad (1.29) \quad [\text{chon.9}]$$

$$\mathbf{v}_{nn}^\Sigma(\mathbf{k}) = \mathbf{v}_{nn}^{\text{LDA}}(\mathbf{k}),$$

and Eq. (1.22) gives

$$\mathbf{r}_{nm}(\mathbf{k}) = \frac{\mathbf{v}_{nm}^\Sigma(\mathbf{k})}{i\omega_{nm}^\Sigma(\mathbf{k})} = \frac{\mathbf{v}_{nm}^{\text{LDA}}(\mathbf{k})}{i\omega_{nm}^{\text{LDA}}(\mathbf{k})} \quad n \notin D_m. \quad (1.30) \quad [\text{chon.10}]$$

The matrix elements of \mathbf{r}_e are the same whether we use the LDA or the scissored Hamiltonian. Therefore, there is no need to label them with either LDA or S superscripts. Thus, we can write

$$\mathbf{r}_{e,nm} \rightarrow \mathbf{r}_{nm}(\mathbf{k}) = \frac{\mathbf{v}_{nm}^{\text{LDA}}(\mathbf{k})}{i\omega_{nm}^{\text{LDA}}(\mathbf{k})} \quad n \notin D_m, \quad (1.31) \quad [\text{chon.98}]$$

which gives the interband matrix elements of the position operator in terms of the matrix elements of $\hat{\mathbf{v}}^{\text{LDA}}$. These matrix elements include the matrix elements of $\mathbf{v}_{nm}^{\text{nl}}(\mathbf{k})$ which can be readily calculated for fully separable nonlocal pseudopotentials in the Kleinman-Bylander form [8, 9, 10]. In Appendix [appvn] we outline how this is accomplished.

1.2 Time-dependent Perturbation Theory

tdpt

In the independent particle approximation, we use the electron density operator $\hat{\rho}$ to obtain the expectation value of any observable \mathcal{O} as

$$\mathcal{O} = \text{Tr}(\hat{\mathcal{O}}\hat{\rho}) = \text{Tr}(\hat{\rho}\hat{\mathcal{O}}), \quad (1.32) \quad [\text{traza}]$$

where Tr is the trace and is invariant under cyclic permutations. The dynamic equation of motion for ρ is given by

$$i\hbar \frac{d\hat{\rho}}{dt} = [\hat{H}, \hat{\rho}], \quad (1.33) \quad [\text{eqrho}]$$

where it is more convenient to work in the interaction picture. We transform all operators according to

$$\hat{\mathcal{O}}_I = \hat{U}\hat{\mathcal{O}}\hat{U}^\dagger, \quad (1.34) \quad [\text{ip}]$$

where

$$\hat{U} = e^{i\hat{H}_0 t/\hbar}, \quad (1.35) \quad [\text{ou}]$$

is the unitary operator that shifts us to the interaction picture. Note that $\hat{\mathcal{O}}_I$ depends on time even if $\hat{\mathcal{O}}$ does not. Then, we transform Eq. (1.33) into

$$i\hbar \frac{d\hat{\rho}_I(t)}{dt} = [-e\hat{\mathbf{r}}_I(t) \cdot \mathbf{E}(t), \hat{\rho}_I(t)], \quad (1.36) \quad [\text{intrho}]$$

that leads to

$$\hat{\rho}_I(t) = \hat{\rho}_I(t = -\infty) + \frac{ie}{\hbar} \int_{-\infty}^t dt' [\hat{\mathbf{r}}_I(t') \cdot \mathbf{E}(t'), \hat{\rho}_I(t')]. \quad (1.37) \quad [\text{intrho2}]$$

We assume that the interaction is switched-on adiabatically and choose a time-periodic perturbing field, to write

$$\mathbf{E}(t) = \mathbf{E}e^{-i\omega t}e^{\eta t} = \mathbf{E}e^{-i\tilde{\omega}t}, \quad (1.38) \quad [\text{efield}]$$

with

$$\tilde{\omega} = \omega + i\eta, \quad (1.39) \quad [\text{got}]$$

where $\eta > 0$ assures that at $t = -\infty$ the interaction is zero and has its full strength \mathbf{E} at $t = 0$. After computing the required time integrals one takes $\eta \rightarrow 0$. Also, $\hat{\rho}_I(t = -\infty)$ should be time independent and thus $[\hat{H}, \hat{\rho}]_{t=-\infty} = 0$. This implies that $\hat{\rho}_I(t = -\infty) = \hat{\rho}(t = -\infty) \equiv \hat{\rho}_0$, where $\hat{\rho}_0$ is the density matrix of the unperturbed ground state, such that

$$\langle n\mathbf{k} | \hat{\rho}_0 | m\mathbf{k}' \rangle = f_n(\hbar\omega_n^\Sigma(\mathbf{k}))\delta_{nm}\delta(\mathbf{k} - \mathbf{k}'), \quad (1.40) \quad [\text{nrhon}]$$

with $f_n(\hbar\omega_n^\Sigma(\mathbf{k})) = f_{n\mathbf{k}}$ as the Fermi-Dirac distribution function.

We solve Eq. (1.37) using the standard iterative solution, for which we write

$$\hat{\rho}_I = \hat{\rho}_I^{(0)} + \hat{\rho}_I^{(1)} + \hat{\rho}_I^{(2)} + \dots, \quad (1.41) \quad [\text{rhop}]$$

where $\hat{\rho}_I^{(N)}$ is the density operator to order N in $\mathbf{E}(t)$. Then, Eq. (1.37) reads

$$\hat{\rho}_I^{(0)} + \hat{\rho}_I^{(1)} + \hat{\rho}_I^{(2)} + \dots = \hat{\rho}_0 + \frac{ie}{\hbar} \int_{-\infty}^t dt' [\hat{\mathbf{r}}_I(t') \cdot \mathbf{E}(t'), \hat{\rho}_I^{(0)} + \hat{\rho}_I^{(1)} + \hat{\rho}_I^{(2)} + \dots], \quad (1.42) \quad [\text{intrho3}]$$

where, by equating equal orders in the perturbation, we find

$$\hat{\rho}_I^{(0)} \equiv \hat{\rho}_0, \quad (1.43) \quad [\text{rho0}]$$

and

$$\hat{\rho}_I^{(N)}(t) = \frac{ie}{\hbar} \int_{-\infty}^t dt' [\hat{\mathbf{r}}_I(t') \cdot \mathbf{E}(t'), \hat{\rho}_I^{(N-1)}(t')]. \quad (1.44) \quad [\text{rhoN}]$$

It is simple to show that matrix elements of Eq. (1.44) satisfy $\langle n\mathbf{k} | \rho_I^{(N+1)}(t) | m\mathbf{k}' \rangle = \rho_{I,nm}^{(N+1)}(\mathbf{k}) \delta(\mathbf{k} - \mathbf{k}')$, with

$$\rho_{I,nm}^{(N+1)}(\mathbf{k}; t) = \frac{ie}{\hbar} \int_{-\infty}^t dt' \langle n\mathbf{k} | [\hat{\mathbf{r}}_I(t'), \hat{\rho}_I^{(N)}(t')] | m\mathbf{k} \rangle \cdot \mathbf{E}(t'). \quad (1.45) \quad [\text{rtilde}]$$

We now work out the commutator of Eq. (1.45). Then,

$$\begin{aligned} \langle n\mathbf{k} | [\hat{\mathbf{r}}_I(t), \hat{\rho}_I^{(N)}(t)] | m\mathbf{k} \rangle &= \langle n\mathbf{k} | [\hat{U} \hat{\mathbf{r}} \hat{U}^\dagger, \hat{U} \hat{\rho}^{(N)}(t) \hat{U}^\dagger] | m\mathbf{k} \rangle \\ &= \langle n\mathbf{k} | \hat{U} [\hat{\mathbf{r}}, \hat{\rho}^{(N)}(t)] \hat{U}^\dagger | m\mathbf{k} \rangle \\ &= e^{i\omega_{nm\mathbf{k}}^\Sigma t} \left(\langle n\mathbf{k} | [\hat{\mathbf{r}}_e, \hat{\rho}^{(N)}(t)] + [\hat{\mathbf{r}}_i, \hat{\rho}^{(N)}(t)] | m\mathbf{k} \rangle \right). \end{aligned} \quad (1.46) \quad [\text{conmu1}]$$

We calculate the interband term first, so using Eq. (1.31) we obtain

$$\begin{aligned} \langle n\mathbf{k} | [\hat{\mathbf{r}}_e, \hat{\rho}^{(N)}(t)] | m\mathbf{k} \rangle &= \sum_\ell \left(\langle n\mathbf{k} | \hat{\mathbf{r}}_e | \ell\mathbf{k} \rangle \langle \ell\mathbf{k} | \hat{\rho}^{(N)}(t) | m\mathbf{k} \rangle \right. \\ &\quad \left. - \langle n\mathbf{k} | \hat{\rho}^{(N)}(t) | \ell\mathbf{k} \rangle \langle \ell\mathbf{k} | \hat{\mathbf{r}}_e | m\mathbf{k} \rangle \right) \\ &= \sum_{\ell \neq n,m} \left(\mathbf{r}_{n\ell}(\mathbf{k}) \rho_{\ell m}^{(N)}(\mathbf{k}; t) - \rho_{n\ell}^{(N)}(\mathbf{k}; t) \mathbf{r}_{\ell m}(\mathbf{k}) \right) \\ &\equiv \mathbf{R}_e^{(N)}(\mathbf{k}; t), \end{aligned} \quad (1.47) \quad [\text{conmu2}]$$

and from Eq. (1.23),

$$\langle n\mathbf{k} | [\hat{\mathbf{r}}_i, \hat{\rho}^{(N)}(t)] | m\mathbf{k}' \rangle = i\delta(\mathbf{k} - \mathbf{k}') (\rho_{nm}^{(N)}(t))_{;\mathbf{k}} \equiv \delta(\mathbf{k} - \mathbf{k}') \mathbf{R}_i^{(N)}(\mathbf{k}; t). \quad (1.48) \quad [\text{conmri4}]$$

Then Eq. (1.45) becomes

$$\rho_{I,nm}^{(N+1)}(\mathbf{k}; t) = \frac{ie}{\hbar} \int_{-\infty}^t dt' e^{i(\omega_{nm\mathbf{k}}^\Sigma - \tilde{\omega})t'} \left[R_e^{(N)}(\mathbf{k}; t') + R_i^{(N)}(\mathbf{k}; t') \right] E^b, \quad (1.49) \quad [\text{rtilde2}]$$

where the roman superindices a, b, c denote Cartesian components that are summed over if repeated. Starting from the linear response and proceeding from Eq. (1.40) and (1.47),

$$\begin{aligned} R_e^{b(0)}(\mathbf{k}; t) &= \sum_{\ell} \left(r_{n\ell}^b(\mathbf{k}) \rho_{\ell m}^{(0)}(\mathbf{k}) - \rho_{n\ell}^{(0)}(\mathbf{k}) r_{\ell m}^b(\mathbf{k}) \right) \\ &= \sum_{\ell} \left(r_{n\ell}^b(\mathbf{k}) \delta_{\ell m} f_m(\hbar\omega_m^\Sigma(\mathbf{k})) - \delta_{n\ell} f_n(\hbar\omega_n^\Sigma(\mathbf{k})) r_{\ell m}^b(\mathbf{k}) \right) \\ &= f_{mn\mathbf{k}} r_{nm}^b(\mathbf{k}), \end{aligned} \quad (1.50) \quad [\text{R0e}]$$

where $f_{mn\mathbf{k}} = f_{m\mathbf{k}} - f_{n\mathbf{k}}$. From now on it should be clear that the matrix elements of \mathbf{r}_{nm} imply $n \notin D_m$. We also have from Eq. (1.48) and Eq. (1.24) that

$$R_i^{b(0)}(\mathbf{k}) = i(\rho_{nm}^{(0)})_{;k^b} = i\delta_{nm}(f_{n\mathbf{k}})_{;k^b} = i\delta_{nm}\nabla_{k^b}f_{n\mathbf{k}}. \quad (1.51) \quad [\text{R0i}]$$

For a semiconductor at $T = 0$, $f_{n\mathbf{k}}$ is one if the state $|n\mathbf{k}\rangle$ is a valence state and zero if it is a conduction state; thus $\nabla_{\mathbf{k}}f_{n\mathbf{k}} = 0$ and $\mathbf{R}_i^{(0)} = 0$ and the linear response has no contribution from intraband transitions. Then,

$$\begin{aligned} \rho_{I,nm}^{(1)}(\mathbf{k}; t) &= \frac{ie}{\hbar} f_{mn\mathbf{k}} r_{nm}^b(\mathbf{k}) E^b \int_{-\infty}^t dt' e^{i(\omega_{nm\mathbf{k}}^\Sigma - \tilde{\omega})t'} \\ &= \frac{e}{\hbar} f_{mn\mathbf{k}} r_{nm}^b(\mathbf{k}) E^b \frac{e^{i(\omega_{nm\mathbf{k}}^\Sigma - \tilde{\omega})t}}{\omega_{nm\mathbf{k}}^\Sigma - \tilde{\omega}} \\ &= e^{i\omega_{nm\mathbf{k}}^\Sigma t} B_{mn}^b(\mathbf{k}) E^b(t) \\ &= e^{i\omega_{nm\mathbf{k}}^\Sigma t} \rho_{nm}^{(1)}(\mathbf{k}; t), \end{aligned} \quad (1.52) \quad [\text{rtilde2n}]$$

with

$$B_{nm}^b(\mathbf{k}, \omega) = \frac{e}{\hbar} \frac{f_{mn\mathbf{k}} r_{nm}^b(\mathbf{k})}{\omega_{nm\mathbf{k}}^\Sigma - \tilde{\omega}}, \quad (1.53) \quad [\text{rho1}]$$

and

$$\rho_{nm}^{(1)}(\mathbf{k}; t) = B_{mn}^b(\mathbf{k}, \omega) E^b(\omega) e^{-i\tilde{\omega}t}. \quad (1.54) \quad [\text{rhono1}]$$

Now, we calculate the second-order response. Then, from Eq. (1.47)

$$\begin{aligned} R_e^{b(1)}(\mathbf{k}; t) &= \sum_{\ell} \left(r_{n\ell}^b(\mathbf{k}) \rho_{\ell m}^{(1)}(\mathbf{k}; t) - \rho_{n\ell}^{(1)}(\mathbf{k}; t) r_{\ell m}^b(\mathbf{k}) \right) \\ &= \sum_{\ell} \left(r_{n\ell}^b(\mathbf{k}) B_{\ell m}^c(\mathbf{k}, \omega) - B_{n\ell}^c(\mathbf{k}, \omega) r_{\ell m}^b(\mathbf{k}) \right) E^c(t), \end{aligned} \quad (1.55) \quad [\text{R1e}]$$

and from Eq. (1.48)

$$R_i^{b(1)}(\mathbf{k}; t) = i(\rho_{nm}^{(1)}(t))_{;k^b} = iE^c(t)(B_{nm}^c(\mathbf{k}, \omega))_{;k^b}. \quad (1.56) \quad [\text{R1i}]$$

Using Eqs. (1.55) and (1.56) in Eq. (1.49), we obtain

$$\begin{aligned}
\rho_{I,nm}^{(2)}(\mathbf{k}; t) &= \frac{ie}{\hbar} \left[\sum_{\ell} \left(r_{n\ell}^b(\mathbf{k}) B_{\ell m}^c(\mathbf{k}, \omega) - B_{n\ell}^c(\mathbf{k}, \omega) r_{\ell m}^b(\mathbf{k}) \right) \right. \\
&\quad \left. + i(B_{nm}^c(\mathbf{k}, \omega))_{;k^b} \right] E_{\omega}^b E_{\omega}^c \int_{-\infty}^t dt' e^{i(\omega_{nm\mathbf{k}}^{\Sigma} - 2\tilde{\omega})t'} \\
&= \frac{e}{\hbar} \left[\sum_{\ell} \left(r_{n\ell}^b(\mathbf{k}) B_{\ell m}^c(\mathbf{k}, \omega) - B_{n\ell}^c(\mathbf{k}, \omega) r_{\ell m}^b(\mathbf{k}) \right) \right. \\
&\quad \left. + i(B_{nm}^c(\mathbf{k}, \omega))_{;k^b} \right] E_{\omega}^b E_{\omega}^c \frac{e^{i(\omega_{nm\mathbf{k}}^{\Sigma} - 2\tilde{\omega})t}}{\omega_{nm\mathbf{k}}^{\Sigma} - 2\tilde{\omega}} \\
&= e^{i\omega_{nm\mathbf{k}}^{\Sigma}t} \rho_{nm}^{(2)}(\mathbf{k}; t). \tag{1.57} \quad [\text{rtilde33}]
\end{aligned}$$

Now, we write $\rho_{nm}^{(2)}(\mathbf{k}; t) = \rho_{nm}^{(2)}(\mathbf{k}; 2\omega) e^{-i2\tilde{\omega}t}$, with

$$\begin{aligned}
\rho_{nm}^{(2)}(\mathbf{k}; 2\omega) &= \frac{e}{i\hbar} \frac{1}{\omega_{nm\mathbf{k}}^{\Sigma} - 2\tilde{\omega}} \left[- (B_{nm}^c(\mathbf{k}, \omega))_{;k^b} \right. \\
&\quad \left. + i \sum_{\ell} \left(r_{n\ell}^b B_{\ell m}^c(\mathbf{k}, \omega) - B_{n\ell}^c(\mathbf{k}, \omega) r_{\ell m}^b \right) \right] E^b(\omega) E^c(\omega) \tag{1.58} \quad [\text{rho2}]
\end{aligned}$$

where $B_{\ell m}^a(\mathbf{k}, \omega)$ are given by Eq. (1.53). We remark that $\mathbf{r}_{nm}(\mathbf{k})$ are the same whether calculated with the LDA or the scissored Hamiltonian. We chose the former in this article.

1.3 Layered Current Density

cd

In this section, we derive the expressions for the microscopic current density of a given layer in the unit cell of the system. The approach we use to study the surface of a semi-infinite semiconductor crystal is as follows. Instead of using a semi-infinite system, we replace it by a slab (see Fig. 1.2). The slab consists of a front and back surface, and in between these two surfaces is the bulk of the system. In general the surface of a crystal reconstructs or relaxes as the atoms move to find equilibrium positions. This is due to the fact that the otherwise balanced forces are disrupted when the surface atoms do not find their partner atoms that are now absent at the surface of the slab.

To take the reconstruction or relaxation into account, we take “surface” to mean the true surface of the first layer of atoms, and some of the atomic sub-layers adjacent to it. Since the front and the back surfaces of the slab are usually identical the total slab is centrosymmetric. This implies that $\chi_{abc}^{\text{slab}} = 0$, and thus we must find a way to bypass this characteristic of a centrosymmetric slab in order to have a finite χ_{abc}^s representative of the surface. Even if the front and back surfaces of the slab are different, breaking the centrosymmetry and therefore giving an overall $\chi_{abc}^{\text{slab}} \neq 0$, we still need a procedure to extract the front surface χ_{abc}^f and the back surface χ_{abc}^b from the nonlinear susceptibility $\chi_{abc}^{\text{slab}} = \chi_{abc}^f - \chi_{abc}^b$ of the entire slab.

A convenient way to accomplish the separation of the SH signal of either surface is to introduce a “cut function”, $\mathcal{C}(z)$, which is usually taken to be unity over one half of the slab and zero over the other half.^{reiningPRB94} In this case $\mathcal{C}(z)$ will give the contribution of the side of the slab for which $\mathcal{C}(z) = 1$. We can generalize this simple choice for $\mathcal{C}(z)$ by a top-hat cut function $\mathcal{C}^\ell(z)$ that selects a given

layer,

$$\mathcal{C}^\ell(z) = \Theta(z - z_\ell + \Delta_\ell^b) \Theta(z_\ell - z + \Delta_\ell^f), \quad (1.59) \quad [\text{sz}]$$

where Θ is the Heaviside function. Here, $\Delta_\ell^{f/b}$ is the distance that the ℓ -th layer extends towards the front (f) or back (b) from its z_ℓ position. $\Delta_\ell^f + \Delta_\ell^b$ is the thickness of layer ℓ (see Fig. 1.2).

Now, we show how this “cut function” $\mathcal{C}^\ell(z)$ is introduced in the calculation of χ_{abc} . The microscopic current density is given by

$$\mathbf{j}(\mathbf{r}, t) = \text{Tr}(\hat{\mathbf{j}}(\mathbf{r})\hat{\rho}(t)), \quad (1.60) \quad [\text{jmic}]$$

where the operator for the electron’s current is

$$\hat{\mathbf{j}}(\mathbf{r}) = \frac{e}{2} (\hat{\mathbf{v}}^\Sigma |\mathbf{r}\rangle\langle\mathbf{r}| + |\mathbf{r}\rangle\langle\mathbf{r}|\hat{\mathbf{v}}^\Sigma), \quad (1.61) \quad [\text{hatjmic}]$$

where $\hat{\mathbf{v}}^\Sigma$ is the electron’s velocity operator to be dealt with below. We define $\hat{\mu} \equiv |\mathbf{r}\rangle\langle\mathbf{r}|$ and use the cyclic invariance of the trace to write

$$\begin{aligned} \text{Tr}(\hat{\mathbf{j}}(\mathbf{r})\hat{\rho}(t)) &= \text{Tr}(\hat{\rho}(t)\hat{\mathbf{j}}(\mathbf{r})) = \frac{e}{2} (\text{Tr}(\hat{\rho}\hat{\mathbf{v}}^\Sigma\hat{\mu}) + \text{Tr}(\hat{\rho}\hat{\mu}\hat{\mathbf{v}}^\Sigma)) \\ &= \frac{e}{2} \sum_{n\mathbf{k}} (\langle n\mathbf{k} | \hat{\rho}\hat{\mathbf{v}}^\Sigma\hat{\mu} | n\mathbf{k} \rangle + \langle n\mathbf{k} | \hat{\rho}\hat{\mu}\hat{\mathbf{v}}^\Sigma | n\mathbf{k} \rangle) \\ &= \frac{e}{2} \sum_{n\mathbf{k}} \langle n\mathbf{k} | \hat{\rho} | m\mathbf{k} \rangle (\langle m\mathbf{k} | \hat{\mathbf{v}}^\Sigma | \mathbf{r} \rangle \langle \mathbf{r} | n\mathbf{k} \rangle + \langle m\mathbf{k} | \mathbf{r} \rangle \langle \mathbf{r} | \hat{\mathbf{v}}^\Sigma | n\mathbf{k} \rangle) \\ \mathbf{j}(\mathbf{r}, t) &= \sum_{n\mathbf{k}} \rho_{nm}(\mathbf{k}; t) \mathbf{j}_{mn}(\mathbf{k}; \mathbf{r}), \end{aligned} \quad (1.62) \quad [\text{jmic2}]$$

where

$$\mathbf{j}_{mn}(\mathbf{k}; \mathbf{r}) = \frac{e}{2} (\langle m\mathbf{k} | \hat{\mathbf{v}}^\Sigma | \mathbf{r} \rangle \langle \mathbf{r} | n\mathbf{k} \rangle + \langle m\mathbf{k} | \mathbf{r} \rangle \langle \mathbf{r} | \hat{\mathbf{v}}^\Sigma | n\mathbf{k} \rangle), \quad (1.63) \quad [\text{jmic3}]$$

are the matrix elements of the microscopic current operator, and we have used the fact that the matrix elements between states $|n\mathbf{k}\rangle$ are diagonal in \mathbf{k} , i.e. proportional to $\delta(\mathbf{k} - \mathbf{k}')$.

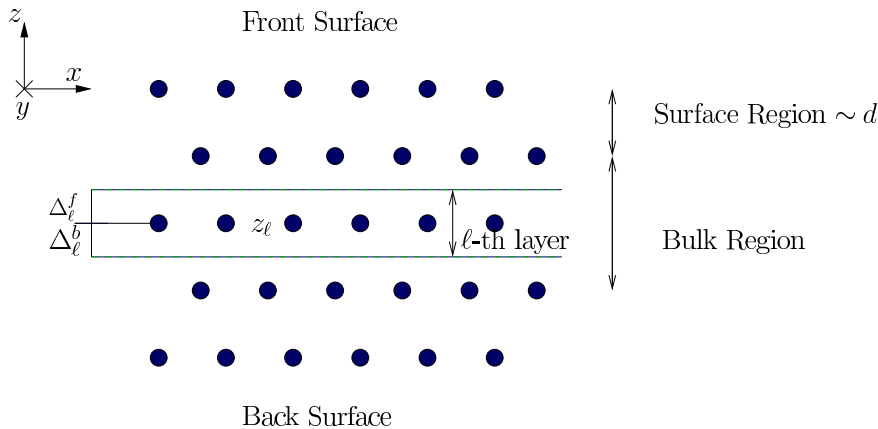


Figure 1.2: A sketch of a slab where the circles represent atoms.

fslab

Integrating the microscopic current $\mathbf{j}(\mathbf{r}, t)$ over the entire slab gives the averaged microscopic current density. If we want the contribution from only one region of the unit cell towards the total current, we can integrate $\mathbf{j}(\mathbf{r}, t)$ over the desired region. The contribution to the current density from the ℓ -th layer of the slab is given by

$$\frac{1}{\Omega} \int d^3r \mathcal{C}^\ell(z) \mathbf{j}(\mathbf{r}, t) \equiv \mathbf{J}^\ell(t), \quad (1.64) \quad [\mathbf{j}_{\mathbf{s}\mathbf{z}}]$$

where $\mathbf{J}^\ell(t)$ is the microscopic current in the ℓ -th layer. Therefore we define

$$e\mathcal{V}_{mn}^{\Sigma,\ell}(\mathbf{k}) \equiv \int d^3r \mathcal{C}^\ell(z) \mathbf{j}_{mn}(\mathbf{k}; \mathbf{r}), \quad (1.65) \quad [\mathbf{v}_{\mathbf{c}\mathbf{a}\mathbf{l}}]$$

to write

$$J_a^{(N,\ell)}(t) = \frac{e}{\Omega} \sum_{mn\mathbf{k}} \mathcal{V}_{mn}^{\Sigma,a,\ell}(\mathbf{k}) \rho_{nm}^{(N)}(\mathbf{k}; t), \quad (1.66) \quad [\mathbf{j}_{\mathbf{m}\mathbf{a}\mathbf{c}}]$$

as the induced microscopic current of the ℓ -th layer, to order N in the external perturbation. The matrix elements of the density operator for $N = 1, 2$ are given by Eqs. (1.53) and (1.58) respectively. The Fourier component of microscopic current of Eq. (1.66) is given by

$$J_a^{(N,\ell)}(\omega_3) = \frac{e}{\Omega} \sum_{mn\mathbf{k}} \mathcal{V}_{mn}^{\Sigma,a,\ell}(\mathbf{k}) \rho_{nm}^{(N)}(\mathbf{k}; \omega_3). \quad (1.67) \quad [\mathbf{j}_{\mathbf{m}\mathbf{a}\mathbf{c}2}]$$

We proceed to give an explicit expression of $\mathcal{V}_{mn}^{\Sigma,\ell}(\mathbf{k})$. From Eqs. (1.65) and (1.63) we obtain

$$\mathcal{V}_{mn}^{\Sigma,\ell}(\mathbf{k}) = \frac{1}{2} \int d^3r \mathcal{C}^\ell(z) \left[\langle m\mathbf{k} | \mathbf{v}^\Sigma | \mathbf{r} \rangle \langle \mathbf{r} | n\mathbf{k} \rangle + \langle m\mathbf{k} | \mathbf{r} \rangle \langle \mathbf{r} | \mathbf{v}^\Sigma | n\mathbf{k} \rangle \right], \quad (1.68) \quad [\mathbf{i}\mathbf{n}\mathbf{t}\mathbf{j}]$$

and using the following property

$$\langle \mathbf{r} | \hat{\mathbf{v}}^\Sigma(\mathbf{r}, \mathbf{r}') | n\mathbf{k} \rangle = \int d^3r'' \langle \mathbf{r} | \hat{\mathbf{v}}^\Sigma(\mathbf{r}, \mathbf{r}') | \mathbf{r}'' \rangle \langle \mathbf{r}'' | n\mathbf{k} \rangle = \hat{\mathbf{v}}^\Sigma(\mathbf{r}, \mathbf{r}'') \int d^3r'' \langle \mathbf{r} | \mathbf{r}'' \rangle \langle \mathbf{r}'' | n\mathbf{k} \rangle = \hat{\mathbf{v}}^\Sigma(\mathbf{r}, \mathbf{r}') \psi_{n\mathbf{k}}(\mathbf{r}), \quad (1.69) \quad [\mathbf{n}\mathbf{l}.2]$$

that stems from the fact that the operator $\mathbf{v}^\Sigma(\mathbf{r}, \mathbf{r}')$ does not act on \mathbf{r}'' , we can write

$$\begin{aligned} \mathcal{V}_{mn}^{\Sigma,\ell}(\mathbf{k}) &= \frac{1}{2} \int d^3r \mathcal{C}^\ell(z) \left[\psi_{n\mathbf{k}}(\mathbf{r}) \hat{\mathbf{v}}^{\Sigma*} \psi_{m\mathbf{k}}^*(\mathbf{r}) + \psi_{m\mathbf{k}}^*(\mathbf{r}) \hat{\mathbf{v}}^\Sigma \psi_{n\mathbf{k}}(\mathbf{r}) \right] \\ &= \int d^3r \psi_{m\mathbf{k}}^*(\mathbf{r}) \left[\frac{\mathcal{C}^\ell(z) \hat{\mathbf{v}}^\Sigma + \mathbf{v}^\Sigma \mathcal{C}^\ell(z)}{2} \right] \psi_{n\mathbf{k}}(\mathbf{r}) \\ &= \int d^3r \psi_{m\mathbf{k}}^*(\mathbf{r}) \mathcal{V}^{\Sigma,\ell} \psi_{n\mathbf{k}}(\mathbf{r}). \end{aligned} \quad (1.70) \quad [\mathbf{n}\mathbf{l}.3]$$

We used the hermitian property of \mathbf{v}^Σ and defined

$$\mathcal{V}^{\Sigma,\ell} = \frac{\mathcal{C}^\ell(z) \hat{\mathbf{v}}^\Sigma + \mathbf{v}^\Sigma \mathcal{C}^\ell(z)}{2}, \quad (1.71) \quad [\mathbf{n}\mathbf{l}.4]$$

where the superscript ℓ is inherited from $\mathcal{C}^\ell(z)$ and we suppress the dependance on z from the increasingly crowded notation. We see that the replacement

$$\hat{\mathbf{v}}^\Sigma \rightarrow \hat{\mathbf{V}}^{\Sigma,\ell} = \left[\frac{\mathcal{C}^\ell(z) \hat{\mathbf{v}}^\Sigma + \hat{\mathbf{v}}^\Sigma \mathcal{C}^\ell(z)}{2} \right], \quad (1.72) \quad [\mathbf{v}_{\mathbf{c}\mathbf{a}\mathbf{l}\mathbf{i}}]$$

is all that is needed to change the velocity operator of the electron $\hat{\mathbf{v}}^\Sigma$ to the new velocity operator $\mathbf{V}^{\Sigma,\ell}$ that implicitly takes into account the contribution of the region of the slab given by $\mathcal{C}^\ell(z)$. From Eq. (1.25),

$$\begin{aligned}\mathbf{V}^{\Sigma,\ell} &= \mathbf{V}^{\text{LDA},\ell} + \mathbf{V}^{S,\ell} \\ \mathbf{V}^{\text{LDA},\ell} &= \mathbf{V}^\ell + \mathbf{V}^{\text{nl},\ell} = \frac{1}{m_e} \mathbf{P}^\ell + \mathbf{V}^{\text{nl},\ell}.\end{aligned}\quad (1.73) \quad \boxed{\text{vopii}}$$

We remark that the simple relationship between $\mathbf{v}_{nm}^\Sigma(\mathbf{k})$ and $\mathbf{v}_{nm}^{\text{LDA}}(\mathbf{k})$, given in Eq. (1.29), does not hold between $\mathbf{V}_{nm}^{\Sigma,\ell}(\mathbf{k})$ and $\mathbf{V}_{nm}^{\text{LDA},\ell}(\mathbf{k})$, i.e. $\mathbf{V}_{nm}^{\Sigma,\ell}(\mathbf{k}) \neq (\omega_{nm}^\Sigma / \omega_{nm}) \mathbf{V}_{nm}^{\text{LDA},\ell}(\mathbf{k})$ and $\mathbf{V}_{nm}^{\Sigma,\ell}(\mathbf{k}) \neq \mathbf{V}_{nm}^{\text{LDA},\ell}(\mathbf{k})$, and thus, to calculate $\mathbf{V}_{nm}^{\Sigma,\ell}(\mathbf{k})$ we must calculate the matrix elements of $\mathbf{V}^{S,\ell}$ and $\mathbf{V}^{\text{LDA},\ell}$ (separately) according to the expressions of Appendix ???. Aeroport Charles de Gaulle, Nov. 30, 2014, see Appendix ??.

To limit the response to one surface, the equivalent of Eq. (1.71) for $\mathbf{V}^\ell = \mathbf{P}^\ell / m_e$ was proposed in Ref. [11] and later used in Refs. [12]–[15], and [16] also in the context of SHG. The layer-by-layer analysis of Refs. [16] and [17] used Eq. (1.59), limiting the current response to a particular layer of the slab and used to obtain the anisotropic linear optical response of semiconductor surfaces. However, the first formal derivation of this scheme is presented in Ref. [18] for the linear response, and here in this article, for the second harmonic optical response of semiconductors.

1.4 Microscopic surface susceptibility

In this section we obtain the expressions for the surface susceptibility tensor χ_{abc}^S . We start with the basic relation $\mathbf{J} = d\mathbf{P}/dt$ with \mathbf{J} the current calculated in Sec. 1.3. From Eq. (1.67) we obtain

$$J_a^{(2,\ell)}(2\omega) = -i2\tilde{\omega}P_a(2\omega) = \frac{e}{\Omega} \sum_{mn\mathbf{k}} \mathcal{V}_{mn}^{\Sigma,a,\ell}(\mathbf{k}) \rho_{nm}^{(2)}(\mathbf{k}; 2\omega), \quad (1.74) \quad \boxed{\text{Pjikn}}$$

and using Eqs. (1.58) and (1.7) leads to

$$\begin{aligned}\chi_{abc}^{S,\ell} &= \frac{ie}{AE_1^b E_2^c 2\tilde{\omega}} \sum_{mn\mathbf{k}} \mathcal{V}_{mn}^{\Sigma,a,\ell}(\mathbf{k}) \rho_{nm}^{(2)}(\mathbf{k}; 2\tilde{\omega}) \\ &= \frac{e^2}{A\hbar 2\tilde{\omega}} \sum_{mn\mathbf{k}} \frac{\mathcal{V}_{mn}^{\Sigma,a,\ell}(\mathbf{k})}{\omega_{nm}^\Sigma - 2\tilde{\omega}} \left[-(B_{nm}^c(\mathbf{k}, \omega))_{;k^b} \right. \\ &\quad \left. + i \sum_\ell \left(r_{n\ell}^b B_{\ell m}^c(\mathbf{k}, \omega) - B_{n\ell}^c(\mathbf{k}, \omega) r_{\ell m}^b \right) \right],\end{aligned}\quad (1.75) \quad \boxed{\text{Pjikn2}}$$

which gives the surface-like susceptibility of ℓ -th layer, where \mathbf{V}^Σ is given in Eq. (1.73), where $A = \Omega/d$ is the surface area of the unit cell that characterizes the surface of the system. Using Eq. (1.53) we split this equation into two contributions from the first and second terms on the right hand side,

$$\chi_{i,abc}^{S,\ell} = -\frac{e^3}{A\hbar^2 2\tilde{\omega}} \sum_{mn\mathbf{k}} \frac{\mathcal{V}_{mn}^{\Sigma,a,\ell}}{\omega_{nm}^\Sigma - 2\tilde{\omega}} \left(\frac{f_{mn} r_{nm}^b}{\omega_{nm}^\Sigma - \tilde{\omega}} \right)_{;k^c}, \quad (1.76) \quad \boxed{\text{chii}}$$

and

$$\chi_{e,abc}^{S,\ell} = \frac{ie^3}{A\hbar^2 2\tilde{\omega}} \sum_{\ell mn\mathbf{k}} \frac{\mathcal{V}_{mn}^{\Sigma,a,\ell}}{\omega_{nm}^\Sigma - 2\tilde{\omega}} \left(\frac{r_{n\ell}^c r_{\ell m}^b f_{ml}}{\omega_{\ell m}^\Sigma - \tilde{\omega}} - \frac{r_{n\ell}^b r_{\ell m}^c f_{\ell n}}{\omega_{n\ell}^\Sigma - \tilde{\omega}} \right), \quad (1.77) \quad \boxed{\text{chie}}$$

where $\chi_i^{S,\ell}$ is related to intraband transitions and $\chi_e^{S,\ell}$ to interband transitions. For the generalized derivative in Eq. (1.76) we use the chain rule

$$\left(\frac{f_{mn}r_{nm}^b}{\omega_{nm}^\Sigma - \tilde{\omega}} \right)_{;k^c} = \frac{f_{mn}}{\omega_{nm}^\Sigma - \tilde{\omega}} \left(r_{nm}^b \right)_{;k^c} - \frac{f_{mn}r_{nm}^b \Delta_{nm}^c}{(\omega_{nm}^\Sigma - \tilde{\omega})^2}, \quad (1.78) \quad [\text{gene2}]$$

and the following result shown in Appendix ???

$$(\omega_{nm}^\Sigma)_{;k^a} = (\omega_{nm}^{\text{LDA}})_{;k^a} = v_{nn}^{\text{LDA,a}} - v_{mm}^{\text{LDA,a}} \equiv \Delta_{nm}^a. \quad (1.79) \quad [\text{eli.13}]$$

In order to calculate the nonlinear susceptibility of any given layer ℓ we simply add the above terms $\chi^{S,\ell} = \chi_e^{S,\ell} + \chi_i^{S,\ell}$ and then calculate the surface susceptibility as

$$\chi^S \equiv \sum_{\ell=1}^N \chi^{S,\ell}, \quad (1.80) \quad [\text{chiijksur}]$$

where $\ell = 1$ is the first layer right at the surface, and $\ell = N$ is the bulk-like layer (at a distance $\sim d$ from the surface as seen in Fig. 1.1), such that

$$\chi^{S,\ell=N} = 0, \quad (1.81) \quad [\text{chiijksur2}]$$

in accordance to Eq. (1.5) valid for a centrosymmetric environment. We note that the value of N is not universal. This means that the slab needs to have enough atomic layers for Eq. (1.81) to be satisfied and to give converged results for χ^S . We can use Eq. (1.80) for either the front or the back surface.

We can see from the prefactors of Eqs. (1.76) and (1.77) that they diverge as $\tilde{\omega} \rightarrow 0$. To remove this apparent divergence of $\chi^{S,\ell}$, we perform a partial fraction expansion over $\tilde{\omega}$. As shown in Appendix ???, we use time-reversal invariance to remove these divergences and obtain the following expressions for χ^S ,

$$\text{Im}[\chi_{e,\omega}^{\text{abc}}] = \frac{\pi|e|^3}{2\hbar^2} \int \frac{d^3k}{8\pi^3} \sum_{vc} \sum_{q \neq (v,c)} \frac{1}{\omega_{cv}^\Sigma} \left[\frac{\text{Im}[\mathcal{V}_{qc}^{\Sigma,a}\{r_{cv}^b r_{vq}^c\}]}{(2\omega_{cv}^\Sigma - \omega_{cq}^\Sigma)} - \frac{\text{Im}[\mathcal{V}_{vq}^{\Sigma,a}\{r_{qc}^c r_{cv}^b\}]}{(2\omega_{cv}^\Sigma - \omega_{qv}^\Sigma)} \right] \delta(\omega_{cv}^\Sigma - \omega), \quad (1.82a)$$

$$\text{Im}[\chi_{i,\omega}^{\text{abc}}] = \frac{\pi|e|^3}{2\hbar^2} \int \frac{d^3k}{8\pi^3} \sum_{cv} \frac{1}{(\omega_{cv}^\Sigma)^2} \left[\text{Re} \left[\left\{ r_{cv}^b (\mathcal{V}_{vc}^{\Sigma,a})_{;k^c} \right\} \right] + \frac{\text{Re} \left[\mathcal{V}_{vc}^{\Sigma,a} \{r_{cv}^b \Delta_{cv}^c\} \right]}{\omega_{cv}^\Sigma} \right] \delta(\omega_{cv}^\Sigma - \omega), \quad (1.82b)$$

$$\text{Im}[\chi_{e,2\omega}^{\text{abc}}] = -\frac{\pi|e|^3}{2\hbar^2} \int \frac{d^3k}{8\pi^3} \sum_{vc} \frac{4}{\omega_{cv}^\Sigma} \left[\sum_{v' \neq v} \frac{\text{Im}[\mathcal{V}_{vc}^{\Sigma,a}\{r_{cv'}^b r_{v'v}^c\}]}{2\omega_{cv'}^\Sigma - \omega_{cv}^\Sigma} - \sum_{c' \neq c} \frac{\text{Im}[\mathcal{V}_{vc}^{\Sigma,a}\{r_{cc'}^c r_{c'v}^b\}]}{2\omega_{c'v}^\Sigma - \omega_{cv}^\Sigma} \right] \delta(\omega_{cv}^\Sigma - 2\omega), \quad (1.82c)$$

$$\text{Im}[\chi_{i,2\omega}^{\text{abc}}] = \frac{\pi|e|^3}{2\hbar^2} \int \frac{d^3k}{8\pi^3} \sum_{vc} \frac{4}{(\omega_{cv}^\Sigma)^2} \left[\text{Re} \left[\mathcal{V}_{vc}^{\Sigma,a} \left\{ \left(r_{cv}^b \right)_{;k^c} \right\} \right] - \frac{2\text{Re} \left[\mathcal{V}_{vc}^{\Sigma,a} \{r_{cv}^b \Delta_{cv}^c\} \right]}{\omega_{cv}^\Sigma} \right] \delta(\omega_{cv}^\Sigma - 2\omega), \quad (1.82d)$$

where the limit of $\eta \rightarrow 0$ has been taken. We have split the interband and intraband 1ω and 2ω contributions. The real part of each contribution can be obtained through a Kramers-Kronig

transformation,^[19] and then $\chi_{abc}^{S,\ell} = \chi_{e,abc,\ell}^{S,\ell} + \chi_{e,abc,2\omega}^{S,\ell} + \chi_{i,abc,\omega}^{S,\ell} + \chi_{i,abc,2\omega}^{S,\ell}$. To fulfill the required intrinsic permutation symmetry,^[20] the $\{\}$ notation symmetrizes the bc Cartesian indices, i.e. $\{u^b s^c\} = (u^b s^c + u^c s^b)/2$, and thus $\chi_{abc}^{S,\ell} = \chi_{acb}^{S,\ell}$. In Appendices ?? and ?? we demonstrate how to calculate the generalized derivatives of $\mathbf{r}_{nm;\mathbf{k}}$ and $\mathcal{V}_{nm;\mathbf{k}}^{\Sigma,a,\ell}$. We find that

$$(r_{nm}^b)_{;k^a} = -i\mathcal{T}_{nm}^{ab} + \frac{r_{nm}^a \Delta_{mn}^b + r_{nm}^b \Delta_{mn}^a}{\omega_{nm}^{\text{LDA}}} + \frac{i}{\omega_{nm}^{\text{LDA}}} \sum_{\ell} \left(\omega_{\ell m}^{\text{LDA}} r_{n\ell}^a r_{\ell m}^b - \omega_{n\ell}^{\text{LDA}} r_{n\ell}^b r_{\ell m}^a \right), \quad (1.83) \quad [\text{rgen.69}]$$

where

$$\mathcal{T}_{nm}^{ab} = [r^a, v^{\text{LDA},b}] = \frac{i\hbar}{m_e} \delta_{ab} \delta_{nm} + \mathcal{L}_{nm}^{ab}, \quad (1.84) \quad [\text{tau.1}]$$

and

$$\mathcal{L}_{nm}^{ab} = \frac{1}{i\hbar} [r^a, v^{\text{nl},b}]_{nm}, \quad (1.85) \quad [\text{tau.2}]$$

is the contribution to the generalized derivative of \mathbf{r}_{nm} coming from the nonlocal part of the pseudopotential. In Appendix ?? we calculate \mathcal{L}_{nm}^{ab} , that is a term with very small numerical value but with a computational time at least an order of magnitude larger than for all the other terms involved in the expressions for $\chi_{abc}^{S,\ell}$.^[21] Therefore, we neglect it throughout this article and take

$$\mathcal{T}_{nm}^{ab} \approx \frac{i\hbar}{m_e} \delta_{ab} \delta_{nm}. \quad (1.86) \quad [\text{tau.69}]$$

Finally, we also need the following term (Eq. (??))

$$\begin{aligned} (v_{nn}^{\text{LDA},a})_{;k^b} &= \nabla_{k^a} v_{nn}^{\text{LDA},b}(\mathbf{k}) = -i\mathcal{T}_{nn}^{ab} - \sum_{\ell \neq n} \omega_{\ell n}^{\text{LDA}} \left(r_{n\ell}^a r_{\ell n}^b + r_{n\ell}^b r_{\ell n}^a \right) \\ &\approx \frac{\hbar}{m_e} \delta_{ab} - \sum_{\ell \neq n} \omega_{\ell n}^{\text{LDA}} \left(r_{n\ell}^a r_{\ell n}^b + r_{n\ell}^b r_{\ell n}^a \right), \end{aligned} \quad (1.87) \quad [\text{a.3c}]$$

among other quantities for $\mathcal{V}_{nm;\mathbf{k}}^{\Sigma,a,\ell}$, where we also use Eq. (1.86). Above is the standard effective-mass sum rule.^[22]

1.5 Conclusions

con

We have presented a complete derivation of the required elements to calculate in the independent particle approach (IPA) the microscopic surface second harmonic susceptibility tensor $\chi^S(-2\omega; \omega, \omega)$ using a layer-by-layer approach. We have done so for semiconductors using the length gauge for the coupling of the external electric field to the electron.

Chapter 2

Surface Second-Harmonic Generation Yield

ap:sshgyield

Outline

2.1	The three layer model for the SSHG yield	16
2.1.1	Multiple SHG reflections	19
2.1.2	Multiple reflections for the linear field	20
2.1.3	Deriving the SSHG yield	21
2.2	\mathcal{R}_{IF} for different polarization cases	23
2.2.1	\mathcal{R}_{pP} (<i>p</i> -in, <i>P</i> -out)	25
2.2.2	\mathcal{R}_{sP} (<i>s</i> -in, <i>P</i> -out)	26
2.2.3	\mathcal{R}_{pS} (<i>p</i> -in, <i>S</i> -out)	26
2.2.4	\mathcal{R}_{sS} (<i>s</i> -in, <i>S</i> -out)	27
2.3	Some scenarios of interest	28
2.3.1	The 3-layer model without multiple reflections	28
2.3.2	The two layer, or Fresnel (2-layer-fresnel) model	29
2.3.3	The 2-layer-bulk model: evaluating $\mathcal{P}(2\omega)$ and $\mathbf{E}(\omega)$ in the bulk	29
2.3.4	The 2-layer-vacuum model: evaluating $\mathcal{P}(2\omega)$ and $\mathbf{E}(\omega)$ in the vacuum	29
2.3.5	The 3-layer-hybrid model: evaluating $\mathcal{P}(2\omega)$ in ℓ and $\mathbf{E}(\omega)$ in the bulk	30
2.4	About coding the SSHG yield	30

In this chapter, I will walk the reader through the considerations for developing the three layer (3-layer) model for the SSHG yield. We will then derive explicit expressions for each of the four polarization configurations for the incoming and outgoing fields. These expressions will be simplified by taking into account the symmetry relations for the (111), (110), and (001) surfaces. I have also included Appendices [B](#), [C](#), [D](#), and [E](#) that contain a wealth of supplementary derivations for all the work contained in this chapter.

2.1 The three layer model for the SSHG yield

c:3layersshg

In this section, we will derive the formulas required for the calculation of the SSHG yield, defined by

$$\mathcal{R}(\omega) = \frac{I(2\omega)}{I^2(\omega)}, \quad (2.1) \quad [\text{eq:rintensit}]$$

with the intensity given by [boyd, sutherland] [23, 24]

$$I(\omega) = \begin{cases} \frac{c}{2\pi} n(\omega) |E(\omega)|^2 & (\text{CGS units}) \\ 2\epsilon_0 c n(\omega) |E(\omega)|^2 & (\text{MKS units}) \end{cases}, \quad (2.2) \quad [\text{eq:intensity}]$$

where $n(\omega) = \sqrt{\epsilon(\omega)}$ is the index of refraction with $\epsilon(\omega)$ as the dielectric function, ϵ_0 is the vacuum permittivity, and c the speed of light in vacuum.

There are several ways to calculate R , one of which is the procedure followed by Cini [25]. This approach calculates the nonlinear susceptibility and at the same time the radiated fields. However, I present an alternative derivation based on the work of Mizrahi and Sipe [26], since the derivation of the 3-layer model is straightforward. In this scheme, the surface is represented by three regions or layers. The first layer is the vacuum region (denoted by v) with a dielectric function $\epsilon_v(\omega) = 1$ from where the fundamental electric field $\mathbf{E}_v(\omega)$ impinges on the material. The second layer is a thin layer (denoted by ℓ) of thickness d characterized by a dielectric function $\epsilon_\ell(\omega)$. It is in this layer where the SHG takes place. The third layer is the bulk region denoted by b and characterized by $\epsilon_b(\omega)$. Both the vacuum and bulk layers are semi-infinite (see Fig. 2.1). [fig:MR3layer2w]

To model the electromagnetic response of the 3-layer model, we follow Ref. [26] and assume a polarization sheet of the form [mizrahiJOSA88]

$$\mathbf{P}(\mathbf{r}, t) = \mathcal{P} e^{i\kappa \cdot \mathbf{R}} e^{-i\omega t} \delta(z - z_\beta) + \text{c.c.}, \quad (2.3) \quad [\text{eq:psheet}]$$

where $\mathbf{R} = (x, y)$, κ is the component of the wave vector ν_β parallel to the surface, and z_β is the position of the sheet within medium β . Ref. [27] demonstrates that the solution of the Maxwell equations for the radiated fields $E_{\beta,p\pm}$ and $E_{\beta,s}$ with $\mathbf{P}(\mathbf{r}, t)$ as a source at points $z \neq 0$, can be written as [sipeJOSAB87]

$$(E_{\beta,p\pm}, E_{\beta,s}) = \left(\frac{\gamma i \tilde{\omega}^2}{\tilde{w}_\beta} \hat{\mathbf{p}}_{\beta\pm} \cdot \mathcal{P}, \frac{\gamma i \tilde{\omega}^2}{\tilde{w}_\beta} \hat{\mathbf{s}} \cdot \mathcal{P} \right), \quad (2.4) \quad [\text{eq:solmaxwel}]$$

where $\gamma = 2\pi$ in CGS units or $\gamma = 1/2\epsilon_0$ in MKS units, and $\tilde{\omega} = \omega/c$. Also, $\hat{\mathbf{s}}$ and $\hat{\mathbf{p}}_{\beta\pm}$ are the unitary vectors for the s and p polarizations of the radiated field, respectively. The \pm refers to upward (+) or downward (-) direction of propagation within medium β , as shown in Fig. 2.1. Also, $\tilde{w}_\beta(\omega) = \tilde{\omega} w_\beta$, where [fig:MR3layer2w]

$$\hat{\mathbf{p}}_{\beta\pm}(\omega) = \frac{\kappa(\omega) \hat{\mathbf{z}} \mp \tilde{w}_\beta(\omega) \hat{\boldsymbol{\kappa}}}{\tilde{w}_\beta n_\beta(\omega)} = \frac{\sin \theta_0 \hat{\mathbf{z}} \mp w_\beta(\omega) \hat{\boldsymbol{\kappa}}}{n_\beta(\omega)}, \quad (2.5) \quad [\text{eq:r4}]$$

with

$$w_\beta(\omega) = (\epsilon_\beta(\omega) - \sin^2 \theta_0)^{1/2}, \quad (2.6) \quad [\text{eq:wavevecto}]$$

θ_0 is the angle of incidence of $\mathbf{E}_v(\omega)$, $\kappa(\omega) = |\kappa| = \tilde{\omega} \sin \theta_0$, $n_\beta(\omega) = \sqrt{\epsilon_\beta(\omega)}$ is the index of refraction of medium β , and z is the direction perpendicular to the surface that points towards the

vacuum. If we consider the plane of incidence along the κz plane, then

$$\hat{\kappa} = \cos \phi \hat{\mathbf{x}} + \sin \phi \hat{\mathbf{y}}, \quad (2.7) \quad [\text{eq:mmc1}]$$

and

$$\hat{\mathbf{s}} = -\sin \phi \hat{\mathbf{x}} + \cos \phi \hat{\mathbf{y}}, \quad (2.8) \quad [\text{eq:mmc2}]$$

where ϕ is the azimuthal angle with respect to the x axis.

It is important to mention that we must also calculate the bulk and surface dielectric functions, $\epsilon_b(\omega)$ and $\epsilon_\ell(\omega)$. For this, we follow the method presented in Ref. [18]. For the bulk, the tensor components are equal in all three directions due to the cubic symmetry,

$$\varepsilon_b(\omega) = \epsilon_b^{xx}(\omega) = \epsilon_b^{yy}(\omega) = \epsilon_b^{zz}(\omega).$$

For the purpose of this calculation, we introduce the average value for the surface dielectric function, $\varepsilon_\ell(\omega)$. This entails that $\epsilon_\ell^{xx}(\omega) = \epsilon_\ell^{yy}(\omega) \approx \epsilon_\ell^{zz}(\omega)$, since symmetry is broken in the zz direction because of the surface. We find the average in the conventional way,

$$\varepsilon_\ell(\omega) = \frac{\epsilon_\ell^{xx}(\omega) + \epsilon_\ell^{yy}(\omega) + \epsilon_\ell^{zz}(\omega)}{3},$$

and use that quantity in the equations for the SSHG yield. In order to obtain a result which does not depend on the size of the vacuum region [28], we have normalized the surface dielectric function to the volume of the slab, instead of the volume of the super-cell. We remark that we could calculate $\epsilon_{\text{half-slab}}^{\text{ab}}(\omega)$ using $\mathcal{C}(z) = 1$ for the upper half of our slab and normalize to the volume of the half-slab. Nevertheless, $\epsilon_\ell^{\text{ab}}(\omega)$ and $\epsilon_{\text{half-slab}}^{\text{ab}}(\omega)$ give the same result [16, 17, 28].

In the 3-layer model the nonlinear polarization responsible for the SHG is immersed in the thin layer ($\beta = \ell$), and is given by

$$\mathcal{P}_{\ell,i}(2\omega) = \begin{cases} \chi^{ijk}(-2\omega; \omega, \omega) E_j(\omega) E_k(\omega) & (\text{CGS units}) \\ \epsilon_0 \chi^{ijk}(-2\omega; \omega, \omega) E_j(\omega) E_k(\omega) & (\text{MKS units}) \end{cases}, \quad (2.9) \quad [\text{eq:tres}]$$

where $\chi(-2\omega; \omega, \omega)$ is the dipolar surface nonlinear susceptibility tensor, and the Cartesian indices i, j, k are summed over if repeated. $\chi^{ijk}(-2\omega; \omega, \omega) = \chi^{ikj}(-2\omega; \omega, \omega)$ is the intrinsic permutation symmetry due to the fact that SHG is degenerate in $E_j(\omega)$ and $E_k(\omega)$. As in Ref. [26], we consider the polarization sheet (Eq. (2.3)) to be oscillating at some frequency ω in order to properly express Eqs. (2.4)-(2.8). However, in the following we find it convenient to use ω exclusively to denote the fundamental frequency and κ to denote the component of the incident wave vector parallel to the surface. The generated nonlinear polarization is oscillating at $\Omega = 2\omega$ and will be characterized by a wave vector parallel to the surface $\mathbf{K} = 2\kappa$. We can carry over Eqs. (2.3)-(2.8) simply by replacing the lowercase symbols $(\omega, \tilde{\omega}, \kappa, n_\beta, \tilde{w}_\beta, w_\beta, \hat{\mathbf{p}}_{\beta\pm}, \hat{\mathbf{s}})$ with uppercase symbols $(\Omega, \tilde{\Omega}, \mathbf{K}, N_\beta, \tilde{W}_\beta, W_\beta, \hat{\mathbf{P}}_{\beta\pm}, \hat{\mathbf{S}})$, all evaluated at 2ω . Of course, we always have that $\hat{\mathbf{S}} = \hat{\mathbf{s}}$.

From Fig. 2.1, we observe the propagation of the SH field as it is refracted at the layer-vacuum interface (ℓv), and reflected multiple times from the layer-bulk (ℓb) and layer-vacuum (ℓv) interfaces. Thus, we can define

$$\mathbf{T}^{\ell v} = \hat{\mathbf{s}} T_s^{\ell v} \hat{\mathbf{s}} + \hat{\mathbf{P}}_{v+} T_p^{\ell v} \hat{\mathbf{P}}_{\ell+}, \quad (2.10) \quad [\text{eq:r5}]$$

as the transmission tensor for the ℓv interface,

$$\mathbf{R}^{\ell b} = \hat{\mathbf{s}} R_s^{\ell b} \hat{\mathbf{s}} + \hat{\mathbf{P}}_{\ell+} R_p^{\ell b} \hat{\mathbf{P}}_{\ell-}, \quad (2.11) \quad [\text{eq:r6}]$$

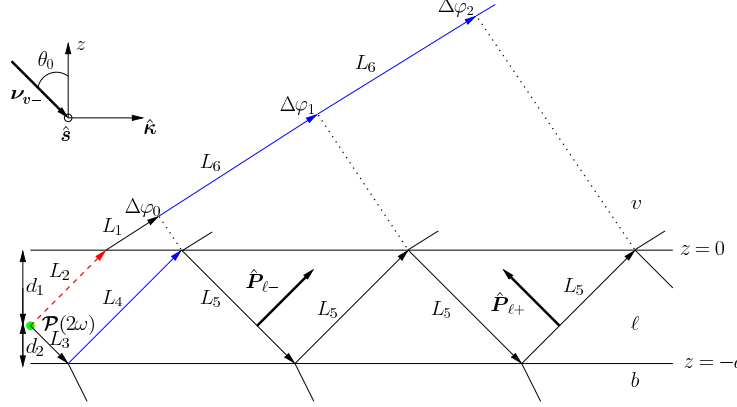


Figure 2.1: Sketch of the three layer model for SHG. The vacuum region (v) is on top with $\epsilon_v = 1$; the layer ℓ of thickness $d = d_1 + d_2$, is characterized with $\epsilon_\ell(\omega)$, and it is where the SH polarization sheet $\mathcal{P}_\ell(2\omega)$ is located at $z_\ell = d_1$. The bulk b is described with $\epsilon_b(\omega)$. The arrows point along the direction of propagation, and the p -polarization unit vector, $\hat{\mathbf{P}}_{\ell- (+)}$, along the downward (upward) direction is denoted with a thick arrow. The s -polarization unit vector $\hat{\mathbf{s}}$, points out of the page. The fundamental field $\mathbf{E}(\omega)$ is incident from the vacuum side along the κz -plane, with θ_0 its angle of incidence and ν_{v-} its wave vector. $\Delta\varphi_i$ denote the phase difference of the multiple reflected beams with respect to the first vacuum transmitted beam (dashed-red arrow), where the dotted lines are perpendicular to this beam.

fig:MR3layer

as the reflection tensor for the ℓb interface, and

$$\mathbf{R}^{\ell v} = \hat{\mathbf{s}} R_s^{\ell v} \hat{\mathbf{s}} + \hat{\mathbf{P}}_{\ell-} R_p^{\ell v} \hat{\mathbf{P}}_{\ell+}, \quad (2.12) \quad \text{eq:r6b}$$

as the reflection tensor for the ℓv interface. The Fresnel factors in uppercase letters, $T_{s,p}^{ij}$ and $R_{s,p}^{ij}$, are evaluated at 2ω from the following well known formulas

$$\begin{aligned} t_s^{ij}(\omega) &= \frac{2w_i(\omega)}{w_i(\omega) + w_j(\omega)}, & t_p^{ij}(\omega) &= \frac{2w_i(\omega)\sqrt{\epsilon_i(\omega)\epsilon_j(\omega)}}{w_i(\omega)\epsilon_j(\omega) + w_j(\omega)\epsilon_i(\omega)}, \\ r_s^{ij}(\omega) &= \frac{w_i(\omega) - w_j(\omega)}{w_i(\omega) + w_j(\omega)}, & r_p^{ij}(\omega) &= \frac{w_i(\omega)\epsilon_j(\omega) - w_j\epsilon_i(\omega)}{w_i(\omega)\epsilon_j(\omega) + w_j(\omega)\epsilon_i(\omega)}. \end{aligned} \quad (2.13) \quad \text{eq:e.f1}$$

With these expressions we easily derive the following useful relations,

$$\begin{aligned} 1 + r_s^{\ell b} &= t_s^{\ell b}, \\ 1 + r_p^{\ell b} &= \frac{n_b}{n_\ell} t_p^{\ell b}, \\ 1 - r_p^{\ell b} &= \frac{n_\ell}{n_b} \frac{w_b}{w_\ell} t_p^{\ell b}, \\ t_p^{\ell v} &= \frac{w_\ell}{w_v} t_p^{v\ell}, \\ t_s^{\ell v} &= \frac{w_\ell}{w_v} t_s^{v\ell}. \end{aligned} \quad (2.14) \quad \text{eq:mf}$$

2.1.1 Multiple SHG reflections

The SH field $\mathbf{E}(2\omega)$ radiated by the SH polarization $\mathcal{P}_\ell(2\omega)$ will radiate directly into the vacuum and the bulk, where it will be reflected back at the layer-bulk interface into the thin layer. This beam will be transmitted and reflected multiple times, as shown in Fig. [fig:MR3layer2w](#). As the two beams propagate, a phase difference will develop between them according to

$$\begin{aligned}\Delta\varphi_m &= \tilde{\Omega} \left((L_3 + L_4 + 2mL_5)N_\ell - (L_2N_\ell + (L_1 + mL_6)N_v) \right) \\ &= \delta_0 + m\delta \quad m = 0, 1, 2, \dots,\end{aligned}\tag{2.15} \quad \text{[eq:m99]}$$

where

$$\delta_0 = 8\pi \left(\frac{d_2}{\lambda_0} \right) W_\ell, \tag{2.16} \quad \text{[eq:delta0]}$$

and

$$\delta = 8\pi \left(\frac{d}{\lambda_0} \right) W_\ell, \tag{2.17} \quad \text{[eq:delta]}$$

where λ_0 is the wavelength of the fundamental field in the vacuum, d is the thickness of layer ℓ , and d_2 is the distance of $\mathcal{P}_\ell(2\omega)$ from the ℓb interface (see Fig. [fig:MR3layer2w](#)). We see that δ_0 is the phase difference of the first and second transmitted beams, and $m\delta$ that of the first and third ($m = 1$), first and fourth ($m = 2$), and so on. Note that the thickness d of the layer ℓ enters through the phase δ , and the position d_2 of the nonlinear polarization sheet $\mathbf{P}(\mathbf{r}, t)$ (Eq. [eq:psheet](#)) enters through δ_0 . In particular, d_2 could be used as a variable to study the effects of multiple reflections on the SHG yield $\mathcal{R}(2\omega)$.

To take into account the multiple reflections of the generated SH field in the layer ℓ , we proceed as follows. I include the algebra for the p -polarized SH field, and the s -polarized field could be worked out along the same steps. The p -polarized $\mathbf{E}_{\ell,p}(2\omega)$ field reflected multiple times is given by

$$\begin{aligned}\mathbf{E}_{\ell,p}(2\omega) &= E_{\ell,p+}(2\omega) \mathbf{T}^{\ell v} \cdot \hat{\mathbf{P}}_{\ell+} + E_{\ell,p-}(2\omega) \mathbf{T}^{\ell v} \cdot \mathbf{R}^{\ell b} \cdot \hat{\mathbf{P}}_{\ell-} e^{i\Delta\varphi_0} \\ &\quad + E_{\ell,p-}(2\omega) \mathbf{T}^{\ell v} \cdot \mathbf{R}^{\ell b} \cdot \mathbf{R}^{\ell v} \cdot \mathbf{R}^{\ell b} \cdot \hat{\mathbf{P}}_{\ell-} e^{i\Delta\varphi_1} \\ &\quad + E_{\ell,p-}(2\omega) \mathbf{T}^{\ell v} \cdot \mathbf{R}^{\ell b} \cdot \mathbf{R}^{\ell v} \cdot \mathbf{R}^{\ell b} \cdot \mathbf{R}^{\ell v} \cdot \mathbf{R}^{\ell b} \cdot \hat{\mathbf{P}}_{\ell-} e^{i\Delta\varphi_2} + \dots \\ &= E_{\ell,p+}(2\omega) \mathbf{T}^{\ell v} \cdot \hat{\mathbf{P}}_{\ell+} + E_{\ell,p-}(2\omega) \mathbf{T}^{\ell v} \cdot \sum_{m=0}^{\infty} (\mathbf{R}^{\ell b} \cdot \mathbf{R}^{\ell v} e^{i\delta})^m \cdot \mathbf{R}^{\ell b} \cdot \hat{\mathbf{P}}_{\ell-} e^{i\delta_0}.\end{aligned}\tag{2.18} \quad \text{[eq:E2wcomplex]}$$

From Eqs. [\(2.10\)](#) - [\(2.12\)](#) it is easy to show that

$$\mathbf{T}^{\ell v} \cdot (\mathbf{R}^{\ell b} \cdot \mathbf{R}^{\ell v})^n \cdot \mathbf{R}^{\ell b} = \hat{\mathbf{s}} T_s^{\ell v} (R_s^{\ell b} R_s^{\ell v})^n R_s^{\ell b} \hat{\mathbf{s}} + \hat{\mathbf{P}}_{v+} T_p^{\ell v} (R_p^{\ell b} R_p^{\ell v})^n R_p^{\ell b} \hat{\mathbf{P}}_{\ell-},$$

then,

$$\mathbf{E}_{\ell,p}(2\omega) = \hat{\mathbf{P}}_{\ell+} T_p^{\ell v} \left(E_{\ell,p+}(2\omega) + \frac{R_p^{\ell b} e^{i\delta_0}}{1 + R_p^{\ell b} R_p^{\ell v} e^{i\delta}} E_{\ell,p-}(2\omega) \right), \tag{2.19} \quad \text{[eq:E2wreduce]}$$

where we used $R_{s,p}^{ij} = -R_{s,p}^{ji}$. Using Eq. [\(2.4\)](#) and [\(2.14\)](#), we can readily write

$$\mathbf{E}_{\ell,p}(2\omega) = \frac{\gamma i \tilde{\Omega}}{W_\ell} \mathbf{H}_\ell \cdot \mathcal{P}_\ell(2\omega), \tag{2.20} \quad \text{[eq:mr8]}$$

where

$$\mathbf{H}_\ell = \frac{W_\ell}{W_v} \left[\hat{\mathbf{s}} T_s^{v\ell} (1 + R_s^M) \hat{\mathbf{s}} + \hat{\mathbf{P}}_{v+} T_p^{v\ell} (\hat{\mathbf{P}}_{\ell+} + R_p^M \hat{\mathbf{P}}_{\ell-}) \right], \quad (2.21) \quad [\text{eq:mr9}]$$

and

$$R_i^M \equiv \frac{R_i^{\ell b} e^{i\delta_0}}{1 + R_i^{v\ell} R_i^{\ell b} e^{i\delta}}, \quad i = s, p, \quad (2.22) \quad [\text{m61}]$$

is defined as the multiple (M) reflection coefficient. This coefficient depends on the thickness d of layer ℓ , and most importantly on the position d_2 of $\mathcal{P}_\ell(2\omega)$ within this layer. The final results will depend on both d and d_2 . However, we can also define an average \bar{R}_i^M as

$$\bar{R}_i^M \equiv \frac{1}{d} \int_0^d R_i^M(x) dx \propto \frac{1}{d} \int_0^d e^{i\alpha x} dx, \quad (2.23) \quad [\text{eq:mcave}]$$

where

$$R_i^M(x) = \frac{R_i^{\ell b} e^{i\alpha x}}{1 + R_i^{v\ell} R_i^{\ell b} e^{i\delta}}, \quad (2.24) \quad [\text{eq:m16}]$$

and $\alpha = 8\pi W_\ell / \lambda_0$. We can evaluate the rightmost integral,

$$\begin{aligned} \frac{1}{d} \int_0^d e^{i\alpha x} dx &= \frac{1}{d} \frac{e^{i\alpha x}}{i\alpha} \Big|_0^d = \frac{1}{i\alpha d} (e^{i\alpha d} - 1) \\ &= \frac{1}{i\delta} (e^{i\delta} - 1) = \frac{1}{i\delta} e^{i\delta/2} \frac{(e^{i\delta/2} - e^{-i\delta/2})}{2i} = e^{i\delta/2} \text{sinc}(\delta/2). \end{aligned} \quad (2.25) \quad [\text{eq:integral}]$$

Therefore, we can establish the average value \bar{R}_i^M as

$$\bar{R}_i^M = \frac{R_i^{\ell b} e^{i\delta/2}}{1 + R_i^{v\ell} R_i^{\ell b} e^{i\delta}} \text{sinc}(\delta/2), \quad (2.26) \quad [\text{eq:mcave2}]$$

that only depends on d through the δ term from Eq. (2.17).

To connect with the work in Ref. [26], where $\mathcal{P}(2\omega)$ is located on top of the vacuum-surface interface and only the vacuum radiated beam and the first (and only) reflected beam need be considered, we take $\ell = v$ and $d_2 = 0$, then $T^{\ell v} = 1$, $R_v^{\ell v} = 0$ and $\delta_0 = 0$, with which $R_i^M = R_i^{vb}$. Thus, Eq. (2.21) coincides with Eq. (3.8) of Ref. [26].

2.1.2 Multiple reflections for the linear field

For a more complete formulation, we must also consider the multiple reflections of the fundamental field $\mathbf{E}_\ell(\omega)$ inside the thin ℓ layer. In Fig. 2.21 present the situation where $\mathbf{E}_v(\omega)$ impinges from the vacuum side with an angle of incidence θ_0 . As the first transmitted beam is multiply reflected from the ℓb and the ℓv interfaces, it accumulates a phase difference of $n\phi$, with $n = 1, 2, 3, \dots$, given by

$$\begin{aligned} \varphi &= \frac{\omega}{c} (2L_1 n_\ell - L_2 n_v) \\ &= 4\pi \left(\frac{d}{\lambda_0} \right) w_\ell, \end{aligned} \quad (2.27) \quad [\text{mphi}]$$

where $n_v = 1$. Besides the equivalent of Eqs. (2.11) and (2.12) for ω , we also need

$$\mathbf{t}^{v\ell} = \hat{\mathbf{s}} t_s^{v\ell} \hat{\mathbf{s}} + \hat{\mathbf{p}}_{\ell-} t_p^{v\ell} \hat{\mathbf{p}}_{v-}, \quad (2.28) \quad [\text{eq:mvv}]$$

to write

$$\begin{aligned} \mathbf{E}(\omega) &= E_0 \left[\mathbf{t}^{v\ell} + \mathbf{r}^{\ell b} \cdot \mathbf{t}^{v\ell} e^{i\varphi} + \mathbf{r}^{\ell b} \cdot \mathbf{r}^{\ell v} \cdot \mathbf{r}^{\ell b} \cdot \mathbf{t}^{v\ell} e^{i2\varphi} + \mathbf{r}^{\ell b} \cdot \mathbf{r}^{\ell v} \cdot \mathbf{r}^{\ell b} \cdot \mathbf{r}^{\ell v} \cdot \mathbf{r}^{\ell b} \cdot \mathbf{t}^{v\ell} e^{i3\varphi} + \dots \right] \cdot \hat{\mathbf{e}}^i \\ &= E_0 \left[1 + \left(1 + \mathbf{r}^{\ell b} \cdot \mathbf{r}^{\ell v} e^{i\varphi} + (\mathbf{r}^{\ell b} \cdot \mathbf{r}^{\ell v})^2 e^{i2\varphi} + \dots \right) \cdot \mathbf{r}^{\ell b} e^{i\varphi} \right] \cdot \mathbf{t}^{v\ell} \cdot \hat{\mathbf{e}}^i \\ &= E_0 \left[\hat{\mathbf{s}} t_s^{v\ell} (1 + r_s^M) \hat{\mathbf{s}} + t_p^{v\ell} (\hat{\mathbf{p}}_{\ell-} + \hat{\mathbf{p}}_{\ell+} r_p^M) \hat{\mathbf{p}}_{v-} \right] \cdot \hat{\mathbf{e}}^i, \end{aligned} \quad (2.29) \quad [\text{eq:mcview}]$$

where E_0 is the intensity of the fundamental field, and $\hat{\mathbf{e}}^i$ is the unit vector of the incoming polarization, with $i = s, p$, and then, $\hat{\mathbf{e}}^s = \hat{\mathbf{s}}$ and $\hat{\mathbf{e}}^p = \hat{\mathbf{p}}_{v-}$. Also,

$$r_i^M \equiv \frac{r_i^{\ell b} e^{i\varphi}}{1 + r_i^{v\ell} r_i^{\ell b} e^{i\varphi}}, \quad i = s, p. \quad (2.30) \quad [\text{mvrM}]$$

r_i^M is defined as the multiple (M) reflection coefficient for the fundamental field. We define $\mathbf{E}_\ell^i(\omega) \equiv E_0 \mathbf{e}_\ell^{\omega, i}$ ($i = s, p$), where

$$\mathbf{e}_\ell^{\omega, i} = \left[\hat{\mathbf{s}} t_s^{v\ell} (1 + r_s^M) \hat{\mathbf{s}} + t_p^{v\ell} (\hat{\mathbf{p}}_{\ell-} + \hat{\mathbf{p}}_{\ell+} r_p^M) \hat{\mathbf{p}}_{v-} \right] \cdot \hat{\mathbf{e}}^i, \quad (2.31) \quad [\text{eq:mcview2}]$$

and using Eq. (2.5) we obtain that

$$\mathbf{e}_\ell^{\omega, p} = \frac{t_p^{v\ell}}{n_\ell} (r_p^{M+} \sin \theta_0 \hat{\mathbf{z}} + r_p^{M-} w_\ell \hat{\boldsymbol{\kappa}}), \quad (2.32) \quad [\text{eq:mcvep}]$$

for p -input polarization with $\hat{\mathbf{e}}^i = \hat{\mathbf{p}}_{v-}$, and

$$\mathbf{e}_\ell^{\omega, s} = t_s^{v\ell} r_s^{M+} \hat{\mathbf{s}}, \quad (2.33) \quad [\text{eq:mcves}]$$

for s -input polarization with $\hat{\mathbf{e}}^i = \hat{\mathbf{s}}$, where

$$r_i^{M\pm} = 1 \pm r_i^M, \quad i = s, p. \quad (2.34) \quad [\text{eq:mvc}]$$

2.1.3 Deriving the SSHG yield

The magnitude of the radiated field is given by $E(2\omega) = \hat{\mathbf{e}}^F \cdot \mathbf{E}_\ell(2\omega)$, where $\hat{\mathbf{e}}^F$ is the unit vector of the final polarization with $F = S, P$, where $\hat{\mathbf{e}}^S = \hat{\mathbf{s}}$ and $\hat{\mathbf{e}}^P = \hat{\mathbf{P}}_{v+}$. We expand the rightmost term in parenthesis of Eq. (2.21) as

$$\begin{aligned} \hat{\mathbf{P}}_{\ell+} + R_p^M \hat{\mathbf{P}}_{\ell-} &= \frac{\sin \theta_0 \hat{\mathbf{z}} - W_\ell \hat{\boldsymbol{\kappa}}}{N_\ell} + R_p^M \frac{\sin \theta_0 \hat{\mathbf{z}} + W_\ell \hat{\boldsymbol{\kappa}}}{N_\ell} \\ &= \frac{1}{N_\ell} (\sin \theta_0 R_p^{M+} \hat{\mathbf{z}} - W_\ell R_p^{M-} \hat{\boldsymbol{\kappa}}), \end{aligned} \quad (2.35)$$

where

$$R_i^{M\pm} \equiv 1 \pm R_i^M, \quad i = s, p. \quad (2.36) \quad [\text{eq:rm}]$$

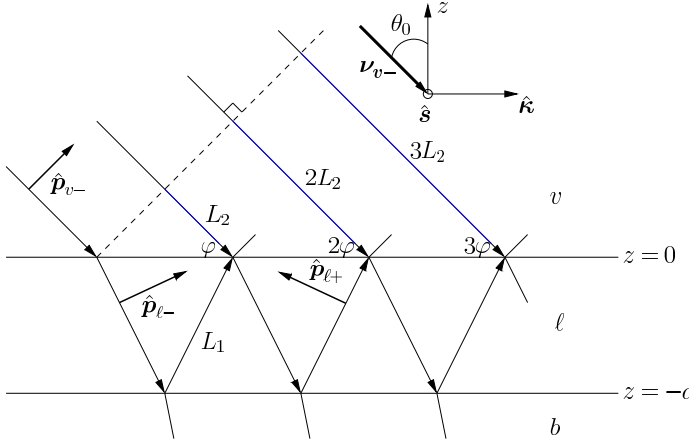


Figure 2.2: Sketch for the multiple reflected fundamental field $\mathbf{E}(\omega)$, which impinges from the vacuum side along the $\hat{\kappa}z$ -plane. θ_0 and ν_{v-} are the angle of incidence and wave vector, respectively. The arrows point along the direction of propagation. The p -polarization unit vectors $\hat{\mathbf{p}}_{\beta\pm}$, point along the downward ($-$) or upward ($+$) directions and are denoted with thick arrows, where $\beta = v$ or ℓ . The s -polarization unit vector $\hat{\mathbf{s}}$ points out of the page. $(1, 2, 3, \dots)\varphi$ denotes the phase difference for the multiple reflected beams with respect to the incident field, where the dotted line is perpendicular to this beam.

`fig:MR3layer`

Using Eq. (2.14) we write Eq. (2.20) as

$$E(2\omega) = \frac{2\gamma i\omega}{cW_\ell} \hat{\mathbf{e}}^F \cdot \mathbf{H}_\ell \cdot \mathcal{P}_\ell(2\omega) = \frac{2\gamma i\omega}{cW_v} \mathbf{e}_\ell^{2\omega,F} \cdot \mathcal{P}_\ell(2\omega), \quad (2.37) \quad [\text{eq:r10}]$$

where

$$\mathbf{e}_\ell^{2\omega,F} = \hat{\mathbf{e}}^F \cdot \left[\hat{\mathbf{s}} T_s^{v\ell} R_s^{M+} \hat{\mathbf{s}} + \hat{\mathbf{P}}_{v+} \frac{T_p^{v\ell}}{N_\ell} (\sin \theta_0 R_p^{M+} \hat{\mathbf{z}} - W_\ell R_p^{M-} \hat{\kappa}) \right]. \quad (2.38) \quad [\text{eq:r12mm}]$$

Replacing $\mathbf{E}(\omega) \rightarrow E_0 \mathbf{e}_\ell^{\omega,i}$, in Eq. (2.9), we obtain that

$$\mathcal{P}_\ell(2\omega) = \begin{cases} E_0^2 \chi : \mathbf{e}_\ell^{\omega,i} \mathbf{e}_\ell^{\omega,i} & (\text{CGS units}) \\ \epsilon_0 E_0^2 \chi : \mathbf{e}_\ell^{\omega,i} \mathbf{e}_\ell^{\omega,i} & (\text{MKS units}) \end{cases}, \quad (2.39) \quad [\text{eq:m4}]$$

where $\mathbf{e}_\ell^{\omega,i}$ is given by Eq. (2.31), and thus Eq. (2.37) reduces to ($W_v = \cos \theta_0$)

$$E_\ell(2\omega) = \frac{2\eta i\omega}{c \cos \theta_0} \mathbf{e}_\ell^{2\omega,F} \cdot \chi : \mathbf{e}_\ell^{\omega,i} \mathbf{e}_\ell^{\omega,i}, \quad (2.40) \quad [\text{eq:mr10}]$$

where $\eta = 2\pi$ in CGS units and $\eta = 1/2$ in MKS units. For ease of notation, we define

$$\Upsilon_{iF} \equiv \mathbf{e}_\ell^{2\omega,F} \cdot \chi : \mathbf{e}_\ell^{\omega,i} \mathbf{e}_\ell^{\omega,i}, \quad (2.41) \quad [\text{eq:mc0}]$$

where i stands for the incoming polarization of the fundamental electric field given by $\hat{\mathbf{e}}^i$ in Eq. (2.31), and F for the outgoing polarization of the SH electric field given by $\hat{\mathbf{e}}^F$ in Eq. (2.38). I purposely omitted the full $\chi(-2\omega; \omega, \omega)$ notation, and will do so from this point on.

From Eqs. (2.1) and (2.2) we obtain that in CGS units ($\eta = 2\pi$),

$$\begin{aligned} |E(2\omega)|^2 &= |E_0|^4 \frac{16\pi^2\omega^2}{c^2 W_v^2} |\Upsilon_{iF}|^2 \\ \frac{c}{2\pi} |\sqrt{N_v} E(2\omega)|^2 &= \frac{32\pi^3\omega^2}{c^3 \cos^2 \theta_0} \left| \frac{\sqrt{N_v}}{n_\ell^2} \Upsilon_{iF} \right|^2 \left(\frac{c}{2\pi} |\sqrt{n_\ell} E_0|^2 \right)^2 \\ I(2\omega) &= \frac{32\pi^3\omega^2}{c^3 \cos^2 \theta_0} \left| \frac{\sqrt{N_v}}{n_\ell^2} \Upsilon_{iF} \right|^2 I^2(\omega) \\ \mathcal{R}_{iF}(2\omega) &= \frac{32\pi^3\omega^2}{c^3 \cos^2 \theta_0} \left| \frac{1}{n_\ell} \Upsilon_{iF} \right|^2, \end{aligned} \quad (2.42) \quad [\text{eq:r01}]$$

and in MKS units ($\eta = 1/2$),

$$\begin{aligned} |E(2\omega)|^2 &= |E_0|^4 \frac{\omega^2}{c^2 W_v^2} \\ 2\epsilon_0 c |\sqrt{N_v} E(2\omega)|^2 &= \frac{2\epsilon_0 \omega^2}{c \cos^2 \theta_0} \left| \frac{\sqrt{N_v}}{n_\ell^2} \Upsilon_{iF} \right|^2 \frac{1}{4\epsilon_0^2 c^2} (2\epsilon_0 c |\sqrt{n_\ell} E_0|^2)^2 \\ I(2\omega) &= \frac{\omega^2}{2\epsilon_0 c^3 \cos^2 \theta_0} \left| \frac{\sqrt{N_v}}{n_\ell^2} \Upsilon_{iF} \right|^2 I^2(\omega) \\ \mathcal{R}_{iF}(2\omega) &= \frac{\omega^2}{2\epsilon_0 c^3 \cos^2 \theta_0} \left| \frac{1}{n_\ell} \Upsilon_{iF} \right|^2. \end{aligned} \quad (2.43) \quad [\text{r01m}]$$

Finally, we condense these results and establish the SSHG yield as

$$\mathcal{R}_{iF}(2\omega) \begin{cases} \frac{32\pi^3\omega^2}{c^3 \cos^2 \theta_0} \left| \frac{1}{n_\ell} \Upsilon_{iF} \right|^2 & (\text{CGS units}) \\ \frac{\omega^2}{2\epsilon_0 c^3 \cos^2 \theta_0} \left| \frac{1}{n_\ell} \Upsilon_{iF} \right|^2 & (\text{MKS units}) \end{cases}, \quad (2.44) \quad [\text{eq:mcs}]$$

where $N_v = 1$ and $W_v = \cos \theta_0$. In the MKS unit system χ is given in m^2/V , since it is a surface second order nonlinear susceptibility, and \mathcal{R}_{iF} is given in m^2/W .

I include a full treatise on this exact procedure without considering the effects of multiple reflections in Appendix C.

2.2 \mathcal{R}_{iF} for different polarization cases

We now have everything we need to derive explicit expressions for \mathcal{R}_{iF} , Eq. (2.44), for the most commonly used polarizations of incoming and outgoing fields ($iF=pP, pS, sP$, and sS). For this, we must expand Υ_{iF} from Eq. (2.41) for each case. By substituting Eqs. (2.7) and (2.8) into Eq. (2.38), we obtain

$$\mathbf{e}_\ell^{2\omega, P} = \frac{T_p^{v\ell}}{N_\ell} (\sin \theta_0 R_p^{M+} \hat{\mathbf{z}} - W_\ell R_p^{M-} \cos \phi \hat{\mathbf{x}} - W_\ell R_p^{M-} \sin \phi \hat{\mathbf{y}}), \quad (2.45) \quad [\text{eq:e2wpmr}]$$

for P ($\hat{\mathbf{e}}^F = \hat{\mathbf{P}}_{v+}$) outgoing polarization, and

$$\mathbf{e}_\ell^{2\omega, S} = T_s^{v\ell} R_s^{M+} (-\sin \phi \hat{\mathbf{x}} + \cos \phi \hat{\mathbf{y}}). \quad (2.46) \quad [\text{eq:e2wsmr}]$$

Case	$\hat{\mathbf{e}}^F$	$\hat{\mathbf{e}}^i$	$\mathbf{e}_\ell^{2\omega,F}$	$\mathbf{e}_\ell^{\omega,i} \mathbf{e}_\ell^{\omega,i}$
\mathcal{R}_{pP}	$\hat{\mathbf{P}}_{v+}$	$\hat{\mathbf{p}}_{v-}$	Eq. (2.45) Eq. (2.46)	Eq. (2.47) Eq. (2.47)
\mathcal{R}_{pS}	$\hat{\mathbf{S}}$	$\hat{\mathbf{p}}_{v-}$	Eq. (2.46) Eq. (2.45)	Eq. (2.47) Eq. (2.48)
\mathcal{R}_{sP}	$\hat{\mathbf{P}}_{v+}$	$\hat{\mathbf{s}}$	Eq. (2.45) Eq. (2.46)	Eq. (2.48) Eq. (2.48)
\mathcal{R}_{sS}	$\hat{\mathbf{S}}$	$\hat{\mathbf{s}}$	Eq. (2.46)	Eq. (2.48)

Table 2.1: Polarization unit vectors for $\hat{\mathbf{e}}^F$ and $\hat{\mathbf{e}}^i$, and equations describing $\mathbf{e}_\ell^{2\omega,F}$ and $\mathbf{e}_\ell^{\omega,i} \mathbf{e}_\ell^{\omega,i}$ for each polarization case.

tab:summary

(111)- C_{3v}	(110)- C_{2v}	(001)- C_{4v}
χ^{zzz}	χ^{zzz}	χ^{zzz}
$\chi^{zxx} = \chi^{zyy}$	$\chi^{zxx} \neq \chi^{zyy}$	$\chi^{zxx} = \chi^{zyy}$
$\chi^{xxz} = \chi^{yyz}$	$\chi^{xxz} \neq \chi^{yyz}$	$\chi^{xxz} = \chi^{yyz}$
$\chi^{xxx} = -\chi^{xyy} = -\chi^{yyx}$		

Table 2.2: Components of χ for the (111), (110) and (001) crystallographic faces, belonging to the C_{3v} , C_{2v} , and C_{4v} , symmetry groups, respectively. For the (111) surface we choose the x and y axes along the $[1\bar{1}\bar{2}]$ and $[1\bar{1}0]$ directions, respectively. For the (110) and (001) we consider the y axis perpendicular to the plane of symmetry.^{sipePRB87} [29] We remark that in general $\chi^{(111)} \neq \chi^{(110)} \neq \chi^{(001)}$.

tab:chis

for S ($\hat{\mathbf{e}}^F = \hat{\mathbf{s}}$) outgoing polarization.

Following a similar procedure, we use Eqs. (2.7) and (2.8) with Eq. (2.32), and obtain

$$\begin{aligned} \mathbf{e}_\ell^{\omega,p} \mathbf{e}_\ell^{\omega,p} &= \left(\frac{t_p^{\ell p}}{n_\ell} \right)^2 \left((r_p^{M-})^2 w_\ell^2 \cos^2 \phi \hat{\mathbf{x}} \hat{\mathbf{x}} + 2(r_p^{M-})^2 w_\ell^2 \sin \phi \cos \phi \hat{\mathbf{x}} \hat{\mathbf{y}} \right. \\ &\quad + 2r_p^{M+} r_p^{M-} w_\ell \sin \theta_0 \cos \phi \hat{\mathbf{x}} \hat{\mathbf{z}} + (r_p^{M-})^2 w_\ell^2 \sin^2 \phi \hat{\mathbf{y}} \hat{\mathbf{y}} \\ &\quad \left. + 2r_p^{M+} r_p^{M-} w_\ell \sin \theta_0 \sin \phi \hat{\mathbf{y}} \hat{\mathbf{z}} + (r_p^{M+})^2 \sin^2 \theta_0 \hat{\mathbf{z}} \hat{\mathbf{z}} \right), \end{aligned} \quad (2.47) \quad [\text{eq:ewewpmr}]$$

for p incoming polarization ($\hat{\mathbf{e}}^i = \hat{\mathbf{p}}_{v-}$), and with Eq. (2.33),

$$\mathbf{e}_\ell^{\omega,s} \mathbf{e}_\ell^{\omega,s} = \left(t_s^{\ell s} r_s^{M+} \right)^2 (\sin^2 \phi \hat{\mathbf{x}} \hat{\mathbf{x}} + \cos^2 \phi \hat{\mathbf{y}} \hat{\mathbf{y}} - 2 \sin \phi \cos \phi \hat{\mathbf{x}} \hat{\mathbf{y}}). \quad (2.48) \quad [\text{eq:ewewsmr}]$$

for s incoming polarization ($\hat{\mathbf{e}}^i = \hat{\mathbf{s}}$).

I have summarized the combination of equations needed to derive the expressions for all four polarization cases of \mathcal{R}_{iF} in Table 2.1. In the following subsections we will derive the explicit expressions for Υ_{iF} for the most general case where the surface has no symmetry other than that of noncentrosymmetry. We will then develop these expressions for particular cases of the most commonly investigated surfaces, the (111), (001), and (110) crystallographic faces. For ease of writing we split Υ_{iF} as

$$\Upsilon_{iF} = \Gamma_{iF} r_{iF}. \quad (2.49) \quad [\text{eq:mc25}]$$

Lastly, in Table 2.2 I list the nonzero components of χ for each surface symmetry [sipePRB87, popovbook 29, 30].

I have provided the full, step-by-step derivation for all of these expressions in Appendix [B](#), with and without the effects of multiple reflections. The avid reader should refer to that chapter if interested in deriving any of the expressions listed below.

2.2.1 \mathcal{R}_{pP} (*p*-in, *P*-out)

`sec:RpP`

Per Table [B.1](#), \mathcal{R}_{pP} requires Eqs. ([2.45](#)) and ([2.47](#)). After some algebra, we obtain that

$$\Gamma_{pP} = \frac{T_p^{v\ell}}{N_\ell} \left(\frac{t_p^{v\ell}}{n_\ell} \right)^2, \quad (2.50) \quad [\text{eq:mc78}]$$

and

$$\begin{aligned} r_{pP} = & -R_p^{M-} (r_p^{M-})^2 w_\ell^2 W_\ell \cos^3 \phi \chi^{xxx} - 2R_p^{M-} (r_p^{M-})^2 w_\ell^2 W_\ell \sin \phi \cos^2 \phi \chi^{xxy} \\ & - 2R_p^{M-} r_p^{M+} r_p^{M-} w_\ell W_\ell \sin \theta_0 \cos^2 \phi \chi^{xxz} - R_p^{M-} (r_p^{M-})^2 w_\ell^2 W_\ell \sin^2 \phi \cos \phi \chi^{xyy} \\ & - 2R_p^{M-} r_p^{M+} r_p^{M-} w_\ell W_\ell \sin \theta_0 \sin \phi \cos \phi \chi^{xyz} - R_p^{M-} (r_p^{M+})^2 W_\ell \sin^2 \theta_0 \cos \phi \chi^{xzz} \\ & - R_p^{M-} (r_p^{M-})^2 w_\ell^2 W_\ell \sin \phi \cos^2 \phi \chi^{yxx} - 2R_p^{M-} (r_p^{M-})^2 w_\ell^2 W_\ell \sin^2 \phi \cos \phi \chi^{yxy} \\ & - 2R_p^{M-} r_p^{M+} r_p^{M-} w_\ell W_\ell \sin \theta_0 \sin \phi \cos \phi \chi^{yxz} - R_p^{M-} (r_p^{M-})^2 w_\ell^2 W_\ell \sin^3 \phi \chi^{yyy} \\ & - 2R_p^{M-} r_p^{M+} r_p^{M-} w_\ell W_\ell \sin \theta_0 \sin^2 \phi \chi^{yyz} - R_p^{M-} (r_p^{M+})^2 W_\ell \sin^2 \theta_0 \sin \phi \chi^{yzz} \\ & + R_p^{M+} (r_p^{M-})^2 w_\ell^2 \sin \theta_0 \cos^2 \phi \chi^{zxx} + 2R_p^{M+} r_p^{M+} r_p^{M-} w_\ell \sin^2 \theta_0 \cos \phi \chi^{zxz} \\ & + 2R_p^{M+} (r_p^{M-})^2 w_\ell^2 \sin \theta_0 \sin \phi \cos \phi \chi^{zxy} + R_p^{M+} (r_p^{M-})^2 w_\ell^2 \sin \theta_0 \sin^2 \phi \chi^{zyy} \\ & + 2R_p^{M+} r_p^{M+} r_p^{M-} w_\ell \sin^2 \theta_0 \sin \phi \chi^{zzy} + R_p^{M+} (r_p^{M+})^2 \sin^3 \theta_0 \chi^{zzz}, \end{aligned} \quad (2.51)$$

where all 18 independent components of χ for a surface with no symmetries, contribute to \mathcal{R}_{pP} . Recall that $\chi^{ijk} = \chi^{ikj}$. We will derive the expressions for each of the three surfaces being considered here, referring to Table [B.2](#). For the (111) surface we obtain

$$\begin{aligned} r_{pP}^{(111)} = & R_p^{M+} \sin \theta_0 \left[(r_p^{M+})^2 \sin^2 \theta_0 \chi^{zzz} + (r_p^{M-})^2 w_\ell^2 \chi^{zxx} \right] \\ & - R_p^{M-} w_\ell W_\ell \left[2r_p^{M+} r_p^{M-} \sin \theta_0 \chi^{xxz} + (r_p^{M-})^2 w_\ell \chi^{xxx} \cos 3\phi \right], \end{aligned} \quad (2.52) \quad [\text{eq:rpp111}]$$

where the three-fold azimuthal symmetry of the SHG signal that is typical of the C_{3v} symmetry group, is seen in the 3ϕ argument of the cosine function. For the (110) surface, we have that

$$\begin{aligned} r_{pP}^{(110)} = & R_p^{M+} \sin \theta_0 \left[(r_p^{M+})^2 \sin^2 \theta_0 \chi^{zzz} + (r_p^{M-})^2 w_\ell^2 \left(\frac{\chi^{zyy} + \chi^{zxx}}{2} + \frac{\chi^{zyy} - \chi^{zxx}}{2} \cos 2\phi \right) \right] \\ & - 2R_p^{M-} r_p^{M+} r_p^{M-} w_\ell W_\ell \sin \theta_0 \left(\frac{\chi^{yyz} + \chi^{xxz}}{2} + \frac{\chi^{yyz} - \chi^{xxz}}{2} \cos 2\phi \right). \end{aligned} \quad (2.53) \quad [\text{eq:rpp110}]$$

The two-fold azimuthal symmetry of the SHG signal that is typical of the C_{2v} symmetry group, is seen in the 2ϕ argument of the cosine function. For the (001) surface we simply make $\chi^{zxx} = \chi^{zyy}$

and $\chi^{xxz} = \chi^{yyz}$ as seen in Table 2.2, and the previous expression reduces to

$$r_{pP}^{(001)} = R_p^{M+} \sin \theta_0 \left[(r_p^{M+})^2 \sin^2 \theta_0 \chi^{zzz} + (r_p^{M-})^2 w_\ell^2 \chi^{zxx} \right] - 2R_p^{M-} r_p^{M+} r_p^{M-} w_\ell W_\ell \sin \theta_0 \chi^{xxz}. \quad (2.54) \quad [\text{rpp001}]$$

This time, the azimuthal 4ϕ symmetry for the C_{4v} group of the (001) surface is absent in this expression since this contribution is only related to the bulk nonlinear quadrupolar SH term [29], that we neglect in this work.

2.2.2 \mathcal{R}_{sP} (*s*-in, *P*-out)

sec:RsP

Per Table 2.1, \mathcal{R}_{sP} requires Eqs. (2.45) and (2.48). After some algebra, we obtain that

$$\Gamma_{sP} = \frac{T_p^{v\ell}}{N_\ell} \left(t_s^{v\ell} r_s^{M+} \right)^2, \quad (2.55) \quad [\text{mcv4}]$$

and

$$\begin{aligned} r_{sP} &= R_p^{M-} W_\ell (-\sin^2 \phi \cos \phi \chi^{xxx} + 2 \sin \phi \cos^2 \phi \chi^{xxy} - \cos^3 \phi \chi^{xyy}) \\ &\quad R_p^{M-} W_\ell (-\sin^3 \phi \chi^{yxx} + 2 \sin^2 \phi \cos \phi \chi^{xyy} - \sin \phi \cos^2 \phi \chi^{yyy}) \\ &\quad R_p^{M+} \sin \theta_0 (\sin^2 \phi \chi^{zxx} - 2 \sin \phi \cos \phi \chi^{zxy} + \cos^2 \phi \chi^{zyy}). \end{aligned} \quad (2.56)$$

In this case, 9 out of the 18 components of χ for a surface with no symmetries, contribute to \mathcal{R}_{sP} . This is because there is no $E_z(\omega)$ component, as the incoming polarization is *s*. From Table 2.2 we get,

$$r_{sP}^{(111)} = R_p^{M+} \sin \theta_0 \chi^{zxx} + R_p^{M-} W_\ell \chi^{xxx} \cos 3\phi, \quad (2.57) \quad [\text{eq:rsp111}]$$

for the (111) surface,

$$r_{sP}^{(110)} = R_p^{M+} \sin \theta_0 \left(\frac{\chi^{zxx} + \chi^{zyy}}{2} + \frac{\chi^{zyy} - \chi^{zxx}}{2} \cos 2\phi \right), \quad (2.58) \quad [\text{eq:rsp110}]$$

for the (110) surface, and

$$r_{sP}^{(001)} = R_p^{M+} \sin \theta_0 \chi^{zxx}, \quad (2.59) \quad [\text{eq:rsp001}]$$

for the (001) surface.

2.2.3 \mathcal{R}_{pS} (*p*-in, *S*-out)

sec:RpS

Per Table 2.1, \mathcal{R}_{pS} requires Eqs. (2.46) and (2.47). After some algebra, we obtain that

$$\Gamma_{pS} = T_s^{v\ell} R_s^{M+} \left(\frac{t_p^{v\ell}}{n_\ell} \right)^2, \quad (2.60) \quad [\text{mcv}]$$

and

$$\begin{aligned}
r_{pS} = & - (r_p^{M-})^2 w_\ell^2 \sin \phi \cos^2 \phi \chi^{xxx} - 2 (r_p^{M-})^2 w_\ell^2 \sin^2 \phi \cos \phi \chi^{xxy} \\
& - 2r_p^{M+} r_p^{M-} w_\ell \sin \theta_0 \sin \phi \cos \phi \chi^{xxz} - (r_p^{M-})^2 w_\ell^2 \sin^3 \phi \chi^{xyy} \\
& - 2r_p^{M+} r_p^{M-} w_\ell \sin \theta_0 \sin^2 \phi \chi^{xzy} - (r_p^{M+})^2 \sin^2 \theta_0 \sin \phi \chi^{xzz} \\
& + (r_p^{M-})^2 w_\ell^2 \cos^3 \phi \chi^{yxx} + 2 (r_p^{M-})^2 w_\ell^2 \sin \phi \cos^2 \phi \chi^{yxy} \\
& + 2r_p^{M+} r_p^{M-} w_\ell \sin \theta_0 \cos^2 \phi \chi^{yxz} + (r_p^{M-})^2 w_\ell^2 \sin^2 \phi \cos \phi \chi^{yyy} \\
& + 2r_p^{M+} r_p^{M-} w_\ell \sin \theta_0 \sin \phi \cos \phi \chi^{yzy} + (r_p^{M+})^2 \sin^2 \theta_0 \cos \phi \chi^{yzz}.
\end{aligned} \tag{2.61}$$

In this case, 12 out of the 18 components of χ for a surface with no symmetries, contribute to \mathcal{R}_{pS} . This is because there is no $\mathcal{P}_z(2\omega)$ component, as the outgoing polarization is S . From Table 2.2 we obtain,

$$r_{pS}^{(111)} = - (r_p^{M-})^2 w_\ell^2 \chi^{xxx} \sin 3\phi, \tag{2.62} \quad [\text{eq:rps111}]$$

for the (111) surface,

$$r_{sP}^{(110)} = r_p^{M+} r_p^{M-} w_\ell \sin \theta_0 (\chi^{yyz} - \chi^{xxz}) \sin 2\phi, \tag{2.63} \quad [\text{eq:rps110}]$$

for the (110) surface, finally,

$$r_{pS}^{(001)} = 0, \tag{2.64} \quad [\text{eq:rps001}]$$

for the (001) surface, where the zero value is only surface related as we neglect the bulk nonlinear quadrupolar contribution [29].

2.2.4 \mathcal{R}_{ss} (*s*-in, *S*-out)

sec:RsS

Per Table 2.1, \mathcal{R}_{ss} requires Eqs. (2.46) and (2.48). After some algebra, we obtain that

$$\Gamma_{ss} = T_s^{v\ell} R_s^{M+} \left(t_s^{v\ell} r_s^{M+} \right)^2, \tag{2.65}$$

and

$$\begin{aligned}
r_{ss} = & - \sin^3 \phi \chi^{xxx} + 2 \sin^2 \phi \cos \phi \chi^{xxy} - \sin \phi \cos^2 \phi \chi^{xyy} \\
& + \sin^2 \phi \cos \phi \chi^{yxx} + \cos^3 \phi \chi^{yyy} - 2 \sin \phi \cos^2 \phi \chi^{yxy}.
\end{aligned} \tag{2.66}$$

In this case, only 6 out of the 18 components of χ for a surface with no symmetries, contribute to \mathcal{R}_{ss} . This is because there is neither an $E_z(\omega)$ component as the incoming polarization is s , nor a $\mathcal{P}_z(2\omega)$ component as the outgoing polarization is S . From Table 2.2, we get

$$r_{ss}^{(111)} = \chi^{xxx} \sin 3\phi, \tag{2.67} \quad [\text{eq:rss111}]$$

for the (111) surface,

$$r_{ss}^{(110)} = 0, \tag{2.68} \quad [\text{eq:rss110}]$$

and

$$r_{ss}^{(001)} = 0, \tag{2.69} \quad [\text{eq:rss001}]$$

for the (110) and (001) surfaces, respectively, both being zero as the bulk nonlinear quadrupolar contribution is not considered here [29].

Label	$\mathcal{P}(2\omega)$	$\mathbf{E}(\omega)$
3-layer	ℓ	ℓ
2-layer-fresnel	v	b
2-layer-bulk	b	b
3-layer-hybrid	ℓ	b
2-layer-vacuum	v	v

Table 2.3: Summary of the SSHG yield models used throughout this work. “Label” is the name used in subsequent figures, while the remaining columns show in which medium we will consider the specified quantity. ℓ is the thin layer below the surface of the material, v is the vacuum region, and b is the bulk region of the material.

`tab:models`

2.3 Some scenarios of interest

In this section we present five different scenarios for placing the nonlinear polarization $\mathcal{P}(2\omega)$ and the fundamental electric field $\mathbf{E}(\omega)$, which are alternatives to the three-layer model presented above. In what follows, we confine ourselves only to the (111) surface and the p -in P -out combination polarizations. This is the case where the proposed scenarios differ the most as the SSHG yield depends on all the finite χ^{ijk} components for this surface. However, the other pS , sP , and sS polarization cases, or the (110) or (001) surfaces could be worked out along the same lines described below. For all the scenarios we omit the multiple SH reflections by taking $R_p^{M\pm} \rightarrow 1 \pm R_p^{\ell b}$ (Eq. [\(2.36\)](#)) and the linear multiple reflections by taking $r_p^{M\pm} \rightarrow 1 \pm r_p^{\ell b}$ (Eq. [\(2.34\)](#)). Using the expressions in Eq. [\(2.14\)](#), we obtain the following useful relationships

$$\begin{aligned} r_p^{M+} &\rightarrow \frac{n_b}{n_\ell} t_p^{\ell b} \\ r_p^{M-} &\rightarrow \frac{n_\ell}{n_b} \frac{w_b}{w_\ell} t_p^{\ell b}, \end{aligned} \tag{2.70} \quad \text{[eq:mvc89]}$$

which will come in handy for expressing Γ_{pP} and $r_{pP}^{(111)}$ in the forms presented below. Recall that these expressions are valid for the 2ω terms by simply capitalizing the relevant quantities as explained in Sec. [2.1](#). We summarize these scenarios in Table [2.3](#) for quick reference. The complete derivations for these different cases are included in Appendix [D](#).

2.3.1 The 3-layer model without multiple reflections

Using Eq. [\(2.70\)](#) in Eq. [\(2.52\)](#) with Eq. [\(2.50\)](#), we obtain

$$\Gamma_{pP} = \frac{T_p^{\ell v} T_p^{\ell b}}{N_\ell^2 N_b} \left(\frac{t_p^{v\ell} t_p^{\ell b}}{n_\ell^2 n_b} \right)^2, \tag{2.71} \quad \text{[eq:gamma11111]}$$

and

$$\begin{aligned} r_{pP}^{(111)} &= N_b^2 \sin \theta_0 \left(n_b^4 \sin^2 \theta_0 \chi^{zzz} + n_\ell^4 w_b^2 \chi^{zxx} \right) \\ &- N_\ell^2 n_\ell^2 w_b W_b \left(2n_b^2 \sin \theta_0 \chi^{xxz} + n_\ell^2 w_b \chi^{xxx} \cos(3\phi) \right). \end{aligned} \tag{2.72} \quad \text{[eq:rpp111nom]}$$

Now that we have neglected multiple SH reflections, we can use these two expressions for Γ_{pP} and r_{pP} to obtain the next four scenarios by using the choices described in each subsection below. Note that by neglecting the multiple reflections, the thickness d of layer ℓ disappears from the formulation, and the location of the nonlinear polarization sheet $\mathbf{P}(\mathbf{r}, t)$ (Eq. (2.3)) at d_2 (see Fig. 2.1) is immaterial.

2.3.2 The two layer, or Fresnel (2-layer-fresnel) model

Historically, this is the model most used in the literature. In Chap. 3, we will see how the 3-layer model, presented in the previous sections, offers a significant improvement over this model.

In the 2-layer-fresnel model, we consider that $\mathcal{P}(2\omega)$ is evaluated in the vacuum region, while the fundamental fields are evaluated in the bulk region [29, 26]. To do this, we evaluate the 2ω radiations factors in the vacuum by taking $\ell = v$, thus $\epsilon_\ell(2\omega) = 1$, $T_p^{\ell v} = 1$, and $T_p^{\ell b} = T_p^{vb}$. We also evaluate the fundamental field inside medium b by taking $\ell = b$, thus $\epsilon_\ell(\omega) = \epsilon_b(\omega)$, $t_p^{v\ell} = t_p^{vb}$, and $t_p^{\ell b} = 1$. With these choices, Eqs. (2.71) and (2.72) reduce to

$$\Gamma_{pP} = \frac{T_p^{vb}(t_p^{vb})^2}{n_b^2 N_b}, \quad (2.73) \quad [\text{eq:m78}]$$

and

$$r_{pP}^{(111)} = N_b^2 \sin \theta_0 \left(\sin^2 \theta_0 \chi^{zzz} + w_b^2 \chi^{zxx} \right) - w_b W_b \left(2 \sin \theta_0 \chi^{xxz} + w_b \chi^{xxx} \cos(3\phi) \right). \quad (2.74) \quad [\text{eq:m82}]$$

These expressions are in perfect agreement with Refs. [29] and [26].

2.3.3 The 2-layer-bulk model: evaluating $\mathcal{P}(2\omega)$ and $\mathbf{E}(\omega)$ in the bulk

We follow the same procedure as above considering that both the 2ω and 1ω terms will be evaluated in the bulk, by taking $\ell = b$. Thus, $\epsilon_\ell(2\omega) = \epsilon_b(2\omega)$, $T_p^{v\ell} = T_p^{vb}$, $T_p^{\ell b} = 1$, and $\epsilon_\ell(\omega) = \epsilon_b(\omega)$, $t_p^{v\ell} = t_p^{vb}$, and $t_p^{\ell b} = 1$. With these choices Eqs. (2.71) and (2.72) reduce to

$$\Gamma_{pP} = \frac{T_p^{vb}(t_p^{vb})^2}{n_b^2 N_b}, \quad (2.75)$$

and

$$r_{pP}^{(111)} = \sin^3 \theta_0 \chi^{zzz} + w_b^2 \sin \theta_0 \chi^{zxx} - 2w_b W_b \sin \theta_0 \chi^{xxz} - w_b^2 W_b \chi^{xxx} \cos 3\phi. \quad (2.76)$$

2.3.4 The 2-layer-vacuum model: evaluating $\mathcal{P}(2\omega)$ and $\mathbf{E}(\omega)$ in the vacuum

We consider both $\mathcal{P}(2\omega)$ and the fundamental fields to be evaluated in the vacuum. We take $\ell = v$, thus $\epsilon_\ell(2\omega) = 1$, $T_p^{\ell v} = 1$, $T_p^{\ell b} = T_p^{vb}$, and $\epsilon_\ell(\omega) = 1$, $t_p^{v\ell} = 1$, and $t_p^{\ell b} = t_p^{vb}$. With these choices Eqs. (2.71) and (2.72) reduce to

$$\Gamma_{pP} = \frac{T_p^{vb}(t_p^{vb})^2}{n_b^2 N_b}, \quad (2.77)$$

and

$$r_{pP}^{(111)} = n_b^4 N_b^2 \sin^3 \theta_0 \chi^{zzz} + N_b^2 w_b^2 \sin \theta_0 \chi^{zxx} - 2n_b^2 w_b W_b \sin \theta_0 \chi^{xxz} - w_b^2 W_b \chi^{xxx} \cos 3\phi. \quad (2.78)$$

2.3.5 The 3-layer-hybrid model: evaluating $\mathcal{P}(2\omega)$ in ℓ and $\mathbf{E}(\omega)$ in the bulk

Again, we follow the same procedure as above considering that 2ω terms are evaluated in the thin layer ℓ , and the 1ω terms will be evaluated in the bulk by taking $\ell = b$, thus $\epsilon_\ell(\omega) = \epsilon_b(\omega)$, $t_p^{v\ell} = t_p^{vb}$, and $t_p^{\ell b} = 1$. With these choices Eqs. (2.71) and (2.72)^{eq:gamma111pp11nomr} reduce to

$$\Gamma_{pP}^{\ell b} = \frac{T_p^{v\ell} T_p^{\ell b} (t_p^{vb})^2}{N_\ell^2 n_b^2 N_b}, \quad (2.79)$$

and

$$r_{pP}^{(111)} = N_b^2 \sin^3 \theta_0 \chi^{zzz} + N_b^2 k_b^2 \sin \theta_0 \chi^{zxx} - 2N_\ell^2 w_b W_b \sin \theta_0 \chi^{xxz} - N_\ell^2 w_b^2 W_b \chi^{xxx} \cos 3\phi. \quad (2.80)$$

2.4 About coding the SSHG yield

Github repository (<https://github.com/roguephysicist/SHGYield>)

```

1 ONEE = np.linspace(0.01, 10, 1000) # 1ω energy array
2
3 # The prefactor,  $\omega^2/2\epsilon_0c^3 \cos^2\theta_0$ 
4 PREFACCTOR = (ONEE**2)/(2*EPS0*HBAR**2 * LSPEED**3 * math.cos(THETA0)**2)
5
6 nl = np.sqrt(epsl1w) # The index of refraction,  $n_\ell = \sqrt{\epsilon_\ell(\omega)}$ 
7 Nl = np.sqrt(epsl2w) # The index of refraction,  $N_\ell = \sqrt{\epsilon_\ell(2\omega)}$ 
8
9 # The wave vectors,  $w_\ell = \sqrt{\epsilon_\ell(\omega) - \sin^2\theta_0}$ , etc.
10 wb1w = np.sqrt(epsb1w - (math.sin(THETA0)**2))
11 wb2w = np.sqrt(epsb2w - (math.sin(THETA0)**2))
12 wl1w = np.sqrt(epsl1w - (math.sin(THETA0)**2))
13 wl2w = np.sqrt(epsl2w - (math.sin(THETA0)**2))
14
15 # The Fresnel factors,  $r_s^{lb} = (w_\ell - w_b)/(w_\ell + w_b)$ , etc.
16 tvls = (2*math.cos(THETA0))/(math.cos(THETA0) + wl1w)
17 Tvlp = (2*math.cos(THETA0)*Nl)/(math.cos(THETA0)*epsl2w + wl2w)
18 rvl = (math.cos(THETA0) - wl1w)/(math.cos(THETA0) + wl1w)
19 rlbs = (wl1w - wb1w)/(wl1w + wb1w)
20 Rvlp = (math.cos(THETA0)*epsl2w - wl2w)/(math.cos(THETA0)*epsl2w + wl2w)
21 Rlbp = (wl2w*epsb2w - wb2w*epsl2w)/(wl2w*epsb2w + wb2w*epsl2w)
22
23 #  $\delta = 8\pi(d/\lambda_0)W_\ell$ ,  $\varphi = 4\pi(d/\lambda_0)w_\ell$ 
24 delta = 8*math.pi*((ONEE*THICKNESS*1e-9)/(PLANCK*LSPEED))*wl2w
25 varphi = 4*math.pi*((ONEE*THICKNESS*1e-9)/(PLANCK*LSPEED))*wl1w
26
27 #  $r_s^M = (r_s^{lb} e^{i\varphi})/(1 + r_s^{v\ell} r_s^{lb} e^{i\varphi})$ , etc.
28 rm = ((rlbs*np.exp(1j*varphi))/(1 + rvl*rlbs*np.exp(1j*varphi)))
29 RMpav = (Rlbp*np.exp(1j*delta/2)*(2/delta)*np.sin(delta/2))* \
30           (1 + Rvlp*Rlbp*np.exp(1j*delta))**-1
31 rMplus = 1 + rm
32 RMplusp = 1 + RMpav
33 RMminusp = 1 - RMpav
34
35 #  $\Gamma_{sP} = (T_p^{v\ell}/N_\ell) (t_s^{v\ell} r_s^{M+})^2$ 
36 GammasP = (Tvlp/Nl)*(tvls*rMplus)**2
37
38 #  $r_{sP} = -R_p^{M-} W_\ell \sin^2\phi \cos\phi \chi^{xxx} + R_p^{M-} W_\ell 2\sin\phi \cos^2\phi \chi^{xy} - \dots$ 
39 rsP = - (RMminusp*wl2w*math.sin(PHI)**2*math.cos(PHI) * XXX) \
40       + (RMminusp*wl2w*2*math.sin(PHI)*math.cos(PHI)**2 * XXY) \
41       - (RMminusp*wl2w*math.cos(PHI)**3 * XYY) \
42       - (RMminusp*wl2w*math.sin(PHI)**3 * YXX) \
43       + (RMminusp*wl2w*2*math.sin(PHI)**2*math.cos(PHI) * YYX) \
44       - (RMminusp*wl2w*math.sin(PHI)*math.cos(PHI)**2 * YYY) \
45       + (RMplusp*math.sin(THETA0)*math.sin(PHI)**2 * ZXX) \
46       - (RMplusp*math.sin(THETA0)*2*math.sin(PHI)*math.cos(PHI) * ZXY) \
47       + (RMplusp*math.sin(THETA0)*math.cos(PHI)**2 * ZYY)
48
49 #  $\mathcal{R}_{sP} = (\omega^2/2\epsilon_0c^3 \cos^2\theta_0) |n_\ell^{-1}\Gamma_{sP} r_{sP}|^2$ 
50 RsP = PREFACCTOR * np.absolute((1/nl) * GammasP * rsP)**2

```

Figure 2.3: A simplified example of using Python code to calculate \mathcal{R}_{sP} .

`fig:code-shg`

Chapter 3

Results

chap:results

Outline

3.1	Results for the Si(001)(2×1) surface	33
3.1.1	Calculating χ^{xxx}	34
3.1.1.1	Full-slab results	35
3.1.1.2	Half-slab vs full-slab	36
3.1.1.3	Half-slab results	38
3.1.2	Overview of the calculated \mathcal{R} spectra	39
3.2	Results for the Si(111)(1×1):H surface	40
3.2.1	Calculating χ^{xxx}	42
3.2.2	Comparing the theoretical \mathcal{R} to experiment	44
3.2.2.1	Overview of the calculated \mathcal{R} spectra	44
3.2.2.2	\mathcal{R}_{pP} (p -in, P -out)	45
3.2.2.3	Calculated \mathcal{R}_{pP} compared to experiment	48
3.2.2.4	Calculated \mathcal{R}_{sP} compared to experiment	51
3.2.2.5	Calculated \mathcal{R}_{pS} compared to experiment	52

In this chapter, we will review the results for the calculation of the nonlinear susceptibility, χ , and the SSHG yield, \mathcal{R}_{iF} , for the the Si(001)(2×1) and the Si(111)(1×1):H surfaces. These results are the direct product of all the theory derived in Chapters [chap:ch1](#) and [chap:ch2](#). These example surfaces provide the perfect testbed for the theory developed in this work, and the resulting spectra yield insight into the various key aspects of the theory.

The first part focuses on using the Si(001)(2×1) surface to review and compare the enhancements that we have added to the framework for calculating χ . This surface is presented in a special configuration that allows us to test each improvement made on the theory; namely, the use of the cut function for extracting the surface susceptibility, the effect of the scissors operator, and the addition of \mathcal{V}^{nl} . I will also present a very brief overview of the calculated SSHG yield, but with no comparison to experimental data as there is very little available for this surface.

The second part features the Si(111)(1×1):H, which is experimentally well-characterized, and thus provides an excellent platform with which to test our robust formulation for the SHG yield. We will first compare the calculated χ^{xxx} component with experimental data from Ref. [\[31\]](#). This will provide a nice confirmation of everything we learned from the Si(001)(2×1) surface. We will then review the calculated spectra for different polarization cases of the incoming fields, and compare them to experimental data from Refs. [\[32, 33, 34\]](#), over a wide energy range covering both the E₁ and E₂ critical point transitions for bulk Si. We will find that this new formalism, that is developed from the 3-layer model and includes the effect of multiple reflections in the material, compares quite favorably with the experimental data. The quality of these calculations affords us some insight into how the SHG spectrum can be affected by several physical factors.

3.1 Results for the Si(001)(2×1) surface

Si2x1results

In this section, let us review the characteristics of the Si(001)(2×1) surface we will be using for the subsequent calculations. This surface provides an excellent test case to check the consistency of our approach for calculating χ with the new elements described in Chap. [\[chap:chi\]](#). For this, I have selected a clean Si(001) surface with a 2×1 surface reconstruction. The slab for such a surface could be made centrosymmetric by creating the front and back surfaces with the same 2×1 reconstruction. However, this particular slab has the lower surface terminated with hydrogen, producing a terminated, “ideal” bulk Si surface. The H atoms [\[fig:2x1struc\]](#) saturate the dangling bonds of the bulk-like Si atoms at the surface, as seen in Fig. [\[3.1\]](#). Consider the z coordinate pointing out of the surface with the x coordinate along the crystallographic [011] direction, parallel to the dimers.

The self-consistent ground state and the Kohn-Sham states were calculated in the DFT-LDA framework using the plane-wave ABINIT code [\[35, 36\]](#), using Troullier-Martins pseudopotentials [\[37\]](#) that are fully separable nonlocal pseudopotentials in the Kleinman-Bylander form [\[9\]](#). The contribution of \mathbf{v}^{nl} and \mathcal{V}^{nl} to Eq. [\(1.82\)](#) was carried out using the DP code [\[38\]](#).

The surface was studied with the experimental lattice constant of 5.43 Å. Structural optimizations were also performed with the ABINIT code. The geometry optimization was carried out in slabs of 12 atomic layers, where the central four layers were fixed at the bulk positions. The structures were relaxed until the Cartesian force components were less than 5 meV/Å. The geometry optimization for the clean surface gives a dimer buckling of 0.721 Å, and a dimer length of 2.301 Å. For the dihydride surface, the obtained Si-H bond distance was 1.48 Å. These results are in good agreement with previous theoretical studies [\[39, 18\]](#). The vacuum size is equivalent to one quarter the size of the slab, avoiding the effects produced by possible wave-function tunneling from the contiguous surfaces of the full crystal formed by the repeated super-cell scheme [\[18\]](#).

Spin-orbit, local field, and electron-hole attraction [\[40\]](#) effects on the SHG process are all neglected. Although these are important factors in the optical response of a semiconductor, their efficient calculation is still theoretically and numerically challenging and under debate. This merits further study but is beyond the scope of this thesis. For a given slab size, I found the converged spectra to obtain the relevant parameters. The most important of these are: an energy cutoff of 10 Ha for the 16, 24, and 32 layered slabs and 13 Ha for the 40 layer slab, an equal number of conduction and valence bands, and a set of 244 \mathbf{k} points in the irreducible Brillouin zone, which are equivalent to 1058 \mathbf{k} points when disregarding symmetry relations. The \mathbf{k} points are used for the linear analytic tetrahedron method for evaluating the 3D Brillouin Zone (BZ) integrals, where special care was taken to examine the double resonances of Eq. [\(1.82\)](#) [\[41\]](#). Note that the Brillouin

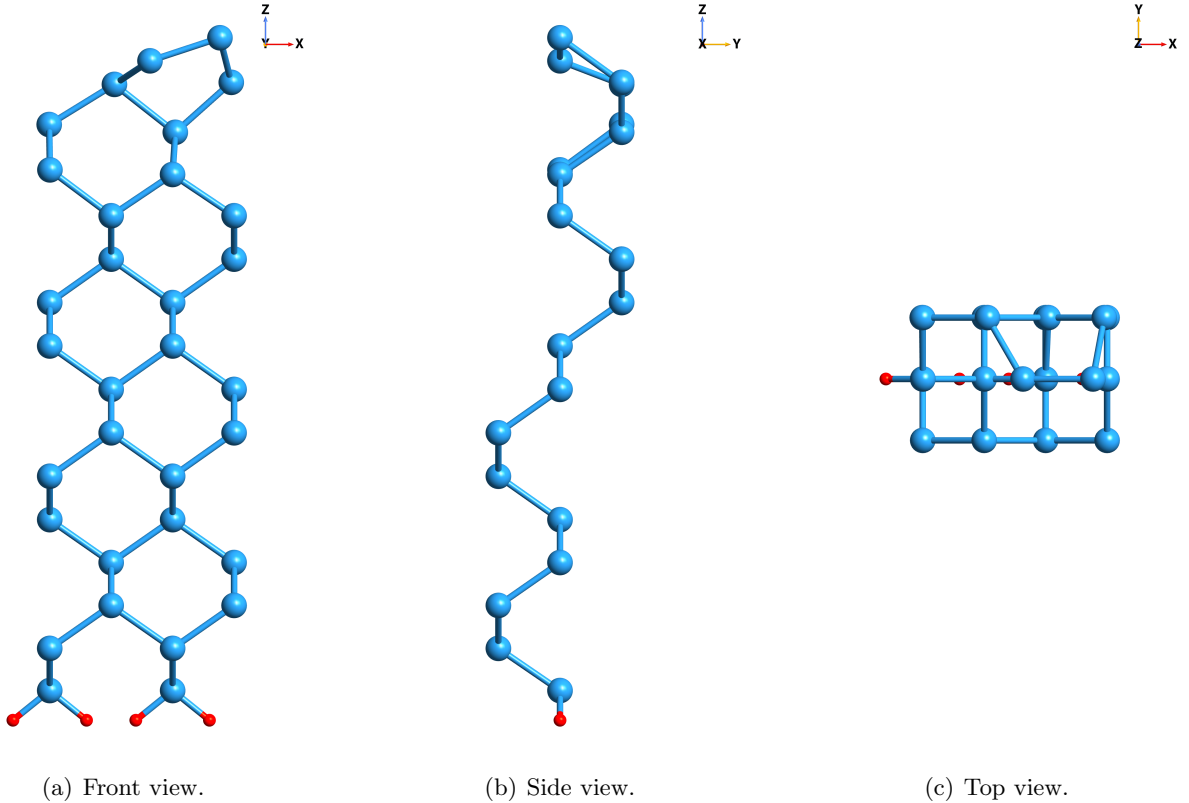


Figure 3.1: Several views of the slab used to represent the Si(001)(2×1) surface. This particular slab has 16 Si atomic layers (large blue balls) with two H atomic layers (small red balls).

`fig:2x1struct`

zone for the slab geometry collapses to a 2D-zone, with only one \mathbf{k} -point along the z -axis.
 $T_{nm}^{ab} = (i/\hbar)[r_{\text{eq:chi}}^b v_{nl,a}^{nl}]_{nm}$ must be evaluated in order to obtain Eqs. (I.84) and (I.85) that are required for Eq. (I.82). Computing second-order derivatives is necessary, making the numerical procedure very time consuming. This adds significantly to the already lengthy time needed for the calculation of the \mathbf{v}^{nl} contribution that is proportional only to the first-order derivatives. Memory requirements are also greatly increased for both \mathbf{v}^{nl} and $[\mathbf{r}, \mathbf{v}^{nl}]$. However, the contribution from $[\mathbf{r}, \mathbf{v}^{nl}]$ is very small [21] and it is therefore neglected in this work.

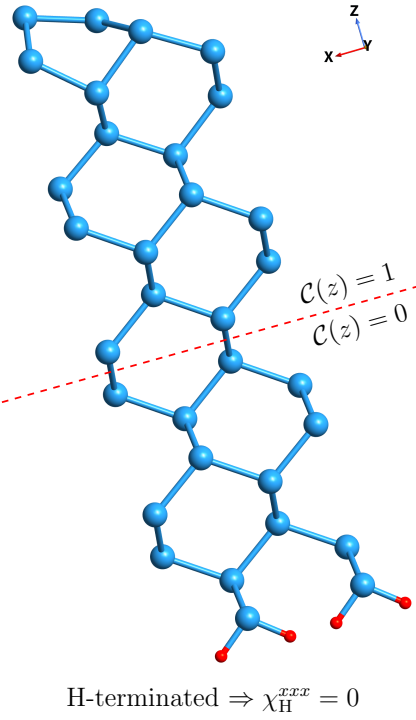
3.1.1 Calculating χ^{xxx}

The idea behind the special slab configuration, pictured in Fig. 3.2, is that the crystalline symmetry of the H terminated surface imposes that $\chi_H^{xxx} = 0$. The 2×1 surface has no such restrictions, so naturally $\chi_{2\times 1}^{xxx} \neq 0$. This is due to the fact that along the y direction there is a mirror plane for the H-saturated surface (causing centrosymmetry), whereas for the 2×1 surface this mirror is lost as the dimers are asymmetric along x . Thus, calculating χ^{xxx} for the full-slab, or the upper half-slab containing the 2×1 surface ^{Note1} [42] should yield the same result, since the contribution from the H saturated surface is zero regardless. The following relationship must be satisfied for this particular

`ec:res2x1chi`

`fig:si2x1slab`

2×1 reconstruction $\Rightarrow \chi_{2\times 1}^{xxx} \neq 0$



H-terminated $\Rightarrow \chi_H^{xxx} = 0$

Figure 3.2: The slab for the Si(001)(2×1) surface. The front (upper) surface is in a 2×1 , clean reconstruction, and the rear (lower) surfaces is H-terminated, with “ideal” bulk-like atomic positions. The dangling bonds are H-saturated.

`fig:si2x1slab`

slab,

$$\chi_{\text{half-slab}}^{xxx} = \chi_{\text{full-slab}}^{xxx},$$

where $\chi_{\text{half-slab}}^{xxx}$ is calculated using $\mathcal{C}(z) = 1$ for the upper half containing the 2×1 surface reconstruction (see Fig. 5.2), and $\chi_{\text{full-slab}}^{xxx}$ is calculated using $\mathcal{C}(z) = 1$ for the entire slab. Again, the dihydride surface on the lower half of the slab must have $\chi_{\text{half-slab}}^{xxx} = 0$.

Note that all spectra for χ^{xxx} presented in this section were calculated with a Gaussian broadening of 0.15 eV.

3.1.1.1 Full-slab results

Fig. 3.3 shows $|\chi_{\text{full-slab}}^{xxx}|$ for the slab with 16, 24, 32, and 40 Si atomic layers, without the contribution of \mathbf{v}^{nl} , and with no scissors correction. Since the clean Si(001) surface is in a 2×1 reconstruction there are two atoms per atomic layer. Thus, the total number of atoms per slab is twice the number of atomic layers of the slab. The slabs were extended in the z directions in steps of 8 layers of bulk-like atomic positions. Note that the response differs substantially for 16 and 24 layers but is quite similar for 32 and 40 layers. As explained above, the calculation of the \mathbf{v}^{nl} contribution is computationally expensive, so it is crucial to minimize the number of atoms in the calculation. I consider a slab with 32 Si atomic layers as a good compromise between the

`sec:fsresults`

`fig:layersconv`

convergence of $\chi_{\text{full-slab}}^{xxx}$ as a function of the number of layers in the slab, and the computational expense.

3.1.1.2 Half-slab vs full-slab

Now that we have established an adequate number of layers to attain convergence, we can proceed to study the spectra produced from the slab with 32 atomic layers. Fig. 3.4 presents a comparison between $\chi_{\text{half-slab}}^{xxx}$ and $\chi_{\text{full-slab}}^{xxx}$ for four different scenarios: with and without the effects of \mathbf{v}^{nl} , and with two values for the scissors correction, $\hbar\Delta$. I have chosen a scissors value of $\hbar\Delta = 0.5$ eV, that is the GW gap reported in Refs. [43, 44]. This is justified by the fact that the surface states from the clean 2×1 surface are rigidly shifted and maintain their dispersion relation with respect to the LDA value, according to the GW calculations of Ref. [43].

We can appreciate that the difference between the half-slab and full-slab responses is quite small for all four scenarios. Indeed, when the value $|\chi^{xxx}|$ is large, the difference between the two is quite small; when $|\chi^{xxx}|$ is small, the difference increases slightly but the spectra is so close to zero that it is negligible. Of course, the difference between the two would decrease as the number of atomic layers increases. Note how 32 layers in the slab is more than enough to confirm that the extraction of the surface second-harmonic susceptibility from the 2×1 surface is readily possible using the formalism contained in Eq. (I.82). Calculating the response from the lower half of the slab substantiates that $|\chi_{\text{half-slab}}^{xxx}| \approx 0$ for the dihydride surface (not shown).

This confirms the validity of the theory developed in I and is an important result of this work. Through the proposed layer formalism, we can calculate the surface χ^{abc} component including the contribution from the nonlocal part of the pseudopotentials, and part of the many-body effects through the scissors correction. Therefore, this scheme is robust and versatile and should work for any crystalline surface.

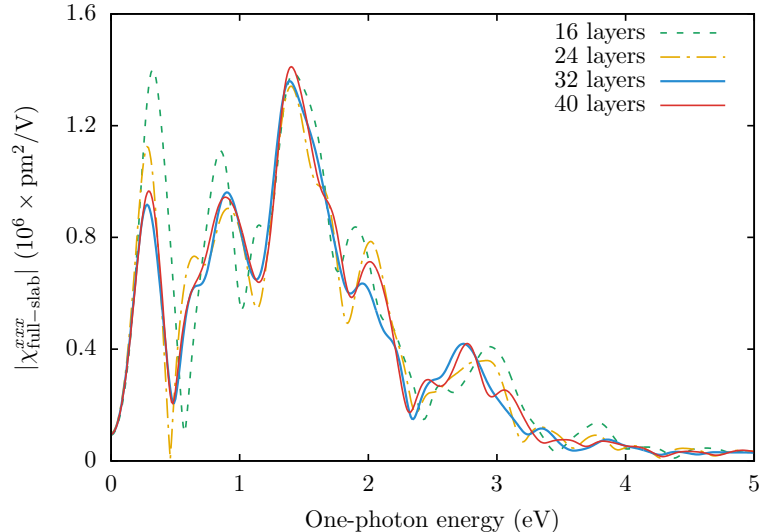


Figure 3.3: $|\chi_{\text{full-slab}}^{xxx}|$ vs $\hbar\omega$ for the slab with 16, 24, 32, and 40 atomic Si layers. Adequate convergence is achieved after 32 layers. The spectra presented here do not include the contribution from \mathbf{v}^{nl} , with a scissors value of $\hbar\Delta = 0$ eV.

`fig:layersco`

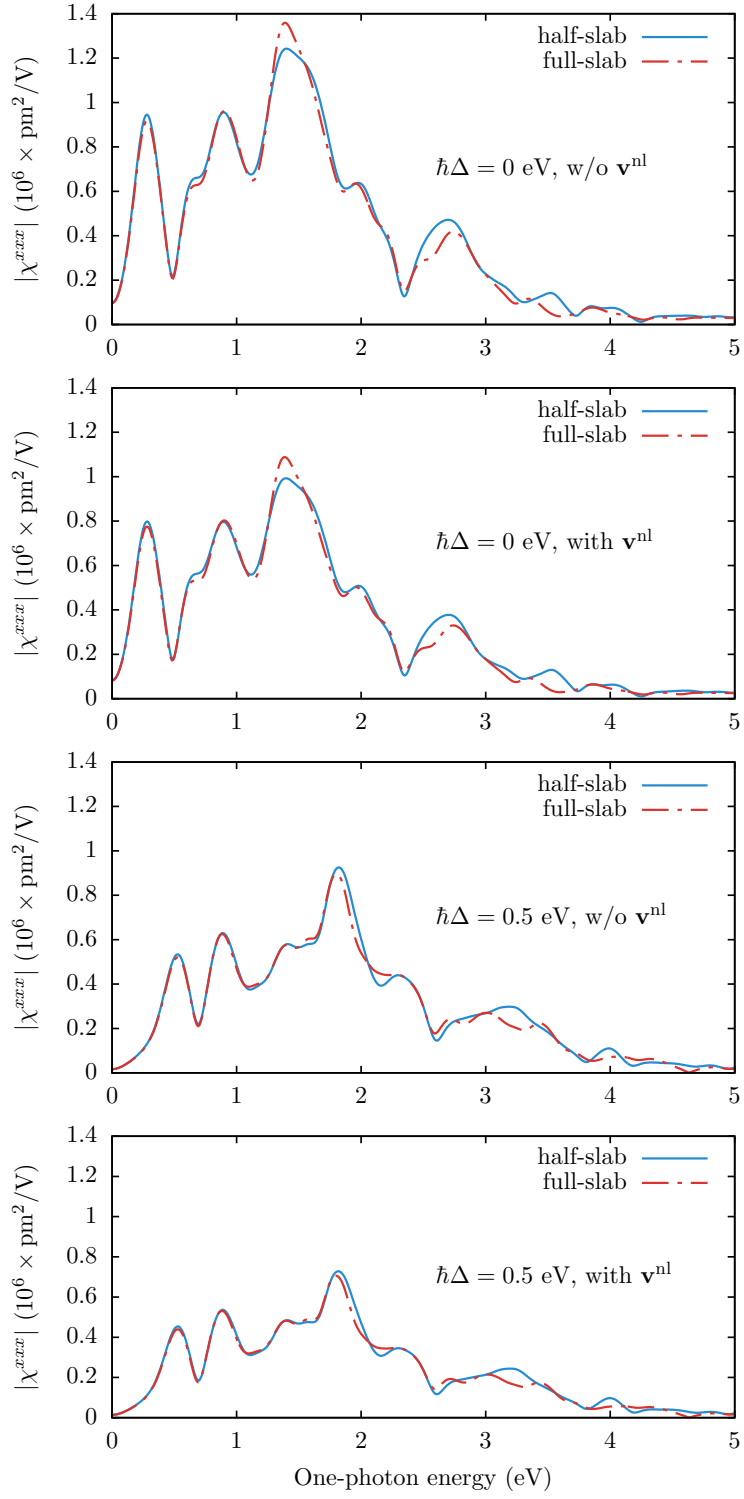


Figure 3.4: $\chi_{\text{half-slab}}^{xxx}$ and $\chi_{\text{full-slab}}^{xxx}$ vs $\hbar\omega$ for four different combinations: with and without the effects of \mathbf{v}^{nl} , and with two values for the scissors correction, $\hbar\Delta$.

`fig:hsvfs`

3.1.1.3 Half-slab results

I proceed to explain some of the features seen in $|\chi_{\text{half-slab}}^{xxx}|$ that is obtained when setting $\mathcal{C}(z) \equiv 1$ for the upper half containing the 2×1 surface reconstruction, as seen in Fig. 3.2. From Fig. 3.4, we note a series of resonances that derive from the 1ω and 2ω terms in Eq. (1.82). Notice that the 2ω resonances start below $E_g/2$, where E_g is the band gap (0.53 eV for LDA, and 1.03 eV if the scissor is used with $\hbar\Delta = 0.5$ eV). These resonances come from the electronic states of the 2×1 surface, that lie inside the bulk band gap of Si and are the well known electronic surface states [43].

Fig. 3.5 shows that the inclusion of \mathbf{v}^{nl} reduces the value of $|\chi_{\text{half-slab}}^{xxx}|$ by 15-20%. This demonstrates the importance of this contribution for a fully correct SHHG calculation. This is in agreement with the analysis for bulk semiconductors [45]. However, the inclusion of \mathbf{v}^{nl} does not change the spectral shape of $|\chi_{\text{half-slab}}^{xxx}|$. We can confirm that this is not unique for this specific scissors shift, as we can appreciate from the upper two panels of Fig. 3.4, with $\hbar\Delta = 0$ eV.

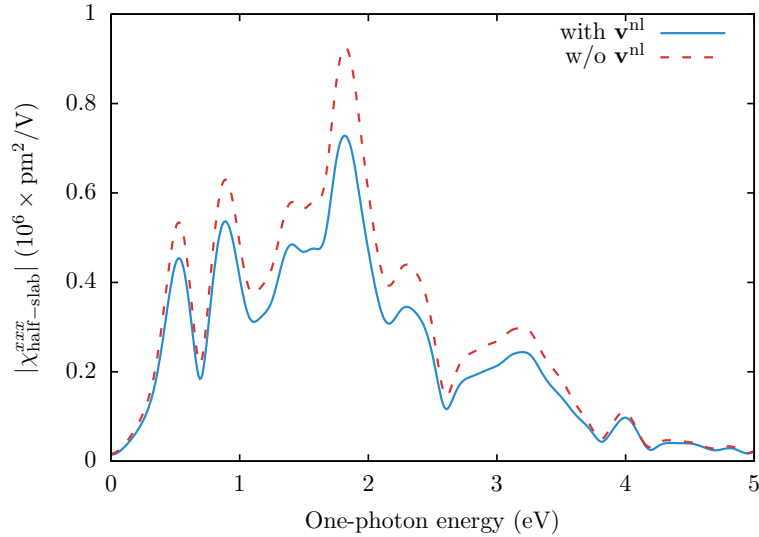


Figure 3.5: $|\chi_{\text{half-slab}}^{xxx}|$ vs $\hbar\omega$, with and without the contribution from \mathbf{v}^{nl} . This spectrum has a scissors value of $\hbar\Delta = 0.5$ eV.

To demonstrate the effect of the scissors correction, I considered two different finite values for $\hbar\Delta$. The first, with a value of $\hbar\Delta = 0.5$ eV that is used in the previous results, is the “average” GW gap taken from Ref. [43] that is in agreement with Ref. [44]. The second, with a value of $\hbar\Delta = 0.63$ eV is the “average” gap taken from Ref. [46], where more \mathbf{k} points in the Brillouin zone were used to calculate the GW value. Fig. 3.6 shows that the scissors correction shifts the spectra from its LDA value to higher energies, as expected. However, contrary to the case of linear optics [47], the shift introduced by the scissors correction is not rigid, which is consistent with the work of Ref. [41]. This is because the second-harmonic optical response mixes 1ω and 2ω transitions (see Eq. (1.82)), and accounts for the non-rigid shift. The reduction of the spectral strength is in agreement with previous calculations for bulk systems [41, 48, 49].

When comparing $|\chi_{\text{half-slab}}^{xxx}|$ for the two finite values of $\hbar\Delta$, it is clear that the first two peaks are almost rigidly shifted with a small difference in height while the rest of the peaks are modified substantially. This behavior comes from the fact that the first two peaks are almost exclusively

related to the 2ω resonances of Eq. (I.82).^{eq:chis} The other peaks are a combination of 1ω and 2ω resonances and yield a more varied spectrum. Note that for large-gap materials the 1ω and 2ω resonances would be split, producing a small interference effect. The 2ω resonances would still strongly depend on the surface states. Thus, small changes in the scissors shift can affect the SSH susceptibility spectrum quite dramatically. In Ref. [50], the authors already noted that the nonlinear optical response of bulk materials is more influenced by the electronic structure of the material than the linear case. For the case of semiconductor surfaces, the problem is even more intricate due to the presence of electronic surface states.

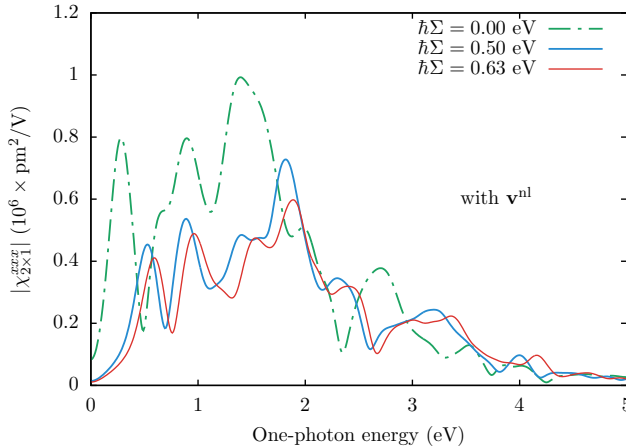


Figure 3.6: $\chi_{\text{half-slab}}^{xxx}$ vs $\hbar\omega$ for a slab with 32 atomic Si layers plus one H layer,

fig:scissors

for three different values of the scissors correction, $\hbar\Delta$.

The high sensitivity of SSHG to the energy position of surface states, as seen in Fig. 3.6,^{fig:scissors} makes SSHG a good benchmark tool for spectroscopically testing the validity of the inclusion of many-body effects, and in particular the quasi-particle correction to the electronic states. Although local fields are neglected, in principle they should be quite small parallel to the interface as the electric field is continuous. χ^{xxx} should have a relatively small influence from these local fields. Excitonic effects should also be explored, but their efficient calculation is theoretically and numerically challenging beyond [40] and far beyond the scope of this work. Unfortunately the experimental measurement of the χ^{xxx} component is difficult as the SH radiated intensity would be proportional not only to this component but also to the other components of χ . However, I will present this exact comparison later on in Sec. 3.2.1 for the Si(111)(1×1):H surface.^{sec:res1x1chi}

3.1.2 Overview of the calculated \mathcal{R} spectra

In Figs. 3.7 and 3.8,^{fig:2x1rP8fig:2x1rS3d} I present the results for the calculation of the SSHG yield for our test surface. The 2×1 surface reconstruction yields a Class 1, primitive triclinic system with all 18 components independent from each other.^{popovbook} We cannot take advantage of any symmetry relations for this surface. However, this is no problem for the robust formulation we derived in Chapter 2 that can accommodate all 18 components disregarding any surface symmetries. Calculating all 18 components is obviously more time consuming, but they can be efficiently parallelized so very little time is actually lost.^{chap:sshgyield}

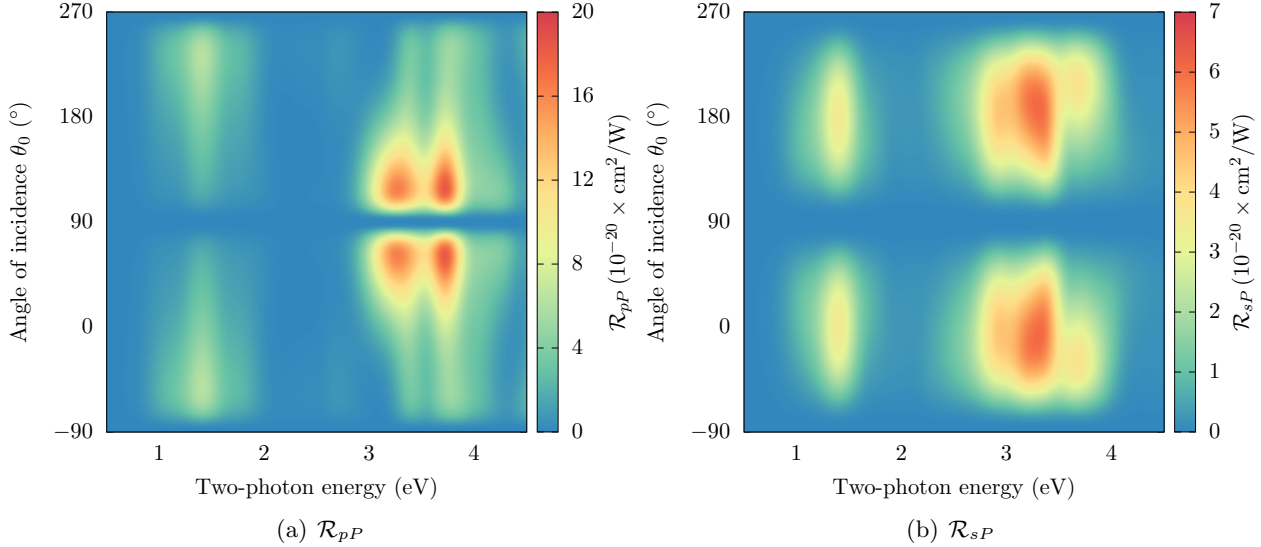


Figure 3.7: \mathcal{R} for outgoing P polarization, versus the angle of incidence (θ_0) for the Si(001)(2×1) surface. The scissor shift used was $\hbar\Delta = 0.5$ eV. Both figures consider an azimuthal angle of $\phi = 45^\circ$. All curves are broadened with $\sigma = 0.10$ eV.

`fig:2x1rP3d`

Fig. 3.7 presents the results for the SSHG yield with outgoing P polarization. I set a fixed azimuthal angle of $\phi = 45^\circ$ and then varied the incoming angle θ_0 from -90° to 270° . We can clearly see that the surface states associated with the 2×1 reconstruction produce significant intensity between 1-2 eV in the two-photon energy range. This is consistent with the findings presented in the previous section and in Ref. [\[51\]](#). The intensity of the peak related to the surface states is significantly lower than the peaks produced in the 2.5-4 eV two-photon energy range. Overall peak intensity is quite high for this surface, which is consistent as it is highly non-centrosymmetric. The spectrum for \mathcal{R}_{pP} is very consistent with other calculations of this type [\[52\]](#), and even with some limited experimental data [\[53\]](#).

Fig. 3.8 presents the results for the SSHG yield with outgoing S polarization. They are quite similar to what we observed in Fig. 3.7, with a peak related to the surface states between 1-2 eV, and a larger set of peaks between 2.4-4 eV in the two-photon energy range. These spectra have a clear maxima around $\theta_0 = 0^\circ$ and $\theta_0 = 180^\circ$.

These plots are presented for mainly illustrative purposes, as there is little experimental data to compare with the theoretical spectrum. However, these kinds of plots will be quite useful to the experimentalist interested in this kind of spectroscopy. Excellent intensity for all polarization cases can be obtained for small beam angles, such as $\theta_0 = 30^\circ$.

3.2 Results for the Si(111)(1×1):H surface

`Si1x1results`

We will now focus our attention on the Si(111)(1×1):H surface. This surface is a C_{3v} , primitive hexagonal system with only 4 nonzero components independent from each other, as shown in Table 2.2 [\[30, 29, 26\]](#). It is composed of stacked layers with one Si atom each, with one H atom

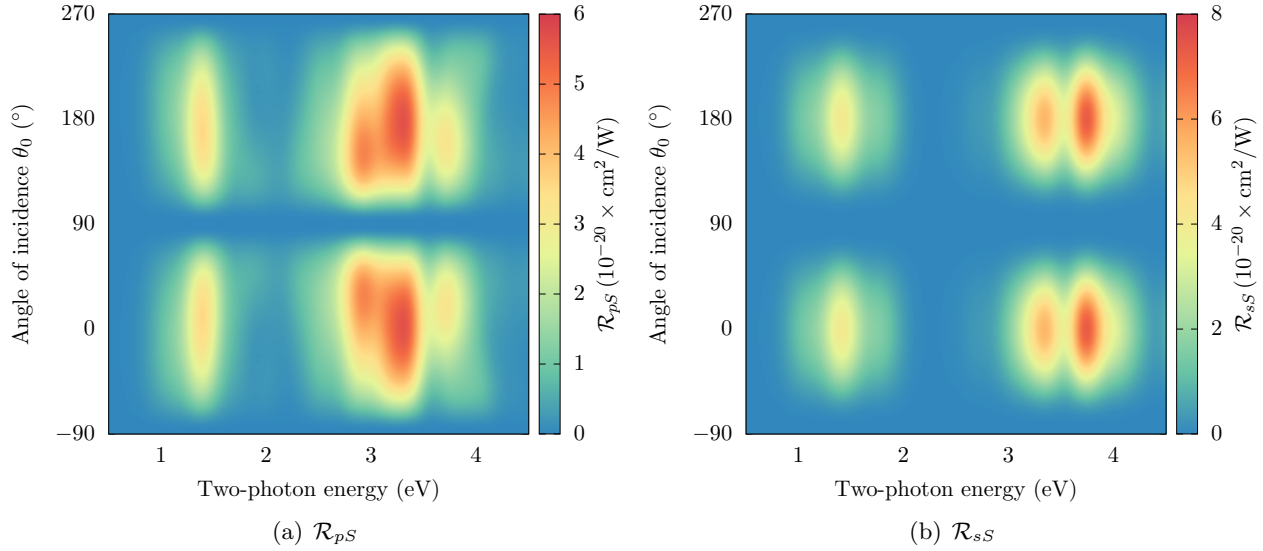


Figure 3.8: \mathcal{R} for outgoing S polarized fields, versus the angle of incidence (θ_0) for the Si(001)(2×1) surface. The scissor shift used was $\hbar\Delta = 0.5$ eV. Both figures consider an azimuthal angle of $\phi = 45^\circ$. All curves are broadened with $\sigma = 0.10$ eV.

`fig:2x1rS3d`

terminating each surface. The added H saturates the surface Si dangling bonds and eliminates any surface-related electronic states in the band gap. Here, the top and bottom surfaces are mirror images (see Fig. 3.9); this provides the centrosymmetry that necessitates the use of the cut function to extract the nonzero surface response. In Sec. 3.2.1 we will compare the spectrum produced by using relaxed and unrelaxed coordinates, so it is worth reviewing this concept here. The specifics of this process are as follows.

The relaxation process was done by my colleague, Nicolas Tancogne-Dejean [\[52\]](#). The structure was initially constructed with the experimental lattice constant of 5.43 Å, and then performed structural optimizations with the ABINIT [\[35, 36\]](#) code. It was then relaxed until the Cartesian force components were less than 5 meV/Å, yielding a final Si-H bond distance of 1.50 Å. The energy cutoff used was 20 Ha, and Troullier-Martin LDA pseudopotentials were used [\[37\]](#). The resulting atomic positions are in good agreement with previous theoretical studies [\[54, 55, 56, 57, 33\]](#), as well as the experimental value for the Si-H distance [\[58\]](#).

I also evaluated the number of layers required for convergence (like Sec. 3.1.1.1) and settled on a slab with 48 atomic Si planes. The geometric optimizations mentioned above are therefore carried out on slabs of 48 atomic layers without fixing any atoms to the bulk positions. Fig. 3.9 depicts a sample slab with 16 layers of Si. The surface susceptibilities must be extracted from only half of the slab. This encompasses 24 layers of Si and the single layer of H that terminates the top surface. The vacuum size is equivalent to one quarter the size of the slab, avoiding the effects produced by possible wave-function tunneling from the contiguous surfaces of the full crystal formed by the repeated super-cell scheme [\[18\]](#).

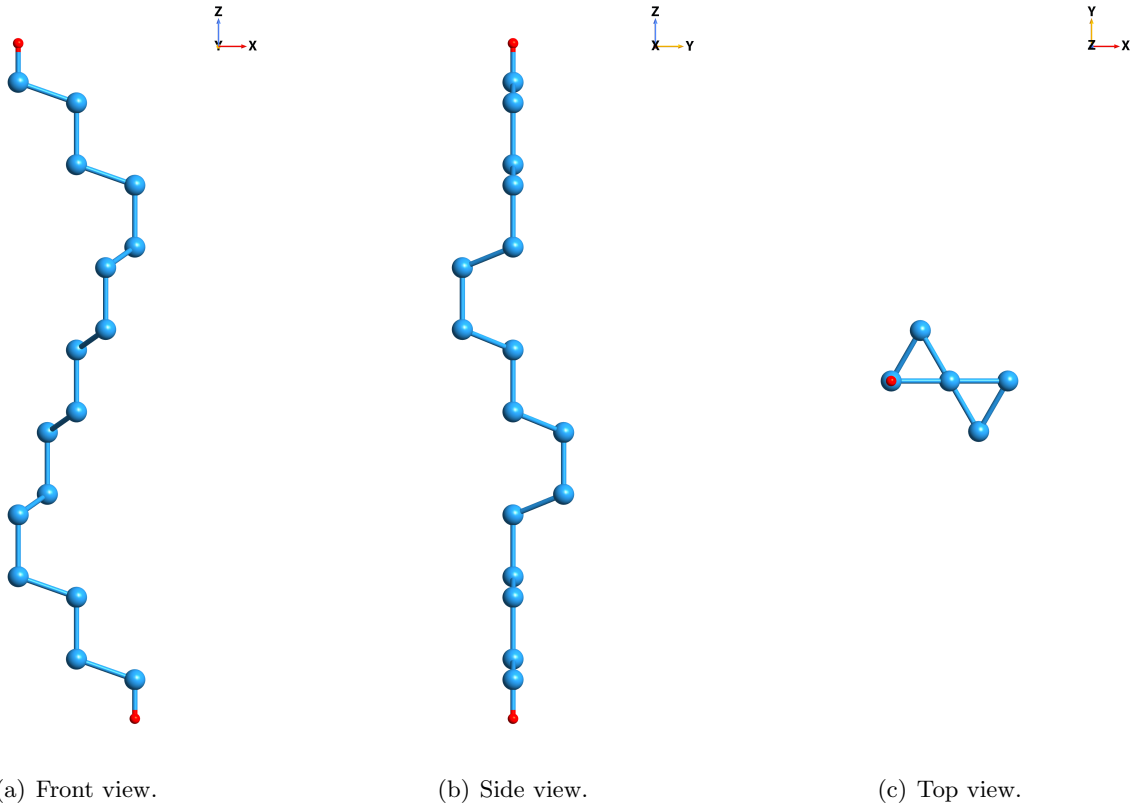


Figure 3.9: Several views of the slab used to represent the Si(111)(1×1):H surface. This particular slab has 16 Si atomic layers (large blue balls) with two H atomic layers (small red balls).

fig:1x1struc

The electronic wave-functions, $\psi_{n\mathbf{k}}(\mathbf{r})$, were also calculated with the ABINIT code using a planewave basis set with an energy cutoff of 15 Hartrees. χ^{abc} was properly converged with 576 \mathbf{k} points in the irreducible Brillouin zone, which are equivalent to 1250 \mathbf{k} points when disregarding symmetry relations. The contribution of \mathcal{V}^{nl} in Eq. (I.82) was carried out using the DP³⁸ code with a basis set of 3000 planewaves. Convergence for the number of bands was achieved at 200, which includes 97 occupied bands and 103 unoccupied bands.

All spectra were produced using a scissors value of 0.7 eV in the χ^{abc} and $\epsilon_\ell(\omega)$ calculations. This value was obtained from Ref. [59], in which the authors carry out a G_0W_0 calculation on this surface for increasing numbers of layers. They calculated the LDA and G_0W_0 band gaps, and found that the difference between the two tends towards ~ 0.7 eV as more layers are added, culminating in a value of 0.68 eV for bulk Si. This calculation is completely *ab-initio*, so I consider 0.7 eV to be a very reasonable value for the scissors correction.

3.2.1 Calculating χ^{xxx}

The pioneering work presented in Ref. [33] showed the effect of artificially moving the atomic position on the resulting SSHG spectra. In this section, I will address the more practical and relevant case of atomic relaxation. More precisely, I compare the fully relaxed structure described

above with an unrelaxed structure where all the Si atoms are at the ideal bulk positions. Note that in both cases, the Si-H bond distance is the same 1.5 Å. The unrelaxed coordinates use the same parameters mentioned above. Fortunately, there exists experimental data that can be compared to the calculated χ^{xxx} for this surface, taken from Ref. [31]. This data provides an excellent point of comparison as it was presented in absolute units and was measured at a very low temperature of 80 K.

[fig:XXXX](#)
 Fig. 3.10 depicts the spectra from the relaxed and unrelaxed coordinates compared to experiment. The theoretical curves were calculated with a scissors shift of $\hbar\Delta = 0.7$ eV, as mentioned in the previous section. The relaxed coordinates have a peak position that is very slightly blueshifted with respect to the experimental peak near 1.7 eV. In contrast, the unrelaxed coordinates have a peak that is redshifted close to 0.05 eV from experiment. There is also a feature between 1.5 eV and 1.6 eV that appears in the relaxed spectrum that coincides partially with the experimental data. Both theoretical curves have half the intensity of the experimental peak. It is important to note that this data was taken at low temperature (80 K); this further favors the comparison, as the theory neglects the effects of temperature. As is shown in Ref. [31], the peaks in the spectrum redshift as the temperature increases. Intensity for both the relaxed and unrelaxed curves are roughly half the intensity of the experimental spectrum. I have converted the units of the experimental data from CGS to MKS units for easier comparison.

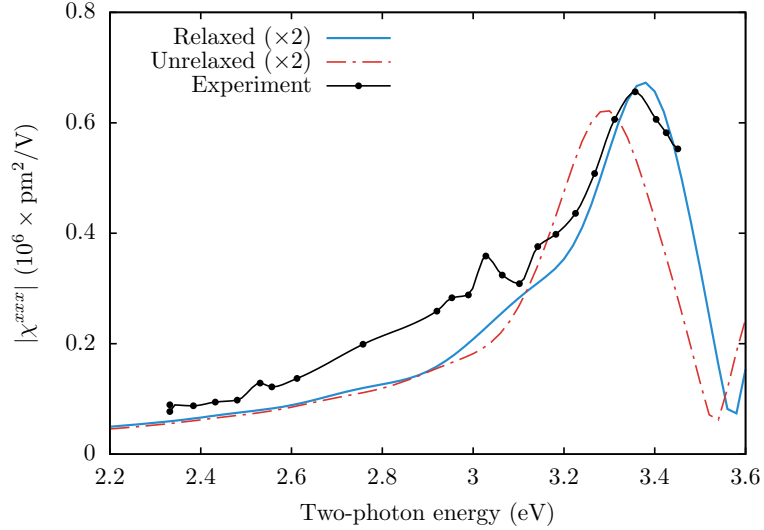


Figure 3.10: Comparison of χ^{xxx} calculated using relaxed and unrelaxed atomic positions, with the experimental data presented in Ref. [31]. The theoretical curves were calculated with a scissors shift of $\hbar\Delta = 0.7$ eV, and are broadened with $\sigma = 0.075$ eV. Experimental data was taken at 80 K.

[fig:XXXX](#)

We can conclude that the most accurate theoretical results are produced by using relaxed atomic positions for the calculation of χ . Although this process can be very time consuming for large numbers of atoms, this should be considered a crucial step. This also further demonstrates that SSHG is very sensitive to the surface atomic positions. In particular, these results show that a correct value of the Si-H bond length is not enough to obtain the most accurate SSHG spectra, and that a full relaxation of the structure is required. Additionally, it seems that the theory may

coincide better with experiments that are conducted under very low temperature conditions.

3.2.2 Comparing the theoretical \mathcal{R} to experiment

All calculations presented from this point on were done using the relaxed atomic positions described in the previous section. I will now present the theoretical SSHG yield for the Si(111)(1×1):H surface compared to experiments from Refs. [34, 33, 32]. These comparisons are good benchmarks to test the complete formalism for calculating the SSHG yield.

The method of calculation is as follows. I first calculated $\varepsilon_b(\omega)$, $\varepsilon_f(\omega)$, and then χ^{abc} from Eq. (1.82). I used these for the Fresnel factors and in Eqs. (2.52), (2.62), and (2.57), and finally, those into Eq. (2.44) to obtain the theoretical SSHG yield for different polarizations that can then be compared with the experimental data. Remember that a scissors shift of $\hbar\Delta = 0.7$ eV is used for all the χ^{abc} components. These were also broadened with a Gaussian broadening of $\sigma = 0.05$ eV, while the calculated \mathcal{R} spectra feature a broadening of $\sigma = 0.10$ eV. These values were selected so that the theoretical calculation best represents the lineshape of the experimental spectrum.

3.2.2.1 Overview of the calculated \mathcal{R} spectra

We will carefully review and compare the calculated \mathcal{R} for each different polarization case in the following sections. However, I first want to present a general overview of the theoretical SSHG yield, as I did in Sec. 3.1.2. In Figs. 3.11 and 3.12, I present these results over a two-photon energy range of 2.5–5 eV. This range corresponds to the experimental measurements featured in Refs. [33] and [32]. Note that the SSHG yield drops to zero very rapidly before for energy values under 3 eV. This is because of the lack of surface states due to the surface H-saturation.

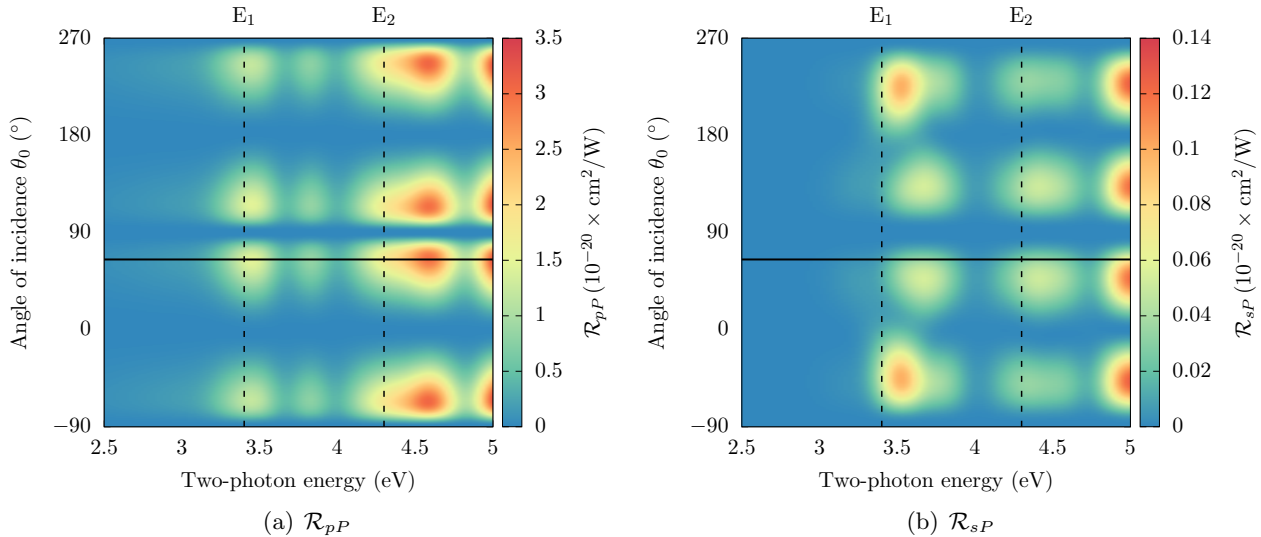


Figure 3.11: \mathcal{R} for outgoing P polarization, versus the angle of incidence (θ_0) for the Si(111)(1×1):H surface. A scissors shift of $\hbar\Delta = 0.7$ eV is applied. The solid line represents $\theta_0 = 65^\circ$, and the dotted lines represent the E_1 and E_2 Si critical points. Both figures consider an azimuthal angle of $\phi = 30^\circ$. All curves are broadened with $\sigma = 0.10$ eV.

fig:1x1rP3d

I have included some helpful markers in these figures. First, the solid black line represents an angle incidence of $\theta_0 = 65^\circ$. This is one of two angles that we will consider for the remainder of this chapter; in particular, this is the angle used in the experiment from Ref. Refs. [33]. It is clear that they chose this particular angle to maximize the \mathcal{R}_{pP} output. Second, the dashed black lines represent the $E_1 \sim 3.4$ eV and $E_2 \sim 4.3$ eV critical points of bulk Si [60]. For the outgoing P polarization in Fig. 3.11, we can see that the calculated SSHG yield does have peaks around those energy values. We will review this in much further detail below.

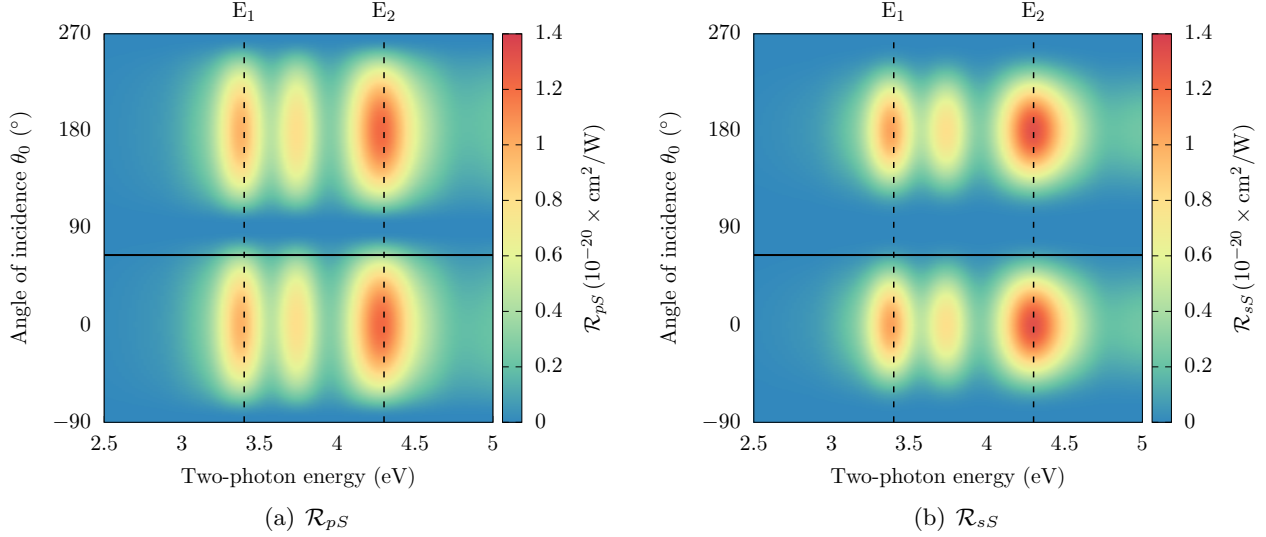


Figure 3.12: \mathcal{R} for outgoing S polarized fields, versus the angle of incidence (θ_0) for the Si(111)(1×1):H surface. A scissors shift of $\hbar\Delta = 0.7$ eV is applied. The solid line represents $\theta_0 = 65^\circ$, and the dotted lines represent the E_1 and E_2 Si critical points. Both figures consider an azimuthal angle of $\phi = 30^\circ$. All curves are broadened with $\sigma = 0.10$ eV.

fig:1x1rS3d

We see similar characteristics, for Fig. 3.12 with the outgoing S polarization cases. Indeed, the theoretical peak values seem to match quite well with the critical points. Again, we will review these findings in much more detail below. Note that I will omit \mathcal{R}_{ss} from this point forward, as I do not have any experimental data to compare it with.

3.2.2.2 \mathcal{R}_{pP} (p -in, P -out)

HERE HERE HERE HERE HERE

I think the first order of business is to review how the inclusion of multiple reflections affects the I think we should first review how the inclusion of multiple reflections affects the produced spectra.

We consider a Si(111)(1×1):H surface as a test case for the three layer model and to study the effects that multiple reflections have on the SSHG radiation. This surface is well characterized experimentally,[34, 33, 32] and there has been success in reproducing these experimental results using the three layer model without multiple reflections.[61] The details of the *ab initio* calculation of χ^{ijk} are not needed for the following discussion, and are left for the reader in Ref. [61]. However, we

mention that we apply a scissors shift of 0.7 eV to the theoretical spectra. In a first approximation, this includes the effects of the electronic many-body interactions within the independent particle approach for the *ab initio* calculation. This 0.7 eV value allows the SH resonant peaks to acquire their corresponding energy positions, and is calculated with what is known as a G_0W_0 calculation [61]. We are interested in finding the thickness of the layer ℓ where $\chi^{ijk} \neq 0$. For this surface, we found well-converged results for a thickness of ~ 5 nm, that is equivalent to 24 atomic sheets of Si along the (111) direction. As this represents only the upper half of the slab, we find it reasonable to choose the thickness of the layer ℓ to be between $d \sim 5 - 10$ nm. This corresponds to a half-slab comprised of 24 to 48 atomic layers to get well-converged values of χ^{ijk} .

We begin our comparisons in Fig. 3.13, in which we compare the theoretical results for the SHG radiation with the experimental results from Ref. [33]. The theoretical curves that include multiple reflections are featured with the ^{meijaPRB02} average value \bar{R}_i^M , Eq. (2.26), with two values for the total thickness, d , and Eqs. (2.50) and (2.52). We contrast these with the standard three layer model excluding the effects of multiple reflections from Sec. 2.3.1. We see that the E_2 peak is blueshifted by around 0.3 eV, and the yield does not go to zero after 4.75 eV. \mathcal{R}_{pP} is by far the most involved calculation out of the four different polarization cases, since it includes all four nonzero components. In particular, χ^{zzz} and χ^{xxz} include out-of-plane incoming fields. These are affected by local field effects that can change both intensity and peak position. [52] Including these effects is computationally very expensive and is beyond the scope of this paper. We speculate that \mathcal{R}_{pP} requires the proper inclusion of these effects in order to accurately describe the experimental peaks.

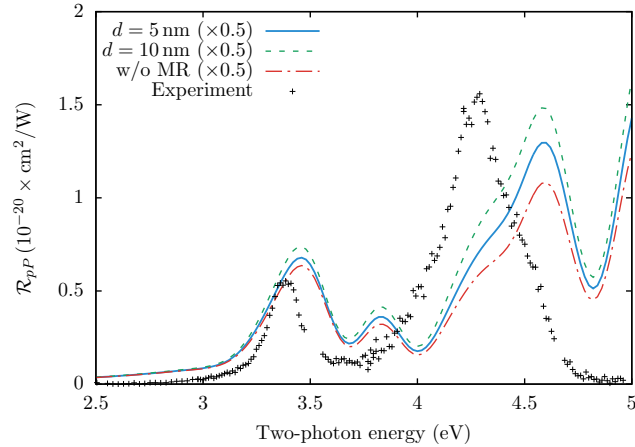


Figure 3.13: Comparison between the three layer model with the effects of multiple reflections for two different values of the total layer thickness d , with the standard three layer model without the effects of multiple reflections, and the experimental data from Ref. [33]. We take $\theta = 65^\circ$, $\phi = 30^\circ$, and a scissors value of $\hbar\Delta = 0.7$ eV. The χ^{ijk} components are broadened with $\sigma = 0.05$ eV, and then \mathcal{R}_{pP} is broadened with $\sigma = 0.10$ eV.

fig:average

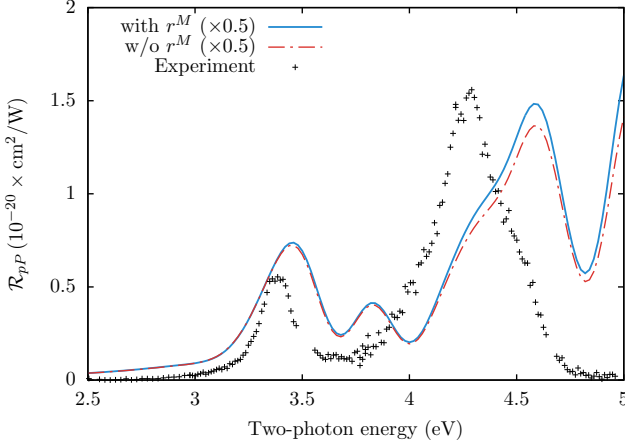


Figure 3.14: Comparison between theoretical models (see Table 3.3) and experiment for \mathcal{R}_{pP} , for $\theta = 65^\circ$, and a scissors value of $\hbar\Delta = 0.7 \text{ eV}$. The χ^{ijk} components are broadened with $\sigma = 0.05 \text{ eV}$, and then \mathcal{R}_{pP} is broadened with $\sigma = 0.10 \text{ eV}$. Experimental data taken from Ref. [34], measured at room temperature.

tab:models
fig:mr2

In Fig. 3.15, we compare the theoretical results for the SSHG yield with the experimental results from Ref. [33]. We mention that the experimental results were produced with an angle of incidence of $\theta = 65^\circ$, and an azimuthal angle of $\phi = 30^\circ$, which eliminates the contribution from χ^{xxx} from Eq. (2.52). First, we note that the experimental spectrum shows two very well defined resonances which come from electronic transitions from the valence to the conduction bands around the well known $E_1 \sim 3.4 \text{ eV}$ and $E_2 \sim 4.3 \text{ eV}$ critical points of Si [60]. As can be seen, the theoretical results reproduce the features of the spectrum, although we see that the E_2 peak is blueshifted by around 0.3 eV. Here we focus on the SSHG yield itself rather than on the physics that lead to such a blueshifted theoretical spectrum. The interested reader can refer to Ref. [61] for those details.

All curves in this figure that include multiple reflections consider $d = 10 \text{ nm}$. We compare the theoretical SSHG yield for $d_2 = 0 \text{ nm}$ and $d_2 = 10 \text{ nm}$, with the SSHG yield that neglects multiple reflections. When $d_2 = 0 \text{ nm}$, we have placed the polarization sheet at the bottom of the layer region. This minimizes the effect of the multiple reflections, and thus the curve is very similar to the three layer model that neglects multiple reflections entirely. When $d_2 = 10 \text{ nm}$, the polarization sheet is placed at the top of the layer region. This maximizes the effect of the multiple reflections and therefore leads to the largest yield. We also notice that the average value obtained by using \bar{R}_i^M (Eq. (2.23)) is intermediate between $d_2 = 0$ and $d_2 = 10 \text{ nm}$, as expected. This is very similar to selecting $d_2 = d/2$, which can be interpreted as placing the nonlinear polarization sheet $\mathbf{P}(\mathbf{r}, t)$ at the middle of layer ℓ . It is important to remark that these enhancements are larger for E_2 than for E_1 . This can be understood from the fact that the corresponding λ_0 for E_1 is larger than that of E_2 . From Eqs. (2.16), (2.17), and (2.27), we see that the phase shifts are larger for E_2 than for E_1 , producing a larger enhancement of the SSHG yield at E_2 from the multiple reflections. As the phase shifts grow with d , so does the enhancement caused by the multiple reflections. We have verified that the effects of the multiple reflections from the linear field are significantly smaller than those of the SH field. This is clear since the phase shift of Eq. (2.27) is not only a factor of 2

smaller than that of Eqs. (2.16) and (2.17), but also $w_\ell < W_\ell$.

From this figure, it becomes evident that the inclusion of multiple reflections is crucial to obtain a better agreement between the theoretical SHHG yield and the experimental spectrum. This is particularly true for larger energies, such as E_2 , as λ_0 becomes smaller and the multiple reflection effects become more noticeable. The selected value for $d \ll \lambda_0$, that comes naturally from the *ab initio* calculation of χ^{ijk} is thus very reasonable in order to model a thin surface layer below the vacuum region where the nonlinear SH conversion takes place.

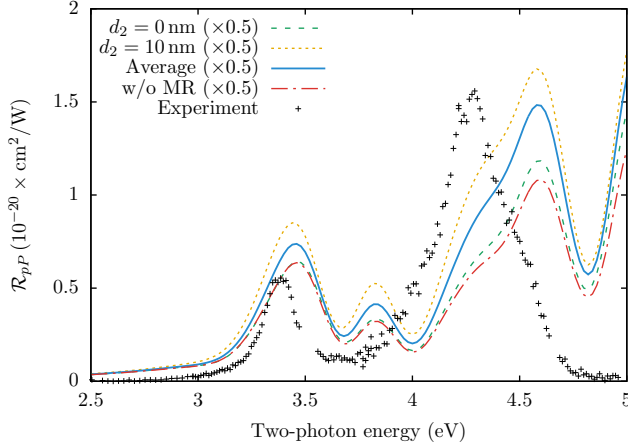


Figure 3.15: Comparison between the three layer model with the effects of multiple reflections for two different values of d_2 , using the average value \bar{R}_i^M Eq. of Eq. (2.26), the three layer model without the effects of multiple reflections, and the experimental data from Ref. [33]. All curves that include multiple reflections consider a layer ℓ thickness of $d = 10 \text{ nm}$.

fig:d2values

3.2.2.3 Calculated \mathcal{R}_{pP} compared to experiment

I present \mathcal{R}_{pP} compared to experimental data from Ref. [33] in Fig. 3.16. Note that peak position for the 3-layer model is similar to experiment with the overall intensity being only two times larger. The E_2 peak is blueshifted by around 0.3 eV, and the yield does not go to zero after 4.75 eV. The 2-layer-fresnel model produces a spectrum with peak positions that are close to the experiment, but are 20 times more intense. The calculated E_2 peak is similar, but the E_1 peak lacks the sharpness present in the experiment. The 2-layer-bulk model is almost identical in lineshape to the 3-layer model, but with eight times less intensity.

From Eq. (2.52), it is clear that \mathcal{R}_{pP} has several 2ω terms that will change between models; this will have a deep effect on the lineshape. Additionally, Γ_{pP}^ℓ also has $\varepsilon_\ell(2\omega)$ in the denominator, and so we have a significant difference in both lineshape and intensity between the 2-layer-fresnel and the other two models. Again, as in the previous sections for \mathcal{R}_{as} and \mathcal{R}_{sp} , the 3-layer model is the closest in intensity to the experiment. Additionally, Ref. [62] shows that low temperature measurements of \mathcal{R}_{pP} will blueshift the spectrum away from room temperature measurements such as those shown in Figs. 3.16 and 3.18, and towards the theoretical results.

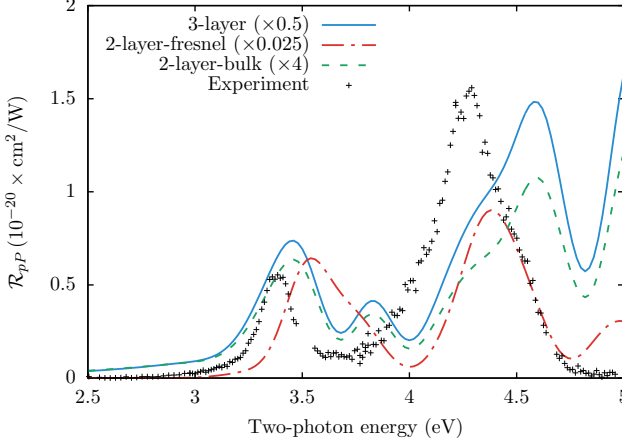


Figure 3.16: Comparison between theoretical models (see Table 2.3) and experiment for \mathcal{R}_{pP} , for $\theta = 65^\circ$, and a scissors value of $\hbar\Delta = 0.7$ eV. All theoretical curves are broadened with $\sigma = 0.10$ eV. Experimental data taken from Ref. [\[33\]](#), measured at room temperature.

`fig:RpP`

I'll take this moment to present some auxiliary results from Sec. 2.3 in Fig. 3.17. Refer to Table 2.3 and Sec. 2.3, and note that there are two additional models that we have ignored thus far. The 3-layer-hybrid (Sec. 2.3.5) evaluates $\mathcal{P}(2\omega)$ in the thin layer ℓ defined by ϵ_{ℓ} , while the fundamental fields are evaluated in the bulk region defined by ϵ_b .

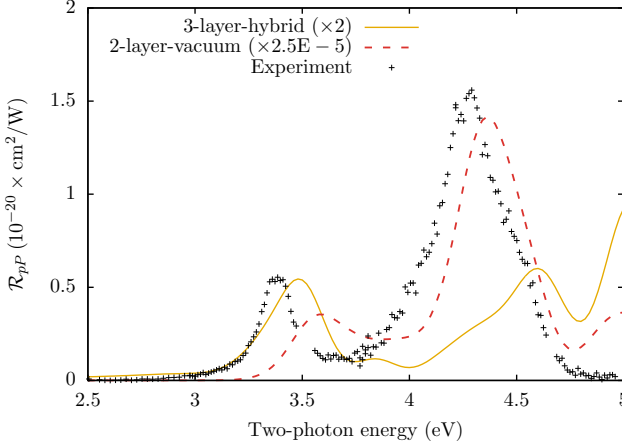


Figure 3.17: Other models.

`fig:othermodels`

It is immediately apparent that the 3-layer-hybrid model shares the same lineshape as 3-layer and 2-layer-bulk models, see Fig. 3.16. This is entirely consistent as ϵ_b and ϵ_ℓ differ only in intensity; this model is intermediate in intensity between the other two. The 3-layer model is still closer to experiment, but this is an interesting alternative. On the other hand, the 2-layer-vacuum model has the most extreme intensity difference with the experiment, over 5 orders of magnitude higher. The lineshape reproduces the E₂ peak quite well, but lacks a sharp E₁ peak with poor peak position. Clearly, the screening provided by ϵ_b and ϵ_ℓ are necessary for accurate results.

Reviewing Eq. (2.52), we see that \mathcal{R}_{pP} is by far the most involved calculation, since it includes all four nonzero components. In particular, χ^{zzz} and χ^{xxz} include out-of-plane incoming fields. These are affected by local field effects^[52] that reveal the inhomogeneities in the material, which are by far more prevalent perpendicular to the surface than in the surface plane. This can be evidenced for Si, as Reflectance Anisotropy Spectroscopy (RAS) measurements are well described by *ab initio* calculations neglecting local field effects.^[63, 64] It is therefore expected that the out-of-plane components will be more sensitive to the inclusion of local fields. These will not change the transition energies, only their relative weights of the resonant peaks,^[52] but including these effects is challenging to compute,^[28] and beyond the scope of this paper. We speculate that \mathcal{R}_{pP} requires the proper inclusion of these effects in order to accurately describe the experimental peaks.

In Fig. 3.18, I compare the theoretical spectra to results from Ref. [34]. The 3-layer model is, as before, close to the experiment in both peak position and intensity. Intensity is almost the same the experimental value. This provides a more compelling argument against the 2-layer-fresnel model than Fig. 3.16. The 2-layer-fresnel model is 20 times more intense and blueshifted by around 0.1 eV. As mentioned above, this surface is of very high quality with measurements taken shortly after surface preparation. The 2-layer-bulk model is intermediate between the other two models in both intensity and lineshape. Under these conditions, the 3-layer model very accurately reproduces the E_1 peak over the 2-layer-fresnel and 2-layer-bulk models.

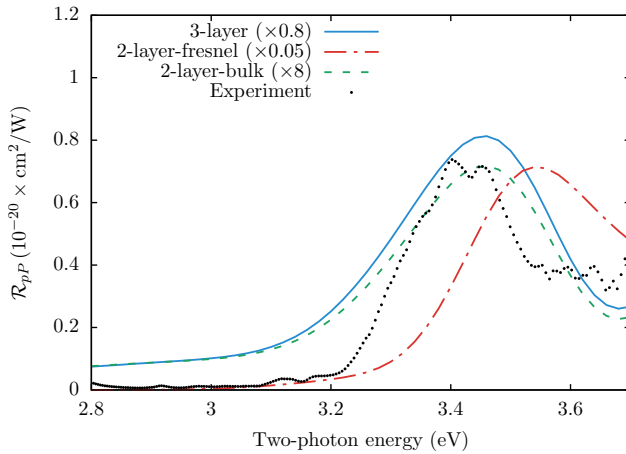


Figure 3.18: Comparison between theoretical models (see Table 2.3) and experiment for \mathcal{R}_{pP} , for $\theta = 45^\circ$, and a scissors value of $\hbar\Delta = 0.7$ eV. All theoretical curves are broadened with $\sigma = 0.075$ eV. Experimental data taken from Ref. [34], measured at room temperature.

fig:mitchell

Lastly, GW transition energies are needed for linear optics and SHG. Doing a Bethe-Salpeter calculation for SSHG will undoubtedly improve the position and the amplitude of the peaks, but is far beyond current capabilities^[65]. I kept the scissors shift constant throughout these calculations as I want to keep this calculation at the *ab initio* level. Remember that the choice of $\hbar\Delta = 0.7$ eV for the scissors shift comes from a GW calculation^[59]. As explained in Fig. 3.22, the lack of surface states causes an almost rigid shift of the spectra by applying the scissors correction. I have checked that it is not possible to have a single scissors value that can reproduce the energy positions of both the E_1 and the E_2 peaks. Of course, the experimental temperature at which the

spectra is measured should be taken into account in a more complete formulation. However, these calculations are always restricted to $T = 0$ K.

3.2.2.4 Calculated \mathcal{R}_{sP} compared to experiment

Next, I analyze and compare the calculated \mathcal{R}_{sP} spectra with experimental data from Ref. [33].
The calculation adheres to the experimental setup by taking an angle of incidence $\theta = 65^\circ$ and an azimuthal angle $\phi = 30^\circ$. As seen in Fig. 3.19, the overall intensity of \mathcal{R}_{sP} is one order of magnitude lower than \mathcal{R}_{pS} . The experimental data is far noisier than in the other cases but the E₁ and E₂ peaks are still discernible. As with the previous comparisons, the 3-layer model is the closest match in both intensity and lineshape to the experimental spectrum. It produces a curve that is very close to the experimental intensity with good proportional heights for the calculated E₁ and E₂ peaks. In contrast, the 2-layer-fresnel model is 100 times more intense than experiment and produces an enlarged E₂ peak. The 2-layer-bulk model is ten times smaller with a very similar lineshape to the 3-layer model.

The differences between the 2-layer-fresnel and 2-layer-bulk models are not derived from Eq. (2.57), as the $\varepsilon_b(2\omega)$ does not change and the second term vanishes for this azimuthal angle of $\phi = 30$. However, Γ_{sP}^ℓ does cause a significant change in the intensity as there is an $\varepsilon_\ell(2\omega)$ term in the denominator. This will become $\varepsilon_v(2\omega) = 1$ for the 2-layer-fresnel model, and $\varepsilon_b(2\omega)$ in the bulk model. This accounts for the significant difference between the intensity of the two models, while the lineshape remains mostly consistent.

At higher energies, the theoretical curve is blueshifted as compared to the experiment. The best explanation for this is the inclusion of the scissor operator, which does not adequately correct the transitions occurring at these higher energies. A full GW calculation would be well suited for this task, but is well beyond the scope of this work.

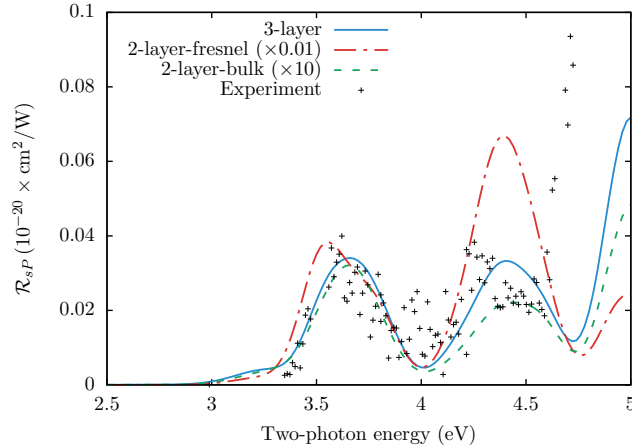


Figure 3.19: Comparison between theoretical models (see Table 2.3) and experiment for \mathcal{R}_{sP} , for $\theta = 65^\circ$, and a scissors value of $\hbar\Delta = 0.7$ eV. All theoretical curves are broadened with $\sigma = 0.075$ eV. Experimental data taken from Ref. [33], measured at room temperature.

3.2.2.5 Calculated \mathcal{R}_{pS} compared to experiment

I first compare the calculated \mathcal{R}_{pS} spectra with room temperature experimental data from Ref. [33]. Adhering to the experimental setup, I set an angle of incidence $\theta = 65^\circ$ and an azimuthal angle of $\phi = 30^\circ$ with respect to the x -axis. This azimuthal angle maximizes r_{pS} , as shown in Eq. (2.62). Fig. 3.20, shows that all three models reproduce the lineshape of the experimental spectrum which includes the peaks corresponding to both the E₁ (3.4 eV) and E₂ (4.3 eV) critical points of bulk silicon, and a smaller feature at around 3.8 eV. The calculated E₁ and E₂ peaks are redshifted by 0.1 eV and 0.06 eV, respectively, compared with the experimental peaks.

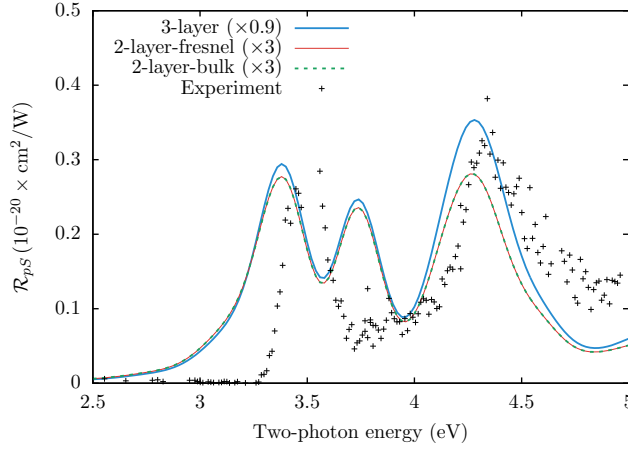


Figure 3.20: Comparison between theoretical models (see Table 2.3) and experiment for \mathcal{R}_{pS} , for $\theta = 65^\circ$, and a scissors value of $\hbar\Delta = 0.7$ eV. All theoretical curves are broadened with $\sigma = 0.075$ eV. Experimental data taken from Ref. [33], measured at room temperature.

tab:models
fig:RpS

The main issue to address here is the discrepancy between the intensity of the E₁ peak. In the theoretical curves, the peaks differ only slightly in overall intensity. Conversely, the experimental E₁ peak is significantly smaller than the E₂ peak. This may be due to the effects of oxidation on the surface. Ref. [32] features similar data to those of Ref. [33] but focuses on the effects of surface oxidation. From Ref. [32] it is clear that as time passes during the experiment, the surface becomes more oxidized and the E₁ peak diminishes substantially, as shown by the experimental data taken 5 hours after initial H-termination. This may be enough time to slightly reduce the E₁ peak intensity, as can be observed here.

In Fig. 3.21, I compare the theoretical \mathcal{R}_{pS} with experimental data from Ref. [34]; this data, however, only encompasses the E₁ peaks, and was obtained at room temperature. This calculation uses an angle of incidence $\theta = 45^\circ$ and an azimuthal angle $\phi = 30^\circ$ to match the experimental conditions. As in the previous comparison, the E₁ peak is slightly redshifted compared to experiment. The intensity of the theoretical yield is smaller than the experimental yield for all three models. The measurements presented in Ref. [34] were taken very shortly after the surface had been prepared, and the surface itself was prepared with a high degree of quality and measured at room temperature. Peak position compared to theory is slightly improved under these conditions. As before, the 3-layer model is closer in intensity to the experimental spectrum.

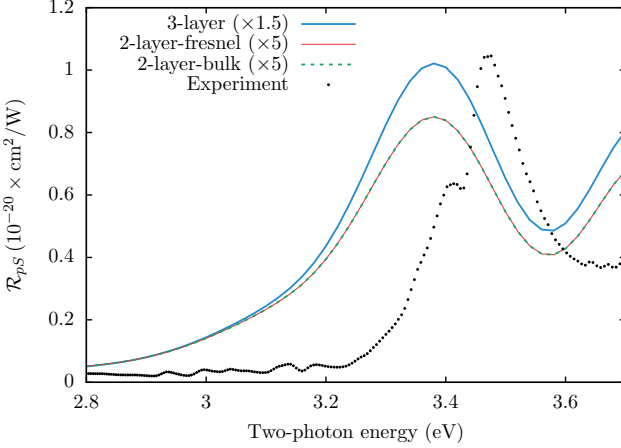


Figure 3.21: Comparison between theoretical models (see Table 2.3) and experiment for \mathcal{R}_{pS} , for $\theta = 45^\circ$. We use a scissors value of $\hbar\Delta = 0.7$ eV. All theoretical curves are broadened with $\sigma = 0.075$ eV. Experimental data taken from Ref. [34], measured at room temperature.

`tab:models`

`fig:mitchell`

From Fig. 3.10, I presented that our calculation for χ^{xxx} coincides with the measurement taken at a low temperature of 80 K. It is well known that temperature causes shifting in the peak position of SSHG spectra [62]. As \mathcal{R}_{pS} only depends on this component (see Eq. (2.62)), the position of the theoretical peak should be correct in Figs. 3.20 and 3.21. Thus, the difference in peak position should stem from the higher temperature at which the experiments were measured.

Both the 2-layer-fresnel and 2-layer-bulk models are identical and roughly four times smaller than the experiment. It is clear from Eq. (2.62) that \mathcal{R}_{pS} only has 1ω terms ($\varepsilon_\ell(\omega)$ and k_b). For both of these models, the fundamental fields are evaluated in the bulk, which means that the only change to Eq. (2.62) is that $\varepsilon_\ell(\omega) \rightarrow \varepsilon_b(\omega)$. Additionally, Γ_{pS}^ℓ also remains identical between the two models and has no 2ω terms in the denominator. Therefore, r_{pS} is identical between these two models. Ultimately, the intensity of the 3-layer model is the closest to the experiment.

Per Eq. (2.62), the intensity of \mathcal{R}_{pS} depends only on χ^{xxx} , which is not affected by local field effects [52]. These effects are neglected in this calculation, but \mathcal{R}_{pS} maintains an accurate lineshape and provides a good quantitative description of the experimental SSHG yield. Note that both the calculated and experimental spectra show two-photon resonances at the energies corresponding to the critical point transitions of bulk Si. Note also that the SSHG yield drops rapidly to zero below E_1 , which is consistent with the absence of surface states due to the H saturation on the surface. This observation holds true for all three polarization cases studied for this surface.

Lastly, in Fig. 3.22 I provide an overview of the different levels of approximation proposed in this article. All curves here were calculated using the 3-layer model. The long dashed line depicts the effect of excluding the contribution from the nonlocal part of the pseduopotentials. This is consistent with the results reported in Ref. [51], where the exclusion of this term increases the intensity of the components of χ by approximately 15% to 20%. Note that the E_1 peak is larger than the E_2 peak, contrasting with the experiment, where the E_1 peak is smaller than E_2 . Lastly, the thin solid line depicts the full calculation with a scissors value of $\hbar\Delta = 0$. The spectrum is almost rigidly redshifted as this H-saturated surface has no electronic surface states [51]. Thus, this demonstrates the importance of including the scissors correction to accurately reproduce the

experimental spectrum. In summary, the inclusion of the contribution from the nonlocal part of the pseudopotentials and the scissors operator on top of the 3-layer model produces spectra with a lineshape and intensity that compare favorably with the experimental data.

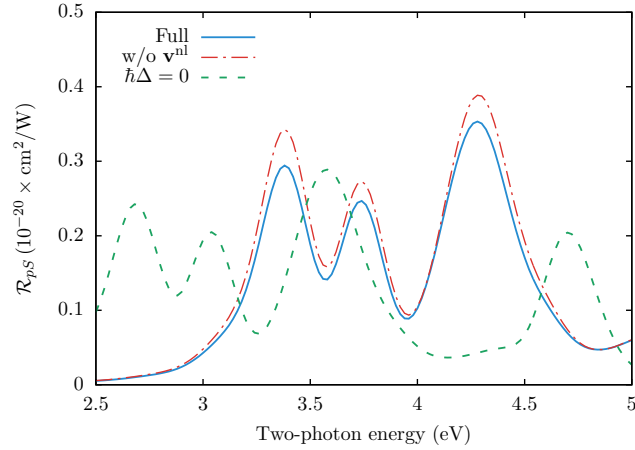


Figure 3.22: Calculated results for \mathcal{R}_{pS} for the different levels of approximation proposed in this article. All curves were calculated using the 3-layer model. We take $\theta = 65^\circ$ for this plot. See text for full details. All curves are broadened with $\sigma = 0.075$ eV.

`fig:improvem`

Chapter 4

Final Remarks

:conclusions

Outline

4.1 Conclusions	55
4.2 Future Work	56

4.1 Conclusions

I was able to learn and successfully apply the XP2SHG/SFG technique to a series of nanoparticles that were unfortunately not of sufficient optical quality to yield meaningful results. This was accomplished by using established methods (with the help of very capable people) to study samples that were not properly characterized. The obvious solution to this would have been to use other nanoparticles, but it was very much beyond my possibilities to obtain other samples within the time constraints imposed by my visit to the Femtosecond Spectroscopy group.

My suggestions for a revisionary work are the following.

Better quality samples. The scattering problem can be completely eliminated with samples that are in good physical condition.

Well characterized samples. The purpose of this work was to characterize the nanoparticles via nonlinear spectroscopy. However, these measurements work much better if applied in conjunction with previous studies of the samples, such as TEM scans, linear measurements, etc.

Apply the XP2SFG technique to metallic nanoparticles. There are few references available on sum frequency studies involving metallic nanoparticles, especially in the two beam configuration. I think that using proper samples with a NOPA in the XP2SFG configuration would provide excellent characterization of the samples and interesting results.

4.2 Future Work

I think that every work of experimental science has its fair share of setbacks, complications, and difficulties. Sometimes the work itself can be very difficult or even dangerous. Other times, the work is so cutting edge that problems have to be solved as they come without the help of literature. Regardless of the scope of the work, *all* experimentation is very touch-and-go business – you arm yourself with the best tools available for the job and hope for the best. This work had its share of complications and setbacks, chief amongst these was the constant breakdown of lasers in both countries. Then, the poor quality of the samples which only came to light after they were in place and ready to be measured. Lastly, the lack of information about the samples did not allow for the systematic study needed to get the most out of this project.

Fortunately, Stephen Jay Gould once said that, “Honorable errors do not count as failures in science, but as seeds for progress in the quintessential activity of correction.” With that in mind I summarize what was learned from this.

First, the XP2SHG/SFG technique is fairly unique and specialized even amongst groups that are dedicated to surface optics and nonlinear optical techniques. Learning how this technique works and how it is used will be invaluable for future work in this field. Actually having seen it in use, and then using it for myself in the company of the people who pioneered it was a rewarding and educational experience.

Second, while the results were inconclusive, the types of measurements done on these types of samples are new and unexplored. There is much work to be done with these kinds of materials and I hope that this work can serve as a starting point for other interested scientists. I have no doubt in my mind that better samples would have yielded excellent new results.

Lastly, this entire work helped broaden my knowledge of nonlinear optics in general, as well as the many experimental techniques used everyday by scientists everywhere. Even so, I only possess a very small portion of the “big picture” needed to understand every aspect of this work. There is still a lot to be learned about surface optics and nonlinear techniques and I hope that this work, at the very least, will pique the readers’ interest on these topics.

Appendix A

Useful derivations for the nonlinear surface susceptibility

pp:chi2deriv

Outline

A.1 \mathbf{r}_e and \mathbf{r}_i	57
---	----

A.1 \mathbf{r}_e and \mathbf{r}_i

In this appendix, we derive the expressions for the matrix elements of the electron position operator \mathbf{r} . The r representation of the Bloch states is given by

$$\psi_{n\mathbf{k}}(\mathbf{r}) = \langle \mathbf{r} | n\mathbf{k} \rangle = \sqrt{\frac{\Omega}{8\pi^3}} e^{i\mathbf{k}\cdot\mathbf{r}} u_{n\mathbf{k}}(\mathbf{r}), \quad (\text{A.1}) \quad [\text{bloch}]$$

where $u_{n\mathbf{k}}(\mathbf{r}) = u_{n\mathbf{k}}(\mathbf{r} + \mathbf{R})$ is cell periodic, and

$$\int_{\Omega} u_{n\mathbf{k}}^*(\mathbf{r}) u_{m\mathbf{k}'}(\mathbf{r}) d^3r = \delta_{nm} \delta_{\mathbf{k},\mathbf{k}'}, \quad (\text{A.2}) \quad [\text{normal}]$$

and Ω is the unit cell volume.

The key ingredient in the calculation are the matrix elements of the position operator \mathbf{r} . We start from the basic relation

$$\langle n\mathbf{k} | m\mathbf{k}' \rangle = \delta_{nm} \delta(\mathbf{k} - \mathbf{k}'), \quad (\text{A.3}) \quad [\text{nbraket}]$$

and take its derivative with respect to \mathbf{k} as follows. On one hand,

$$\frac{\partial}{\partial \mathbf{k}} \langle n\mathbf{k} | m\mathbf{k}' \rangle = \delta_{nm} \frac{\partial}{\partial \mathbf{k}} \delta(\mathbf{k} - \mathbf{k}'), \quad (\text{A.4}) \quad [\text{ddk1}]$$

and on the other,

$$\frac{\partial}{\partial \mathbf{k}} \langle n\mathbf{k} | m\mathbf{k}' \rangle = \frac{\partial}{\partial \mathbf{k}} \int \langle n\mathbf{k} | \mathbf{r} \rangle \langle \mathbf{r} | m\mathbf{k}' \rangle d\mathbf{r} = \int \left(\frac{\partial}{\partial \mathbf{k}} \psi_{n\mathbf{k}}^*(\mathbf{r}) \right) \psi_{m\mathbf{k}'}(\mathbf{r}) d\mathbf{r}. \quad (\text{A.5}) \quad [\text{dkbraket}]$$

The derivative of the wavefunction is simply given by

$$\frac{\partial}{\partial \mathbf{k}} \psi_{n\mathbf{k}}^*(\mathbf{r}) = \sqrt{\frac{\Omega}{8\pi^3}} \left(\frac{\partial}{\partial \mathbf{k}} u_{n\mathbf{k}}^*(\mathbf{r}) \right) e^{-i\mathbf{k}\cdot\mathbf{r}} - i\mathbf{r} \psi_{n\mathbf{k}}^*(\mathbf{r}). \quad (\text{A.6}) \quad [\text{dpsi}]$$

Substituting into Eq. (A.5), we obtain

$$\begin{aligned} \frac{\partial}{\partial \mathbf{k}} \langle n\mathbf{k}|m\mathbf{k}' \rangle &= \sqrt{\frac{\Omega}{8\pi^3}} \int \left(\frac{\partial}{\partial \mathbf{k}} u_{n\mathbf{k}}^*(\mathbf{r}) \right) e^{-i\mathbf{k}\cdot\mathbf{r}} \psi_{m\mathbf{k}'}(\mathbf{r}) d\mathbf{r} - i \int \psi_{n\mathbf{k}}^*(\mathbf{r}) \mathbf{r} \psi_{m\mathbf{k}'}(\mathbf{r}) d\mathbf{r} \\ &= \frac{\Omega}{8\pi^3} \int e^{-i(\mathbf{k}-\mathbf{k}')\cdot\mathbf{r}} \left(\frac{\partial}{\partial \mathbf{k}} u_{n\mathbf{k}}^*(\mathbf{r}) \right) u_{m\mathbf{k}'}(\mathbf{r}) d\mathbf{r} - i \langle n\mathbf{k}|\hat{\mathbf{r}}|m\mathbf{k}' \rangle. \end{aligned} \quad (\text{A.7}) \quad [\text{dkbraket2}]$$

Restricting \mathbf{k} and \mathbf{k}' to the first Brillouin zone, we use the following result that is valid for any periodic function $f(\mathbf{r}) = f(\mathbf{r} + \mathbf{R})$,

$$\int e^{i(\mathbf{q}-\mathbf{k})\cdot\mathbf{r}} f(\mathbf{r}) d^3r = \frac{8\pi^3}{\Omega} \delta(\mathbf{q} - \mathbf{k}) \int_{\Omega} f(\mathbf{r}) d^3r, \quad (\text{A.8}) \quad [\text{periodic}]$$

to finally write [6]

$$\frac{\partial}{\partial \mathbf{k}} \langle n\mathbf{k}|m\mathbf{k}' \rangle = \delta(\mathbf{k} - \mathbf{k}') \int_{\Omega} \left(\frac{\partial}{\partial \mathbf{k}} u_{n\mathbf{k}}^*(\mathbf{r}) \right) u_{m\mathbf{k}}(\mathbf{r}) d\mathbf{r} - i \langle n\mathbf{k}|\hat{\mathbf{r}}|m\mathbf{k}' \rangle. \quad (\text{A.9}) \quad [\text{dkbraket3}]$$

From

$$\int_{\Omega} u_{m\mathbf{k}} u_{n\mathbf{k}}^* d\mathbf{r} = \delta_{nm}, \quad (\text{A.10}) \quad [\text{dnm1}]$$

we easily find that

$$\int_{\Omega} \left(\frac{\partial}{\partial \mathbf{k}} u_{m\mathbf{k}}(\mathbf{r}) \right) u_{n\mathbf{k}}^*(\mathbf{r}) d\mathbf{r} = - \int_{\Omega} u_{m\mathbf{k}}(\mathbf{r}) \left(\frac{\partial}{\partial \mathbf{k}} u_{n\mathbf{k}}^*(\mathbf{r}) \right) d\mathbf{r}. \quad (\text{A.11}) \quad [\text{dnm2}]$$

Therefore, we define

$$\xi_{nm}(\mathbf{k}) \equiv i \int_{\Omega} u_{n\mathbf{k}}^*(\mathbf{r}) \nabla_{\mathbf{k}} u_{m\mathbf{k}}(\mathbf{r}) d\mathbf{r}, \quad (\text{A.12}) \quad [\text{zeta}]$$

with $\nabla_{\mathbf{k}} = \partial/\partial \mathbf{k}$. Now, from Eqs. (A.4), (A.7), and (A.12), we have that the matrix elements of the position operator of the electron are given by

$$\langle n\mathbf{k}|\hat{\mathbf{r}}|m\mathbf{k}' \rangle = \delta(\mathbf{k} - \mathbf{k}') \xi_{nm}(\mathbf{k}) + i \delta_{nm} \nabla_{\mathbf{k}} \delta(\mathbf{k} - \mathbf{k}'), \quad (\text{A.13}) \quad [\text{erre}]$$

Then, from Eq. (A.13) and writing $\hat{\mathbf{r}} = \hat{\mathbf{r}}_e + \hat{\mathbf{r}}_i$, with $\hat{\mathbf{r}}_e$ ($\hat{\mathbf{r}}_i$) the interband (intraband) part, we obtain that

$$\langle n\mathbf{k}|\hat{\mathbf{r}}_i|m\mathbf{k}' \rangle = \delta_{nm} [\delta(\mathbf{k} - \mathbf{k}') \xi_{nn}(\mathbf{k}) + i \nabla_{\mathbf{k}} \delta(\mathbf{k} - \mathbf{k}')], \quad (\text{A.14}) \quad [\text{rnmi}]$$

$$\langle n\mathbf{k}|\hat{\mathbf{r}}_e|m\mathbf{k}' \rangle = (1 - \delta_{nm}) \delta(\mathbf{k} - \mathbf{k}') \xi_{nm}(\mathbf{k}). \quad (\text{A.15}) \quad [\text{rnme}]$$

To proceed, we relate Eq. (A.15) to the matrix elements of the momentum operator as follows. For the intraband part, we derive the following general result,

$$\begin{aligned}\langle n\mathbf{k}| [\hat{\mathbf{r}}_i, \hat{\mathcal{O}}] |m\mathbf{k}'\rangle &= \sum_{\ell, \mathbf{k}''} \left(\langle n\mathbf{k}|\hat{\mathbf{r}}_i|\ell\mathbf{k}''\rangle \langle \ell\mathbf{k}''|\hat{\mathcal{O}}|m\mathbf{k}'\rangle - \langle n\mathbf{k}|\hat{\mathcal{O}}|\ell\mathbf{k}''\rangle \langle \ell\mathbf{k}''|\hat{\mathbf{r}}_i|m\mathbf{k}'\rangle \right) \\ &= \sum_{\ell} \left(\langle n\mathbf{k}|\hat{\mathbf{r}}_i|\ell\mathbf{k}'\rangle \mathcal{O}_{\ell m}(\mathbf{k}') - \mathcal{O}_{n\ell}(\mathbf{k}) |\ell\mathbf{k}\rangle \langle \ell\mathbf{k}|\hat{\mathbf{r}}_i|m\mathbf{k}'\rangle \right),\end{aligned}\tag{A.16} \quad [\text{conmri}]$$

where we have taken $\langle n\mathbf{k}|\hat{\mathcal{O}}|\ell\mathbf{k}''\rangle = \delta(\mathbf{k} - \mathbf{k}'')\mathcal{O}_{n\ell}(\mathbf{k})$. We substitute Eq. (A.14) to obtain

$$\begin{aligned}\sum_{\ell} (\delta_{n\ell}[\delta(\mathbf{k} - \mathbf{k}')\boldsymbol{\xi}_{nn}(\mathbf{k}) + i\nabla_{\mathbf{k}}\delta(\mathbf{k} - \mathbf{k}')]\mathcal{O}_{\ell m}(\mathbf{k}') - \mathcal{O}_{n\ell}(\mathbf{k})\delta_{\ell m}[\delta(\mathbf{k} - \mathbf{k}')\boldsymbol{\xi}_{mm}(\mathbf{k}) + i\nabla_{\mathbf{k}}\delta(\mathbf{k} - \mathbf{k}')]) \\ = ([\delta(\mathbf{k} - \mathbf{k}')\boldsymbol{\xi}_{nn}(\mathbf{k}) + i\nabla_{\mathbf{k}}\delta(\mathbf{k} - \mathbf{k}')]\mathcal{O}_{nm}(\mathbf{k}') - \mathcal{O}_{nm}(\mathbf{k}) [\delta(\mathbf{k} - \mathbf{k}')\boldsymbol{\xi}_{mm}(\mathbf{k}) + i\nabla_{\mathbf{k}}\delta(\mathbf{k} - \mathbf{k}')]) \\ = \delta(\mathbf{k} - \mathbf{k}')\mathcal{O}_{nm}(\mathbf{k}) (\boldsymbol{\xi}_{nn}(\mathbf{k}) - \boldsymbol{\xi}_{mm}(\mathbf{k})) + i\mathcal{O}_{nm}(\mathbf{k}')\nabla_{\mathbf{k}}\delta(\mathbf{k} - \mathbf{k}') + i\delta(\mathbf{k} - \mathbf{k}')\nabla_{\mathbf{k}}\mathcal{O}_{nm}(\mathbf{k}) - i\mathcal{O}_{nm}(\mathbf{k}')\nabla_{\mathbf{k}}\delta(\mathbf{k} - \mathbf{k}') \\ = i\delta(\mathbf{k} - \mathbf{k}')(\nabla_{\mathbf{k}}\mathcal{O}_{nm}(\mathbf{k}) - i\mathcal{O}_{nm}(\mathbf{k}) (\boldsymbol{\xi}_{nn}(\mathbf{k}) - \boldsymbol{\xi}_{mm}(\mathbf{k}))) \\ \equiv i\delta(\mathbf{k} - \mathbf{k}')(\mathcal{O}_{nm})_{;\mathbf{k}}.\end{aligned}\tag{A.17} \quad [\text{conmri2}]$$

Then,

$$\langle n\mathbf{k}|[\hat{\mathbf{r}}_i, \hat{\mathcal{O}}]|m\mathbf{k}'\rangle = i\delta(\mathbf{k} - \mathbf{k}')(\mathcal{O}_{nm})_{;\mathbf{k}},\tag{A.18} \quad [\text{conmri3}]$$

where

$$(\mathcal{O}_{nm})_{;\mathbf{k}} = \nabla_{\mathbf{k}}\mathcal{O}_{nm}(\mathbf{k}) - i\mathcal{O}_{nm}(\mathbf{k}) (\boldsymbol{\xi}_{nn}(\mathbf{k}) - \boldsymbol{\xi}_{mm}(\mathbf{k})),\tag{A.19} \quad [\text{gendev}]$$

is the generalized derivative of \mathcal{O}_{nm} with respect to \mathbf{k} . Note that the highly singular term $\nabla_{\mathbf{k}}\delta(\mathbf{k}-\mathbf{k}')$ cancels in Eq. (A.17), thus giving a well defined commutator of the intraband position operator with any arbitrary operator $\hat{\mathcal{O}}$.

Appendix B

Derived expressions for the SHG yield

ressions_rif

Outline

B.1	Some useful expressions	60
B.1.1	2ω terms	61
B.1.2	1ω terms	62
B.1.3	Nonzero components of $\chi(-2\omega; \omega, \omega)$	63
B.2	\mathcal{R}_{pP}	64
B.2.1	For the (111) surface	65
B.2.2	For the (110) surface	68
B.2.3	For the (001) surface	69
B.3	\mathcal{R}_{pS}	70
B.3.1	For the (111) surface	71
B.3.2	For the (110) surface	71
B.3.3	For the (001) surface	72
B.4	\mathcal{R}_{sP}	72
B.4.1	For the (111) surface	73
B.4.2	For the (110) surface	74
B.4.3	For the (001) surface	74
B.5	\mathcal{R}_{ss}	75
B.5.1	For the (111) surface	75
B.5.2	For the (110) surface	76
B.5.3	For the (001) surface	76

B.1 Some useful expressions

We are interested in finding

$$\Upsilon = \mathbf{e}_\ell^{2\omega} \cdot \boldsymbol{\chi} : \mathbf{e}_\ell^\omega \mathbf{e}_\ell^\omega$$

for each different polarization case. We choose the plane of incidence along the κz plane, and define

$$\hat{\kappa} = \cos \phi \hat{x} + \sin \phi \hat{y}, \quad (\text{B.1}) \quad [\text{eqapp:kappa}]$$

and

$$\hat{s} = -\sin \phi \hat{x} + \cos \phi \hat{y}, \quad (\text{B.2}) \quad [\text{eqapp:svec}]$$

where ϕ the angle with respect to the x axis.

B.1.1 2ω terms

Including multiple reflecions, the $\mathbf{e}_\ell^{2\omega}$ term is

$$\mathbf{e}_\ell^{2\omega} = \hat{\mathbf{e}}^{\text{out}} \cdot \left[\hat{\mathbf{s}} T_s^{v\ell} R_s^{M+} \hat{\mathbf{s}} + \hat{\mathbf{P}}_{v+} \frac{T_p^{v\ell}}{N_\ell} (\sin \theta_0 R_p^{M+} \hat{\mathbf{z}} - W_\ell R_p^{M-} \hat{\kappa}) \right], \quad (\text{B.3}) \quad [\text{eqapp:e2well}]$$

and neglecting the multiple reflections reduces this expression to

$$\mathbf{e}_\ell^{2\omega} = \hat{\mathbf{e}}^{\text{out}} \cdot \left[\hat{\mathbf{s}} T_s^{v\ell} T_s^{\ell b} \hat{\mathbf{s}} + \hat{\mathbf{P}}_{v+} \frac{T_p^{v\ell} T_p^{\ell b}}{N_\ell^2 N_b} (N_b^2 \sin \theta_0 \hat{\mathbf{z}} - N_\ell^2 W_b \hat{\kappa}) \right]. \quad (\text{B.4}) \quad [\text{eqapp:e2well}]$$

We first expand these equations for clarity. Substituting Eqs. (B.1) and (B.2) into Eq. (B.3),

$$\begin{aligned} \mathbf{e}_\ell^{2\omega} = & \hat{\mathbf{e}}^{\text{out}} \cdot \left[\hat{\mathbf{s}} T_s^{v\ell} R_s^{M+} (-\sin \phi \hat{x} + \cos \phi \hat{y}) \right. \\ & \left. + \hat{\mathbf{P}}_{v+} \frac{T_p^{v\ell}}{N_\ell} (\sin \theta_0 R_p^{M+} \hat{\mathbf{z}} - W_\ell R_p^{M-} \cos \phi \hat{x} - W_\ell R_p^{M-} \sin \phi \hat{y}) \right]. \end{aligned}$$

We now have $\mathbf{e}_\ell^{2\omega}$ in terms of $\hat{\mathbf{P}}_{v+}$,

$$\mathbf{e}_\ell^{2\omega} = \frac{T_p^{v\ell}}{N_\ell} (\sin \theta_0 R_p^{M+} \hat{\mathbf{z}} - W_\ell R_p^{M-} \cos \phi \hat{x} - W_\ell R_p^{M-} \sin \phi \hat{y}), \quad (\text{B.5}) \quad [\text{eqapp:e2wpmr}]$$

and in terms of $\hat{\mathbf{s}}$,

$$\mathbf{e}_\ell^{2\omega} = T_s^{v\ell} R_s^{M+} (-\sin \phi \hat{x} + \cos \phi \hat{y}). \quad (\text{B.6}) \quad [\text{eqapp:e2wsmr}]$$

If we wish to neglect the effects from the multiple reflections, we do the exact same for Eq. (B.4), and get the following term for $\hat{\mathbf{P}}_{v+}$,

$$\mathbf{e}_\ell^{2\omega} = \frac{T_p^{v\ell} T_p^{\ell b}}{N_\ell^2 N_b} (N_b^2 \sin \theta_0 \hat{\mathbf{z}} - N_\ell^2 W_b \cos \phi \hat{x} - N_\ell^2 W_b \sin \phi \hat{y}), \quad (\text{B.7}) \quad [\text{eqapp:e2wp}]$$

and $\hat{\mathbf{s}}$,

$$\mathbf{e}_\ell^{2\omega} = T_s^{v\ell} T_s^{\ell b} [-\sin \phi \hat{x} + \cos \phi \hat{y}]. \quad (\text{B.8}) \quad [\text{eqapp:e2ws}]$$

B.1.2 1ω terms

We have that the \mathbf{e}_ℓ^ω term is

$$\mathbf{e}_\ell^\omega = \left[\hat{\mathbf{s}} t_s^{v\ell} r_s^{M+} \hat{\mathbf{s}} + \frac{t_p^{v\ell}}{n_\ell} (r_p^{M+} \sin \theta_0 \hat{\mathbf{z}} + r_p^{M-} w_\ell \hat{\boldsymbol{\kappa}}) \hat{\mathbf{p}}_{v-} \right] \cdot \hat{\mathbf{e}}^{\text{in}}.$$

We are interested in finding $\mathbf{e}_\ell^\omega \mathbf{e}_\ell^\omega$ for both polarizations. For $\hat{\mathbf{e}}^{\text{in}} = \hat{\mathbf{p}}_{v-}$ we have

$$\mathbf{e}_\ell^\omega = \frac{t_p^{v\ell}}{n_\ell} (r_p^{M+} \sin \theta_0 \hat{\mathbf{z}} + r_p^{M-} w_\ell \cos \phi \hat{\mathbf{x}} + r_p^{M-} w_\ell \sin \phi \hat{\mathbf{y}}),$$

so

$$\begin{aligned} \mathbf{e}_\ell^\omega \mathbf{e}_\ell^\omega &= \left(\frac{t_p^{v\ell}}{n_\ell} \right)^2 \left((r_p^{M-})^2 w_\ell^2 \cos^2 \phi \hat{\mathbf{x}} \hat{\mathbf{x}} + 2(r_p^{M-})^2 w_\ell^2 \sin \phi \cos \phi \hat{\mathbf{x}} \hat{\mathbf{y}} \right. \\ &\quad + 2r_p^{M+} r_p^{M-} w_\ell \sin \theta_0 \cos \phi \hat{\mathbf{x}} \hat{\mathbf{z}} + (r_p^{M-})^2 w_\ell^2 \sin^2 \phi \hat{\mathbf{y}} \hat{\mathbf{y}} \\ &\quad \left. + 2r_p^{M+} r_p^{M-} w_\ell \sin \theta_0 \sin \phi \hat{\mathbf{z}} \hat{\mathbf{y}} + (r_p^{M+})^2 \sin^2 \theta_0 \hat{\mathbf{z}} \hat{\mathbf{z}} \right), \end{aligned} \quad (\text{B.9}) \quad [\text{eqapp:ewewpm}]$$

and for $\hat{\mathbf{e}}^{\text{in}} = \hat{\mathbf{s}}$,

$$\mathbf{e}_\ell^\omega \mathbf{e}_\ell^\omega = \left(t_s^{v\ell} r_s^{M+} \right)^2 (\sin^2 \phi \hat{\mathbf{x}} \hat{\mathbf{x}} + \cos^2 \phi \hat{\mathbf{y}} \hat{\mathbf{y}} - 2 \sin \phi \cos \phi \hat{\mathbf{x}} \hat{\mathbf{y}}). \quad (\text{B.10}) \quad [\text{eqapp:ewewsm}]$$

Neglecting the effects of the multiple reflections for the \mathbf{e}_ℓ^ω term yields

$$\mathbf{e}_\ell^\omega = \left[\hat{\mathbf{s}} t_s^{v\ell} t_s^{\ell b} \hat{\mathbf{s}} + \frac{t_p^{v\ell} t_p^{\ell b}}{n_\ell^2 n_b} (n_b^2 \sin \theta_0 \hat{\mathbf{z}} + n_\ell^2 w_b \hat{\boldsymbol{\kappa}}) \hat{\mathbf{p}}_{v-} \right] \cdot \hat{\mathbf{e}}^{\text{in}}.$$

For all cases, we require a $\mathbf{e}_\ell^\omega \mathbf{e}_\ell^\omega$ product. For brevity, we will directly list these terms for both polarizations. For $\hat{\mathbf{e}}^{\text{in}} = \hat{\mathbf{p}}_{v-}$,

$$\begin{aligned} \mathbf{e}_\ell^\omega \mathbf{e}_\ell^\omega &= \left(\frac{t_p^{v\ell} t_p^{\ell b}}{n_\ell^2 n_b} \right)^2 (n_\ell^4 w_b^2 \cos^2 \phi \hat{\mathbf{x}} \hat{\mathbf{x}} + 2n_\ell^4 w_b^2 \sin \phi \cos \phi \hat{\mathbf{x}} \hat{\mathbf{y}} \\ &\quad + 2n_\ell^2 n_b^2 w_b \sin \theta_0 \cos \phi \hat{\mathbf{x}} \hat{\mathbf{z}} + n_\ell^4 w_b^2 \sin^2 \phi \hat{\mathbf{y}} \hat{\mathbf{y}} \\ &\quad + 2n_\ell^2 n_b^2 w_b \sin \theta_0 \sin \phi \hat{\mathbf{y}} \hat{\mathbf{z}} + n_b^4 \sin^2 \theta_0 \hat{\mathbf{z}} \hat{\mathbf{z}}), \end{aligned} \quad (\text{B.11}) \quad [\text{eqapp:ewewp}]$$

and for $\hat{\mathbf{e}}^{\text{in}} = \hat{\mathbf{s}}$,

$$\mathbf{e}_\ell^\omega \mathbf{e}_\ell^\omega = \left(t_s^{v\ell} t_s^{\ell b} \right)^2 (\sin^2 \phi \hat{\mathbf{x}} \hat{\mathbf{x}} + \cos^2 \phi \hat{\mathbf{y}} \hat{\mathbf{y}} - 2 \sin \phi \cos \phi \hat{\mathbf{x}} \hat{\mathbf{y}}). \quad (\text{B.12}) \quad [\text{eqapp:ewews}]$$

We summarize these expressions in Table B.1. In order to derive the equations for a given polarization case, we refer to the equations listed there. Then it is simply a matter of multiplying the terms correctly and obtaining the appropriate components of $\chi(-2\omega; \omega, \omega)$.

B.1.3 Nonzero components of $\chi(-2\omega; \omega, \omega)$

For a (111) surface with C_{3v} symmetry, we have the following nonzero components:

$$\begin{aligned}\chi_{xxx} &= -\chi_{xyy} = -\chi_{yyx}, \\ \chi_{xxz} &= \chi_{yyz}, \\ \chi_{zxx} &= \chi_{zyy}, \\ \chi_{zzz}.\end{aligned}\tag{B.13} \quad \boxed{\text{eqapp:nonzer}}$$

For a (110) surface with C_{2v} symmetry, we have the following nonzero components:

$$\chi_{xxz}, \chi_{yyz}, \chi_{zxx}, \chi_{zyy}, \chi_{zzz}.\tag{B.14} \quad \boxed{\text{eqapp:nonzer}}$$

Lastly, for a (001) surface with C_{4v} symmetry, we have the following nonzero components:

$$\begin{aligned}\chi_{xxz} &= \chi_{yyz}, \\ \chi_{zxx} &= \chi_{zyy}, \\ \chi_{zzz}.\end{aligned}\tag{B.15} \quad \boxed{\text{eqapp:nonzer}}$$

Case	$\hat{\mathbf{e}}^{\text{out}}$	$\hat{\mathbf{e}}^{\text{in}}$	$\mathbf{e}_\ell^{2\omega}$	$\mathbf{e}_\ell^\omega \mathbf{e}_\ell^\omega$
\mathcal{R}_{pP}	$\hat{\mathbf{P}}_{v+}$	$\hat{\mathbf{p}}_{v-}$	Eq. (B.5) or (B.7) eqapp:e2w eqapp e2wp	Eq. (B.9) or Eq. (B.11) eqapp:ewewpmr eqapp eqapp:ewwp
\mathcal{R}_{pS}	$\hat{\mathbf{s}}$	$\hat{\mathbf{p}}_{v-}$	Eq. (B.6) or (B.8) eqapp:e2w eqapp e2ws	Eq. (B.9) or Eq. (B.11) eqapp:ewewpmr eqapp eqapp:ewwp
\mathcal{R}_{sP}	$\hat{\mathbf{P}}_{v+}$	$\hat{\mathbf{s}}$	Eq. (B.5) or (B.7) eqapp:e2w eqapp e2wp	Eq. (B.10) or Eq. (B.12) eqapp:ewewsmr eqapp eqapp:ewews
\mathcal{R}_{sS}	$\hat{\mathbf{s}}$	$\hat{\mathbf{s}}$	Eq. (B.6) or (B.8) eqapp:e2w eqapp e2ws	Eq. (B.10) or Eq. (B.12) eqapp:ewewsmr eqapp eqapp:ewews

Table B.1: Polarization unit vectors for $\hat{\mathbf{e}}^{\text{out}}$ and $\hat{\mathbf{e}}^{\text{in}}$, and equations describing $\mathbf{e}_\ell^{2\omega}$ and $\mathbf{e}_\ell^\omega \mathbf{e}_\ell^\omega$ for each polarization case. When there are two equations to choose from, the former includes the effects of multiple reflections, and the latter neglects them.

`tab:review`

B.2 \mathcal{R}_{pP}

Per Table B.1, \mathcal{R}_{pP} requires Eqs. (B.5) and (B.9). After some algebra, we obtain that

$$\Upsilon_{pP}^{\text{MR}} = \Gamma_{pP}^{\text{MR}} \left[-R_p^{M-} (r_p^{M-})^2 w_\ell^2 W_\ell \cos^3 \phi \chi_{xxx} \right. \\ - 2R_p^{M-} (r_p^{M-})^2 w_\ell^2 W_\ell \sin \phi \cos^2 \phi \chi_{xxy} \\ - 2R_p^{M-} r_p^{M+} r_p^{M-} w_\ell W_\ell \sin \theta_0 \cos^2 \phi \chi_{xxz} \\ - R_p^{M-} (r_p^{M-})^2 w_\ell^2 W_\ell \sin^2 \phi \cos \phi \chi_{xyy} \\ - 2R_p^{M-} r_p^{M+} r_p^{M-} w_\ell W_\ell \sin \theta_0 \sin \phi \cos \phi \chi_{xyz} \\ - R_p^{M-} (r_p^{M+})^2 W_\ell \sin^2 \theta_0 \cos \phi \chi_{xzz} \\ - R_p^{M-} (r_p^{M-})^2 w_\ell^2 W_\ell \sin \phi \cos^2 \phi \chi_{yxx} \\ - 2R_p^{M-} (r_p^{M-})^2 w_\ell^2 W_\ell \sin^2 \phi \cos \phi \chi_{yxy} \\ - 2R_p^{M-} r_p^{M+} r_p^{M-} w_\ell W_\ell \sin \theta_0 \sin \phi \cos \phi \chi_{yxz} \\ - R_p^{M-} (r_p^{M-})^2 w_\ell^2 W_\ell \sin^3 \phi \chi_{yyy} \\ - 2R_p^{M-} r_p^{M+} r_p^{M-} w_\ell W_\ell \sin \theta_0 \sin^2 \phi \chi_{yyz} \\ - R_p^{M-} (r_p^{M+})^2 W_\ell \sin^2 \theta_0 \sin \phi \chi_{yzz} \\ + R_p^{M+} (r_p^{M-})^2 w_\ell^2 \sin \theta_0 \cos^2 \phi \chi_{zxx} \\ + 2R_p^{M+} r_p^{M+} r_p^{M-} w_\ell \sin^2 \theta_0 \cos \phi \chi_{zxz} \\ + 2R_p^{M+} (r_p^{M-})^2 w_\ell^2 \sin \theta_0 \sin \phi \cos \phi \chi_{zxy} \\ + R_p^{M+} (r_p^{M-})^2 w_\ell^2 \sin \theta_0 \sin^2 \phi \chi_{zyy} \\ + 2R_p^{M+} r_p^{M+} r_p^{M-} w_\ell \sin^2 \theta_0 \sin \phi \chi_{zzy} \\ \left. + R_p^{M+} (r_p^{M+})^2 \sin^3 \theta_0 \chi_{zzz} \right], \quad (\text{B.16}) \quad [\text{eqapp:rppfull}]$$

We take this opportunity to introduce a quantity that will be repeated throughout this section,

$$\Gamma_{pP}^{\text{MR}} = \frac{T_p^{v\ell}}{N_\ell} \left(\frac{t_p^{v\ell}}{n_\ell} \right)^2. \quad (\text{B.17}) \quad [\text{eqapp:gammapp}]$$

If we neglect the multiple reflections, as described in the manuscript, we have that

$$\begin{aligned}
\Upsilon_{pP} = \Gamma_{pP} & \left[-N_\ell^2 W_b \left(+ n_\ell^4 w_b^2 \cos^3 \phi \chi_{xxx} + 2n_\ell^4 w_b^2 \sin \phi \cos^2 \phi \chi_{xxy} \right. \right. \\
& + 2n_b^2 n_\ell^2 w_b \sin \theta_0 \cos^2 \phi \chi_{xxz} + n_\ell^4 w_b^2 \sin^2 \phi \cos \phi \chi_{xyy} \\
& \left. \left. + 2n_b^2 n_\ell^2 w_b \sin \theta_0 \sin \phi \cos \phi \chi_{xyz} + n_b^4 \sin^2 \theta_0 \cos \phi \chi_{xzz} \right) \right. \\
& - N_\ell^2 W_b \left(+ n_\ell^4 w_b^2 \sin \phi \cos^2 \phi \chi_{yxx} + 2n_\ell^4 w_b^2 \sin^2 \phi \cos \phi \chi_{xyy} \right. \\
& + 2n_b^2 n_\ell^2 w_b \sin \theta_0 \sin \phi \cos \phi \chi_{yxz} + n_\ell^4 w_b^2 \sin^3 \phi \chi_{yyy} \\
& \left. \left. + 2n_b^2 n_\ell^2 w_b \sin \theta_0 \sin^2 \phi \chi_{yyz} + n_b^4 \sin^2 \theta_0 \sin \phi \chi_{yzz} \right) \right. \\
& + N_b^2 \sin \theta_0 \left(+ n_\ell^4 w_b^2 \cos^2 \phi \chi_{zxx} + 2n_\ell^4 w_b^2 \sin \phi \cos \phi \chi_{zxy} \right. \\
& + n_\ell^4 w_b^2 \sin^2 \phi \chi_{zyy} + 2n_\ell^2 n_b^2 w_b \sin \theta_0 \cos \phi \chi_{zzx} \\
& \left. \left. + 2n_\ell^2 n_b^2 w_b \sin \theta_0 \sin \phi \chi_{zzy} + n_b^4 \sin^2 \theta_0 \chi_{zzz} \right) \right], \tag{B.18} \quad \boxed{\text{eqapp:rppfull}}
\end{aligned}$$

and again we introduce a quantity that will be repeated throughout this section,

$$\Gamma_{pP} = \frac{T_p^{v\ell} T_p^{\ell b}}{N_\ell^2 N_b} \left(\frac{t_p^{v\ell} t_p^{\ell b}}{n_\ell^2 n_b} \right)^2. \tag{B.19} \quad \boxed{\text{gammapp}}$$

B.2.1 For the (111) surface

We take Eqs. (B.16) and (B.13), eliminate the components that do not contribute, and apply the symmetry relations as follows,

$$\begin{aligned}
\Upsilon_{pP}^{\text{MR},(111)} = \Gamma_{pP}^{\text{MR}} & \left[-R_p^{M-} (r_p^{M-})^2 w_\ell^2 W_\ell \cos^3 \phi \chi_{xxx} \right. \\
& + R_p^{M-} (r_p^{M-})^2 w_\ell^2 W_\ell \sin^2 \phi \cos \phi \chi_{xxx} \\
& + 2R_p^{M-} (r_p^{M-})^2 w_\ell^2 W_\ell \sin^2 \phi \cos \phi \chi_{xxx} \\
& - 2R_p^{M-} r_p^{M+} r_p^{M-} w_\ell W_\ell \sin \theta_0 \cos^2 \phi \chi_{xxz} \\
& - 2R_p^{M-} r_p^{M+} r_p^{M-} w_\ell W_\ell \sin \theta_0 \sin^2 \phi \chi_{xxz} \\
& + R_p^{M+} (r_p^{M-})^2 w_\ell^2 \sin \theta_0 \cos^2 \phi \chi_{zxx} \\
& + R_p^{M+} (r_p^{M-})^2 w_\ell^2 \sin \theta_0 \sin^2 \phi \chi_{zxx} \\
& \left. + R_p^{M+} (r_p^{M+})^2 \sin^3 \theta_0 \chi_{zzz} \right]. \tag{B.16} \quad \boxed{\text{eqapp:rppfull}\atop\text{eqapp:nonzero111}}
\end{aligned}$$

We reduce terms,

$$\begin{aligned}
\Upsilon_{pP}^{\text{MR},(111)} &= \Gamma_{pP}^{\text{MR}} \left[R_p^{M-} (r_p^{M-})^2 w_\ell^2 W_\ell (3 \sin^2 \phi \cos \phi - \cos^3 \phi) \chi_{xxx} \right. \\
&\quad - 2R_p^{M-} r_p^{M+} r_p^{M-} w_\ell W_\ell \sin \theta_0 (\sin^2 \phi + \cos^2 \phi) \chi_{xxz} \\
&\quad + R_p^{M+} (r_p^{M+})^2 w_\ell^2 \sin \theta_0 (\sin^2 \phi + \cos^2 \phi) \chi_{zxx} \\
&\quad \left. + R_p^{M+} (r_p^{M+})^2 \sin^3 \theta_0 \chi_{zzz} \right] \\
&= \Gamma_{pP}^{\text{MR}} \left[R_p^{M+} \sin \theta_0 \left((r_p^{M+})^2 \sin^2 \theta_0 \chi_{zzz} + (r_p^{M-})^2 w_\ell^2 \chi_{zxx} \right) \right. \\
&\quad \left. - R_p^{M-} w_\ell W_\ell \left(2r_p^{M+} r_p^{M-} \sin \theta_0 \chi_{xxz} + (r_p^{M-})^2 w_\ell \chi_{xxx} \cos 3\phi \right) \right] \\
&= \Gamma_{pP}^{\text{MR}} r_{pP}^{\text{MR},(111)},
\end{aligned}$$

where

$$\begin{aligned}
r_{pP}^{\text{MR},(111)} &= R_p^{M+} \sin \theta_0 \left((r_p^{M+})^2 \sin^2 \theta_0 \chi_{zzz} + (r_p^{M-})^2 w_\ell^2 \chi_{zxx} \right) \\
&\quad - R_p^{M-} w_\ell W_\ell \left(2r_p^{M+} r_p^{M-} \sin \theta_0 \chi_{xxz} + (r_p^{M-})^2 w_\ell \chi_{xxx} \cos 3\phi \right).
\end{aligned} \tag{B.20} \quad \boxed{\text{eqapp:final-}}$$

If we wish to neglect the effects of the multiple reflections, we follow the exact same procedure but starting with Eq. (B.18),

$$\begin{aligned}
\Upsilon_{pP}^{(111)} &= \Gamma_{pP} \left[+ n_b^4 N_b^2 \sin^3 \theta_0 \chi_{zzz} \right. \\
&\quad + n_\ell^4 N_b^2 w_b^2 \sin \theta_0 \cos^2 \phi \chi_{zxx} \\
&\quad + n_\ell^4 N_b^2 w_b^2 \sin \theta_0 \sin^2 \phi \chi_{zxx} \\
&\quad - 2n_b^2 n_\ell^2 N_\ell^2 w_b W_b \sin \theta_0 \cos^2 \phi \chi_{xxz} \\
&\quad - 2n_b^2 n_\ell^2 N_\ell^2 w_b W_b \sin \theta_0 \sin^2 \phi \chi_{xxz} \\
&\quad - n_\ell^4 N_\ell^2 w_b^2 W_b \cos^3 \phi \chi_{xxx} \\
&\quad + n_\ell^4 N_\ell^2 w_b^2 W_b \sin^2 \phi \cos \phi \chi_{xxx} \\
&\quad \left. + 2n_\ell^4 N_\ell^2 w_b^2 W_b \sin^2 \phi \cos \phi \chi_{xxx} \right],
\end{aligned}$$

and reduce,

$$\begin{aligned}
\Upsilon_{pP}^{(111)} &= \Gamma_{pP} \left[+ n_b^4 N_b^2 \sin^3 \theta_0 \chi_{zzz} \right. \\
&\quad + n_\ell^4 N_b^2 w_b^2 \sin \theta_0 (\sin^2 \phi + \cos^2 \phi) \chi_{zxx} \\
&\quad - 2n_b^2 n_\ell^2 N_\ell^2 w_b W_b \sin \theta_0 (\sin^2 \phi + \cos^2 \phi) \phi \chi_{xxz} \\
&\quad \left. + n_\ell^4 N_\ell^2 w_b^2 W_b (3 \sin^2 \phi \cos \phi - \cos^3 \phi) \chi_{xxx} \right] \\
&= \Gamma_{pP} \left[N_b^2 \sin \theta_0 (n_b^4 \sin^2 \theta_0 \chi_{zzz} + n_\ell^4 w_b^2 \chi_{zxx}) \right. \\
&\quad \left. - n_\ell^2 N_\ell^2 w_b W_b (2n_b^2 \sin \theta_0 \chi_{xxz} + n_\ell^2 w_b \chi_{xxx} \cos 3\phi) \right] \\
&= \Gamma_{pP} r_{pP}^{(111)},
\end{aligned}$$

where

$$\begin{aligned}
r_{pP}^{(111)} &= N_b^2 \sin \theta_0 (n_b^4 \sin^2 \theta_0 \chi_{zzz} + n_\ell^4 w_b^2 \chi_{zxx}) \\
&\quad - n_\ell^2 N_\ell^2 w_b W_b (2n_b^2 \sin \theta_0 \chi_{xxz} + n_\ell^2 w_b \chi_{xxx} \cos 3\phi).
\end{aligned} \tag{B.21} \boxed{\text{eqapp:final-}}$$

B.2.2 For the (110) surface

We take Eqs. (B.16) and (B.14), eliminate the components that do not contribute, and apply the symmetry relations as follows,

$$\begin{aligned}
\Upsilon_{pP}^{\text{MR},(110)} &= \Gamma_{pP}^{\text{MR}} \left[R_p^{M+} (r_p^{M+})^2 \sin^3 \theta_0 \chi_{zzz} \right. \\
&\quad + R_p^{M+} (r_p^{M-})^2 w_\ell^2 \sin \theta_0 \sin^2 \phi \chi_{zyy} \\
&\quad + R_p^{M+} (r_p^{M-})^2 w_\ell^2 \sin \theta_0 \cos^2 \phi \chi_{zxx} \\
&\quad - 2R_p^{M-} r_p^{M+} r_p^{M-} w_\ell W_\ell \sin \theta_0 \sin^2 \phi \chi_{yyz} \\
&\quad \left. - 2R_p^{M-} r_p^{M+} r_p^{M-} w_\ell W_\ell \sin \theta_0 \cos^2 \phi \chi_{xxz} \right] \\
&= \Gamma_{pP}^{\text{MR}} \left[R_p^{M+} \sin \theta_0 \left((r_p^{M+})^2 \sin^2 \theta_0 \chi_{zzz} \right. \right. \\
&\quad + (r_p^{M-})^2 w_\ell^2 \left(\frac{1}{2}(1 - \cos 2\phi) \chi_{zyy} + \frac{1}{2}(\cos 2\phi + 1) \chi_{zxx} \right) \left. \right) \\
&\quad - 2R_p^{M-} r_p^{M+} r_p^{M-} w_\ell W_\ell \sin \theta_0 \left(\frac{1}{2}(1 - \cos 2\phi) \chi_{yyz} \right. \\
&\quad \left. \left. + \frac{1}{2}(\cos 2\phi + 1) \chi_{xxz} \right) \right] \\
&= \Gamma_{pP}^{\text{MR}} \left[R_p^{M+} \sin \theta_0 \left((r_p^{M+})^2 \sin^2 \theta_0 \chi_{zzz} \right. \right. \\
&\quad + (r_p^{M-})^2 w_\ell^2 \left(\frac{\chi_{zyy} + \chi_{zxx}}{2} + \frac{\chi_{zyy} - \chi_{zxx}}{2} \cos 2\phi \right) \left. \right) \\
&\quad - 2R_p^{M-} r_p^{M+} r_p^{M-} w_\ell W_\ell \sin \theta_0 \left(\frac{\chi_{yyz} + \chi_{xxz}}{2} + \frac{\chi_{yyz} - \chi_{xxz}}{2} \cos 2\phi \right) \right] \\
&= \Gamma_{pP}^{\text{MR}} r_{pP}^{\text{MR},(110)},
\end{aligned}$$

where

$$\begin{aligned}
r_{pP}^{\text{MR},(110)} &= R_p^{M+} \sin \theta_0 \left((r_p^{M+})^2 \sin^2 \theta_0 \chi_{zzz} \right. \\
&\quad + (r_p^{M-})^2 w_\ell^2 \left(\frac{\chi_{zyy} + \chi_{zxx}}{2} + \frac{\chi_{zyy} - \chi_{zxx}}{2} \cos 2\phi \right) \left. \right) \\
&\quad - 2R_p^{M-} r_p^{M+} r_p^{M-} w_\ell W_\ell \sin \theta_0 \left(\frac{\chi_{yyz} + \chi_{xxz}}{2} + \frac{\chi_{yyz} - \chi_{xxz}}{2} \cos 2\phi \right).
\end{aligned} \tag{B.22} \quad [\text{eqapp:final-}]$$

If we wish to neglect the effects of the multiple reflections, we follow the exact same procedure

but starting with Eq. (B.18),

$$\begin{aligned}
\Upsilon_{pP}^{(110)} &= \Gamma_{pP} \left[N_b^2 \sin \theta_0 \left(n_b^4 \sin^2 \theta_0 \chi_{zzz} + n_\ell^4 w_b^2 (\sin^2 \phi \chi_{zyy} + \cos^2 \phi \chi_{zxx}) \right) \right. \\
&\quad \left. - 2n_b^2 n_\ell^2 N_\ell^2 w_b W_b \sin \theta_0 (\sin^2 \phi \chi_{yyz} + \cos^2 \phi \chi_{xxz}) \right] \\
&= \Gamma_{pP} \left[N_b^2 \sin \theta_0 \left(n_b^4 \sin^2 \theta_0 \chi_{zzz} \right. \right. \\
&\quad \left. + n_\ell^4 w_b^2 \left(\frac{\chi_{zyy} + \chi_{zxx}}{2} + \frac{\chi_{zyy} - \chi_{zxx}}{2} \cos 2\phi \right) \right) \\
&\quad \left. - 2n_b^2 n_\ell^2 N_\ell^2 w_b W_b \sin \theta_0 \left(\frac{\chi_{yyz} + \chi_{xxz}}{2} + \frac{\chi_{yyz} - \chi_{xxz}}{2} \cos 2\phi \right) \right] \\
&= \Gamma_{pP} r_{pP}^{(110)},
\end{aligned}$$

where

$$\begin{aligned}
r_{pP}^{(110)} &= N_b^2 \sin \theta_0 \left[n_b^4 \sin^2 \theta_0 \chi_{zzz} + n_\ell^4 w_b^2 \left(\frac{\chi_{zyy} + \chi_{zxx}}{2} + \frac{\chi_{zyy} - \chi_{zxx}}{2} \cos 2\phi \right) \right] \\
&\quad - 2n_b^2 n_\ell^2 N_\ell^2 w_b W_b \sin \theta_0 \left(\frac{\chi_{yyz} + \chi_{xxz}}{2} + \frac{\chi_{yyz} - \chi_{xxz}}{2} \cos 2\phi \right). \tag{B.23} \quad \text{[eqapp:final-]}
\end{aligned}$$

B.2.3 For the (001) surface

We take Eqs. (B.16) and (B.14), eliminate the components that do not contribute, and apply the symmetry relations as follows,

$$\begin{aligned}
\Upsilon_{pP}^{\text{MR},(001)} &= \Gamma_{pP}^{\text{MR}} \left[R_p^{M+} (r_p^{M+})^2 \sin^3 \theta_0 \chi_{zzz} \right. \\
&\quad + R_p^{M+} (r_p^{M-})^2 w_\ell^2 \sin \theta_0 \sin^2 \phi \chi_{zxx} \\
&\quad + R_p^{M+} (r_p^{M-})^2 w_\ell^2 \sin \theta_0 \cos^2 \phi \chi_{zxx} \\
&\quad - 2R_p^{M-} r_p^{M+} r_p^{M-} w_\ell W_\ell \sin \theta_0 \sin^2 \phi \chi_{xxz} \\
&\quad \left. - 2R_p^{M-} r_p^{M+} r_p^{M-} w_\ell W_\ell \sin \theta_0 \cos^2 \phi \chi_{xxz} \right] \\
&= \Gamma_{pP}^{\text{MR}} \left[R_p^{M+} \sin \theta_0 \left((r_p^{M+})^2 \sin^2 \theta_0 \chi_{zzz} + (r_p^{M-})^2 w_\ell^2 \chi_{zxx} \right) \right. \\
&\quad \left. - 2R_p^{M-} r_p^{M+} r_p^{M-} w_\ell W_\ell \sin \theta_0 \chi_{xxz} \right] \\
&= \Gamma_{pP}^{\text{MR}} r_{pP}^{\text{MR},(001)},
\end{aligned}$$

where

$$r_{pP}^{\text{MR},(001)} = R_p^{M+} \sin \theta_0 \left((r_p^{M+})^2 \sin^2 \theta_0 \chi_{zzz} + (r_p^{M-})^2 w_\ell^2 \chi_{zxx} \right) - 2R_p^{M-} r_p^{M+} r_p^{M-} w_\ell W_\ell \sin \theta_0 \chi_{xxz}, \quad (\text{B.24}) \quad [\text{eqapp:final}]$$

If we wish to neglect the effects of the multiple reflections, we follow the exact same procedure but starting with Eq. (B.18),

$$\begin{aligned} \Upsilon_{pP}^{(001)} &= \Gamma_{pP} [N_b^2 \sin \theta_0 (n_b^4 \sin^2 \theta_0 \chi_{zzz} + n_\ell^4 w_b^2 \chi_{zxx}) \\ &\quad - 2n_b^2 n_\ell^2 N_\ell^2 w_b W_b \sin \theta_0 \chi_{xxz}] \\ &= \Gamma_{pP} r_{pp}^{(001)}, \end{aligned}$$

where

$$r_{pP}^{(001)} = N_b^2 \sin \theta_0 (n_b^4 \sin^2 \theta_0 \chi_{zzz} + n_\ell^4 w_b^2 \chi_{zxx}) - 2n_b^2 n_\ell^2 N_\ell^2 w_b W_b \sin \theta_0 \chi_{xxz}. \quad (\text{B.25}) \quad [\text{eqapp:final}]$$

B.3 \mathcal{R}_{pS}

Per Table B.1, \mathcal{R}_{pS} requires Eqs. (B.6) and (B.9). After some algebra, we obtain that

$$\begin{aligned} \Upsilon_{pS}^{\text{MR}} &= \Gamma_{pS}^{\text{MR}} [- (r_p^{M-})^2 w_\ell^2 \sin \phi \cos^2 \phi \chi_{xxx} - 2(r_p^{M-})^2 w_\ell^2 \sin^2 \phi \cos \phi \chi_{xxy} \\ &\quad - 2r_p^{M+} r_p^{M-} w_\ell \sin \theta_0 \sin \phi \cos \phi \chi_{xxz} - (r_p^{M-})^2 w_\ell^2 \sin^3 \phi \chi_{xyy} \\ &\quad - 2r_p^{M+} r_p^{M-} w_\ell \sin \theta_0 \sin^2 \phi \chi_{xzy} - (r_p^{M+})^2 \sin^2 \theta_0 \sin \phi \chi_{xzz} \\ &\quad + (r_p^{M-})^2 w_\ell^2 \cos^3 \phi \chi_{yxx} + 2(r_p^{M-})^2 w_\ell^2 \sin \phi \cos^2 \phi \chi_{yxy} \\ &\quad + 2r_p^{M+} r_p^{M-} w_\ell \sin \theta_0 \cos^2 \phi \chi_{yxz} + (r_p^{M-})^2 w_\ell^2 \sin^2 \phi \cos \phi \chi_{yyy} \\ &\quad + 2r_p^{M+} r_p^{M-} w_\ell \sin \theta_0 \sin \phi \cos \phi \chi_{yzy} + (r_p^{M+})^2 \sin^2 \theta_0 \cos \phi \chi_{yzz}]. \end{aligned} \quad (\text{B.26}) \quad [\text{eqapp:rpsful}]$$

We take this opportunity to introduce a quantity that will be repeated throughout this section,

$$\Gamma_{pS}^{\text{MR}} = T_s^{v\ell} R_s^{M+} \left(\frac{t_p^{v\ell}}{n_\ell} \right)^2 \quad (\text{B.27}) \quad [\text{eqapp:gammapp}]$$

If we neglect the multiple reflections, as described in the manuscript, we have that

$$\begin{aligned} \Upsilon_{pS} &= \Gamma_{pS} [- n_\ell^4 w_b^2 \sin \phi \cos^2 \phi \chi_{xxx} - 2n_\ell^4 w_b^2 \sin^2 \phi \cos \phi \chi_{xxy} \\ &\quad - 2n_\ell^2 n_b^2 w_b \sin \theta_0 \sin \phi \cos \phi \chi_{xxz} - n_\ell^4 w_b^2 \sin^3 \phi \chi_{xyy} \\ &\quad - 2n_\ell^2 n_b^2 w_b \sin \theta_0 \sin^2 \phi \chi_{xzy} - n_b^4 \sin^2 \theta_0 \sin \phi \chi_{xzz} \\ &\quad + n_\ell^4 w_b^2 \cos^3 \phi \chi_{yxx} + 2n_\ell^4 w_b^2 \sin \phi \cos^2 \phi \chi_{yxy} \\ &\quad + 2n_\ell^2 n_b^2 w_b \sin \theta_0 \cos^2 \phi \chi_{yxz} + n_\ell^4 w_b^2 \sin^2 \phi \cos \phi \chi_{yyy} \\ &\quad + 2n_\ell^2 n_b^2 w_b \sin \theta_0 \sin \phi \cos \phi \chi_{yzy} + n_b^4 \sin^2 \theta_0 \cos \phi \chi_{yzz}], \end{aligned} \quad (\text{B.28}) \quad [\text{eqapp:rpsful}]$$

and again we introduce a quantity that will be repeated throughout this section,

$$\Gamma_{pS} = T_s^{v\ell} T_s^{\ell b} \left(\frac{t_p^{v\ell} t_p^{\ell b}}{n_\ell^2 n_b} \right)^2. \quad (\text{B.29}) \quad [\text{eqapp:gammapp}]$$

B.3.1 For the (111) surface

We take Eqs. (B.26) and (B.13), eliminate the components that do not contribute, and apply the symmetry relations as follows,

$$\begin{aligned}\Upsilon_{pS}^{\text{MR},(111)} &= \Gamma_{pS}^{\text{MR}} [2r_p^{M+}r_p^{M-}w_\ell \sin \theta_0 \sin \phi \cos \phi \chi_{xxz} \\ &\quad - 2r_p^{M+}r_p^{M-}w_\ell \sin \theta_0 \sin \phi \cos \phi \chi_{xxz} \\ &\quad - (r_p^{M-})^2 w_\ell^2 \sin \phi \cos^2 \phi \chi_{xxx} \\ &\quad - 2(r_p^{M-})^2 w_\ell^2 \sin \phi \cos^2 \phi \chi_{xxx} \\ &\quad + (r_p^{M-})^2 w_\ell^2 \sin^3 \phi \chi_{xxx}].\end{aligned}$$

We reduce terms,

$$\begin{aligned}\Upsilon_{pS}^{\text{MR},(111)} &= \Gamma_{pS}^{\text{MR}} [(r_p^{M-})^2 w_\ell^2 (\sin^3 \phi - 3 \sin \phi \cos^2 \phi) \chi_{xxx}] \\ &= \Gamma_{pS}^{\text{MR}} [-(r_p^{M-})^2 w_\ell^2 \chi_{xxx} \sin 3\phi] \\ &= \Gamma_{pS}^{\text{MR}} r_{pS}^{\text{MR},(111)},\end{aligned}$$

where

$$r_{pS}^{\text{MR},(111)} = -(r_p^{M-})^2 w_\ell^2 \chi_{xxx} \sin 3\phi. \quad (\text{B.30}) \quad [\text{eqapp:final-}]$$

If we wish to neglect the effects of the multiple reflections, we follow the exact same procedure but starting with Eq. (B.28),

$$\begin{aligned}\Upsilon_{pS} &= \Gamma_{pS} [n_\ell^4 w_b^2 (\sin^3 \phi - 3 \sin \phi \cos^2 \phi) \chi_{xxx}] \\ &= \Gamma_{pS} [- n_\ell^4 w_b^2 \chi_{xxx} \sin 3\phi] \\ &= \Gamma_{pS} r_{pS}^{(111)},\end{aligned} \quad (\text{B.31})$$

where

$$r_{pS}^{(111)} = -n_\ell^4 w_b^2 \chi_{xxx} \sin 3\phi, \quad (\text{B.32}) \quad [\text{eqapp:final-}]$$

and we use Γ_{pS} instead of Γ_{pS}^{MR} .

B.3.2 For the (110) surface

We take Eqs. (B.26) and (B.14), eliminate the components that do not contribute, and apply the symmetry relations as follows,

$$\begin{aligned}\Upsilon_{pS}^{\text{MR},(110)} &= \Gamma_{pS}^{\text{MR}} [2r_p^{M+}r_p^{M-}w_\ell \sin \theta_0 \sin \phi \cos \phi (\chi_{yyz} - \chi_{xxz})] \\ &= \Gamma_{pS}^{\text{MR}} [r_p^{M+}r_p^{M-}w_\ell \sin \theta_0 (\chi_{yyz} - \chi_{xxz}) \sin 2\phi] \\ &= \Gamma_{pS}^{\text{MR}} r_{pS}^{\text{MR},(110)}.\end{aligned}$$

where

$$r_{pS}^{\text{MR},(110)} = r_p^{M+} r_p^{M-} w_\ell \sin \theta_0 (\chi_{yyz} - \chi_{xxz}) \sin 2\phi. \quad (\text{B.33}) \quad [\text{eqapp:final-}]$$

If we neglect the effects of the multiple reflections as mentioned above, we have

$$r_{pS}^{(110)} = n_\ell^2 n_b^2 w_b \sin \theta_0 (\chi_{yyz} - \chi_{xxz}) \sin 2\phi, \quad (\text{B.34}) \quad [\text{eqapp:final-}]$$

and we use Γ_{pS} instead of Γ_{pS}^{MR} .

B.3.3 For the (001) surface

We take Eqs. (B.26) and (B.14), eliminate the components that do not contribute, and apply the symmetry relations as follows,

$$\begin{aligned} \Upsilon_{pS}^{\text{MR},(001)} &= \Gamma_{pS}^{\text{MR}} [-2r_p^{M+} r_p^{M-} w_\ell \sin \theta_0 \sin \phi \cos \phi \chi_{xxz} \\ &\quad + 2r_p^{M+} r_p^{M-} w_\ell \sin \theta_0 \sin \phi \cos \phi \chi_{xxz}] = 0. \end{aligned}$$

Neglecting the effects of multiple reflections will obviously yield the same result, thus

$$\Upsilon_{pS}^{\text{MR},(001)} = \Upsilon_{pS}^{(001)} = 0. \quad (\text{B.35}) \quad [\text{eqapp:final-}]$$

B.4 \mathcal{R}_{sP}

Per Table B.1, \mathcal{R}_{sP} requires Eqs. (B.5) and (B.10). After some algebra, we obtain that

$$\begin{aligned} \Upsilon_{sP}^{\text{MR}} &= \Gamma_{sP}^{\text{MR}} \left[R_p^{M-} W_\ell (-\sin^2 \phi \cos \phi \chi_{xxx} + 2 \sin \phi \cos^2 \phi \chi_{xxy} - \cos^3 \phi \chi_{xyy}) \right. \\ &\quad + R_p^{M-} W_\ell (-\sin^3 \phi \chi_{yxx} + 2 \sin^2 \phi \cos \phi \chi_{yyx} - \sin \phi \cos^2 \phi \chi_{yyy}) \\ &\quad \left. + R_p^{M+} \sin \theta_0 (\sin^2 \phi \chi_{zxx} - 2 \sin \phi \cos \phi \chi_{zxy} + \cos^2 \phi \chi_{zyy}) \right]. \end{aligned} \quad (\text{B.36}) \quad [\text{eqapp:rspful}]$$

We take this opportunity to introduce a quantity that will be repeated throughout this section,

$$\Gamma_{sP}^{\text{MR}} = \frac{T_p^{v\ell}}{N_\ell} \left(t_s^{v\ell} r_s^{M+} \right)^2 \quad (\text{B.37}) \quad [\text{eqapp:gammamr}]$$

If we neglect the multiple reflections, as described in the manuscript, we have that

$$\begin{aligned} \Upsilon_{sP} &= \Gamma_{sP} \left[N_\ell^2 W_b (-\sin^2 \phi \cos \phi \chi_{xxx} + 2 \sin \phi \cos^2 \phi \chi_{xxy} - \cos^3 \phi \chi_{xyy}) \right. \\ &\quad + N_\ell^2 W_b (-\sin^3 \phi \chi_{yxx} + 2 \sin^2 \phi \cos \phi \chi_{yyx} - \sin \phi \cos^2 \phi \chi_{yyy}) \\ &\quad \left. + N_b^2 \sin \theta_0 (+\sin^2 \phi \chi_{zxx} - 2 \sin \phi \cos \phi \chi_{zxy} + \cos^2 \phi \chi_{zyy}) \right], \end{aligned} \quad (\text{B.38}) \quad [\text{eqapp:rspful}]$$

and again we introduce a quantity that will be repeated throughout this section,

$$\Gamma_{sP} = \frac{T_p^{v\ell} T_p^{\ell b}}{N_\ell^2 N_b} \left(t_s^{v\ell} t_s^{\ell b} \right)^2. \quad (\text{B.39}) \quad [\text{eqapp:gammamr}]$$

B.4.1 For the (111) surface

We take Eqs. (B.36) and (B.13), eliminate the components that do not contribute, and apply the symmetry relations as follows,

$$\begin{aligned}\Upsilon_{sP}^{\text{MR},(111)} &= \Gamma_{sP}^{\text{MR}} \left[+ R_p^{M-} W_\ell \cos^3 \phi \chi_{xxx} \right. \\ &\quad - R_p^{M-} W_\ell \sin^2 \phi \cos \phi \chi_{xxx} \\ &\quad - 2R_p^{M-} W_\ell \sin^2 \phi \cos \phi \chi_{xxx} \\ &\quad + R_p^{M+} \sin \theta_0 \sin^2 \phi \chi_{zxx} \\ &\quad \left. + R_p^{M+} \sin \theta_0 \cos^2 \phi \chi_{zxx} \right].\end{aligned}$$

We reduce terms,

$$\begin{aligned}\Upsilon_{sP}^{\text{MR},(111)} &= \Gamma_{sP}^{\text{MR}} \left[R_p^{M-} W_\ell (\cos^3 \phi - 3 \sin^2 \phi \cos \phi) \chi_{xxx} \right. \\ &\quad \left. + R_p^{M+} \sin \theta_0 (\sin^2 \phi + \cos^2 \phi) \chi_{zxx} \right] \\ &= \Gamma_{sP}^{\text{MR}} \left[R_p^{M-} W_\ell \chi_{xxx} \cos 3\phi + R_p^{M+} \sin \theta_0 \chi_{zxx} \right] \\ &= \Gamma_{sP}^{\text{MR}} r_{sP}^{\text{MR},(111)},\end{aligned}$$

where

$$r_{sP}^{\text{MR},(111)} = R_p^{M+} \sin \theta_0 \chi_{zxx} + R_p^{M-} W_\ell \chi_{xxx} \cos 3\phi. \quad (\text{B.40})$$

If we wish to neglect the effects of the multiple reflections, we follow the exact same procedure but starting with Eq. (B.38),

$$\begin{aligned}\Upsilon_{sP}^{(111)} &= \Gamma_{sP} \left[- N_\ell^2 W_b \sin^2 \phi \cos \phi \chi_{xxx} \right. \\ &\quad + N_\ell^2 W_b \cos^3 \phi \chi_{xxx} \\ &\quad - 2N_\ell^2 W_b \sin^2 \phi \cos \phi \chi_{yyx} \\ &\quad + N_b^2 \sin \theta_0 \sin^2 \phi \chi_{zxx} \\ &\quad \left. + N_b^2 \sin \theta_0 \cos^2 \phi \chi_{zxx} \right],\end{aligned}$$

and reduce,

$$\begin{aligned}\Upsilon_{sP}^{(111)} &= \Gamma_{sP} \left[N_\ell^2 W_b (\cos^3 \phi - 3 \sin^2 \phi \cos \phi) \chi_{xxx} \right. \\ &\quad \left. + N_b^2 \sin \theta_0 (\sin^2 \phi + \cos^2 \phi) \chi_{zxx} \right] \\ &= \Gamma_{sP} \left[N_\ell^2 W_b \chi_{xxx} \cos 3\phi + N_b^2 \sin \theta_0 \chi_{zxx} \right] \\ &= \Gamma_{sP} r_{sP}^{(111)},\end{aligned}$$

where

$$r_{sP}^{(111)} = N_b^2 \sin \theta_0 \chi_{zxx} + N_\ell^2 W_b \chi_{xxx} \cos 3\phi. \quad (\text{B.41})$$

B.4.2 For the (110) surface

We take Eqs. (B.36) and (B.14), eliminate the components that do not contribute, and apply the symmetry relations as follows,

$$\begin{aligned}\Upsilon_{sP}^{\text{MR},(110)} &= \Gamma_{sP}^{\text{MR}} [R_p^{M+} \sin \theta_0 (\sin^2 \phi \chi_{zxx} + \cos^2 \phi \chi_{zyy})] \\ &= \Gamma_{sP}^{\text{MR}} \left[R_p^{M+} \sin \theta_0 \left(\frac{1}{2}(1 - \cos 2\phi) \chi_{zxx} + \frac{1}{2}(\cos 2\phi + 1) \chi_{zyy} \right) \right] \\ &= \Gamma_{sP}^{\text{MR}} \left[R_p^{M+} \sin \theta_0 \left(\frac{\chi_{zyy} + \chi_{zxx}}{2} + \frac{\chi_{zyy} - \chi_{zxx}}{2} \cos 2\phi \right) \right] \\ &= \Gamma_{sP}^{\text{MR}} r_{sP}^{\text{MR},(110)},\end{aligned}$$

where

$$r_{sP}^{\text{MR},(110)} = R_p^{M+} \sin \theta_0 \left(\frac{\chi_{zxx} + \chi_{zyy}}{2} + \frac{\chi_{zyy} - \chi_{zxx}}{2} \cos 2\phi \right). \quad (\text{B.42})$$

If we wish to neglect the effects of the multiple reflections, we follow the exact same procedure but starting with Eq. (B.38),

$$\begin{aligned}\Upsilon_{sP}^{(110)} &= \Gamma_{sP} [N_b^2 \sin \theta_0 (\sin^2 \phi \chi_{zxx} + \cos^2 \phi \chi_{zyy})] \\ &= \Gamma_{sP} \left[N_b^2 \sin \theta_0 \left(\frac{1}{2}(1 - \cos 2\phi) \chi_{zxx} + \frac{1}{2}(\cos 2\phi + 1) \chi_{zyy} \right) \right] \\ &= \Gamma_{sP} \left[N_b^2 \sin \theta_0 \left(\frac{\chi_{zyy} + \chi_{zxx}}{2} + \frac{\chi_{zyy} - \chi_{zxx}}{2} \cos 2\phi \right) \right] \\ &= \Gamma_{sP} r_{sP}^{(110)},\end{aligned}$$

where

$$r_{sP}^{(110)} = N_b^2 \sin \theta_0 \left(\frac{\chi_{zxx} + \chi_{zyy}}{2} + \frac{\chi_{zyy} - \chi_{zxx}}{2} \cos 2\phi \right). \quad (\text{B.43})$$

B.4.3 For the (001) surface

We take Eqs. (B.36) and (B.14), eliminate the components that do not contribute, and apply the symmetry relations as follows,

$$\begin{aligned}\Upsilon_{sP}^{\text{MR},(001)} &= \Gamma_{sP}^{\text{MR}} [R_p^{M+} \sin \theta_0 (\sin^2 \phi + \cos^2 \phi) \chi_{zxx}] \\ &= \Gamma_{sP}^{\text{MR}} [R_p^{M+} \sin \theta_0 \chi_{zxx}] \\ &= \Gamma_{sP}^{\text{MR}} r_{sP}^{\text{MR},(001)}.\end{aligned}$$

where

$$r_{sP}^{\text{MR},(001)} = R_p^{M+} \sin \theta_0 \chi_{zxx}. \quad (\text{B.44}) \quad [\text{eqapp:final-}]$$

If we wish to neglect the effects of the multiple reflections, we follow the exact same procedure but starting with Eq. (B.38),

$$\begin{aligned} \Upsilon_{sP}^{(001)} &= \Gamma_{sP} [N_b^2 \sin \theta_0 (\sin^2 \phi + \cos^2 \phi) \chi_{zxx}] \\ &= \Gamma_{sP} [N_b^2 \sin \theta_0 \chi_{zxx}] \\ &= \Gamma_{sP} r_{sP}^{(001)}, \end{aligned}$$

where

$$r_{sP}^{(001)} = N_b^2 \sin \theta_0 \chi_{zxx}. \quad (\text{B.45}) \quad [\text{eqapp:final-}]$$

B.5 \mathcal{R}_{sS}

Per Table B.1, \mathcal{R}_{sS} requires Eqs. (B.6) and (B.10). After some algebra, we obtain that

$$\begin{aligned} \Upsilon_{sS}^{\text{MR}} &= \Gamma_{sS}^{\text{MR}} [-\sin^3 \phi \chi_{xxx} + 2 \sin^2 \phi \cos \phi \chi_{xxy} - \sin \phi \cos^2 \phi \chi_{xyy} \\ &\quad + \sin^2 \phi \cos \phi \chi_{yxx} - 2 \sin \phi \cos^2 \phi \chi_{yxy} + \cos^3 \phi \chi_{yyy}]. \end{aligned} \quad (\text{B.46}) \quad [\text{eqapp:rssful}]$$

We take this opportunity to introduce a quantity that will be repeated throughout this section,

$$\Gamma_{sS}^{\text{MR}} = T_s^{v\ell} R_s^{M+} (t_s^{v\ell} r_s^{M+})^2. \quad (\text{B.47}) \quad [\text{eqapp:gammamr}]$$

If we neglect the multiple reflections, as described in the manuscript, we have that

$$\begin{aligned} \Upsilon_{sS} &= \Gamma_{sS} [-\sin^3 \phi \chi_{xxx} + 2 \sin^2 \phi \cos \phi \chi_{xxy} - \sin \phi \cos^2 \phi \chi_{xyy} \\ &\quad + \sin^2 \phi \cos \phi \chi_{yxx} - 2 \sin \phi \cos^2 \phi \chi_{yxy} + \cos^3 \phi \chi_{yyy}], \end{aligned} \quad (\text{B.48}) \quad [\text{eqapp:rssful}]$$

and again we introduce a quantity that will be repeated throughout this section,

$$\Gamma_{sS} = T_s^{v\ell} T_s^{\ell b} (t_s^{v\ell} t_s^{\ell b})^2. \quad (\text{B.49}) \quad [\text{eqapp:gammamr}]$$

We note that both Eqs. (B.46) and (B.48) are identical save for the different Γ_{sS} terms. Therefore, we can safely derive the equations only once, and then use Γ_{sS}^{MR} when we wish to include multiple reflections, or Γ_{sS} when we do not.

B.5.1 For the (111) surface

We take Eqs. (B.46) and (B.13), eliminate the components that do not contribute, and apply the symmetry relations as follows,

$$\begin{aligned} \Upsilon_{sS}^{\text{MR}} &= \Gamma_{sS}^{\text{MR}} [(3 \sin \phi \cos^2 \phi - \sin^3 \phi) \chi_{xxx}] \\ &= \Gamma_{sS}^{\text{MR}} [\chi_{xxx} \sin 3\phi] \\ &= \Gamma_{sS}^{\text{MR}} r_{sS}^{\text{MR},(111)}, \end{aligned}$$

where

$$r_{sS}^{\text{MR},(111)} = \chi_{xxx} \sin 3\phi. \quad (\text{B.50}) \quad [\text{eqapp:final-}]$$

As mentioned above,

$$r_{sS}^{(111)} = r_{sS}^{\text{MR},(111)}, \quad (\text{B.51}) \quad [\text{eqapp:final-}]$$

so if we wish to neglect the effects of the multiple reflections, we simply use Γ_{sS} instead of Γ_{sS}^{MR} .

B.5.2 For the (110) surface

When considering Eqs. (B.46) and (B.14), we see that there are no nonzero components that contribute. Therefore,

$$\Upsilon_{pS}^{\text{MR},(110)} = \Upsilon_{pS}^{(110)} = 0. \quad (\text{B.52}) \quad [\text{eqapp:final-}]$$

B.5.3 For the (001) surface

When considering Eqs. (B.46) and (B.14), we see that there are no nonzero components that contribute. Therefore,

$$\Upsilon_{sS}^{\text{MR},(001)} = \Upsilon_{sS}^{(001)} = 0. \quad (\text{B.53}) \quad [\text{eqapp:final-}]$$

Appendix C

Deriving the SSHG yield without multiple reflections

shgyieldnomr

Outline

C.1 Three layer model for SSHG radiation	77
C.1.1 SSHG Yield	80

C.1 Three layer model for SSHG radiation

c:threelayer

In this section we derive the formulas required for the calculation of the SSHG yield, defined by

$$\mathcal{R} = \frac{I(2\omega)}{I^2(\omega)}, \quad (\text{C.1}) \quad \boxed{\text{uno}}$$

with the intensity given by $\boxed{\text{poyd}}$ [23]

$$I(\omega) = \begin{cases} \frac{c}{2\pi} n(\omega) |E(\omega)|^2 & (\text{cgs units}) \\ 2\epsilon_0 c n(\omega) |E(\omega)|^2 & (\text{MKS units}) \end{cases}, \quad (\text{C.2}) \quad \boxed{\text{dos}}$$

where $n(\omega) = \sqrt{\epsilon(\omega)}$ is the index of refraction with $\epsilon(\omega)$ the dielectric function, ϵ_0 is the vacuum permittivity, and c the speed of light in vacuum. We use Ref. [26] as a starting point for this work, as the derivation of the three layer model is direct. In this scheme, we represent the surface by three regions or layers. The first layer is the vacuum region (denoted by v) with a dielectric function $\epsilon_v(\omega) = 1$ from where the fundamental electric field $\mathbf{E}_v(\omega)$ impinges on the material. The second layer is a thin layer (denoted by ℓ) of thickness d characterized by a dielectric function $\epsilon_\ell(\omega)$. It is in this layer where the second harmonic generation takes place. The third layer is the bulk region denoted by b and characterized by $\epsilon_b(\omega)$. Both the vacuum layer and the bulk layer are semi-infinite (see Fig. $\boxed{\text{fig:3layer}}$).

To model the electromagnetic response of the three layer model we follow Ref. [26], and assume a polarization sheet of the form

$$\mathbf{P}(\mathbf{r}, t) = \mathcal{P} e^{i\kappa \cdot \mathbf{R}} e^{-i\omega t} \delta(z - z_\beta) + \text{c.c.}, \quad (\text{C.3}) \quad [\text{m31}]$$

where \mathcal{P} is the nonlinear polarization (given below), $\mathbf{R} = (x, y)$, κ is the component of the wave vector ν_α parallel to the surface, and z_β is the position of the sheet within medium β (see Fig. 3.1). It is shown in Ref. [27] that the solution of the Maxwell equations for the radiated fields $E_{\beta,p\pm}$ and $E_{\beta,s}$, at points $z \neq 0$, with $\mathbf{P}(\mathbf{r}, t)$ acting as a source can be written as

$$(E_{\beta,p\pm}, E_{\beta,s}) = \left(\frac{\gamma i \tilde{\omega}^2}{\tilde{w}_\beta} \hat{\mathbf{p}}_{\beta\pm} \cdot \mathcal{P}, \frac{\gamma i \tilde{\omega}^2}{\tilde{w}_\beta} \hat{\mathbf{s}} \cdot \mathcal{P} \right), \quad (\text{C.4}) \quad [\text{r2}]$$

where $\gamma = 2\pi$ in cgs units and $\gamma = 1/2\epsilon_0$ in MKS units. $E_{\beta,p\pm}$ represents the electric field for p -polarization propagating downward ($-$) or upward ($+$), and $E_{\beta,s}$ that for s -polarization, both in medium β . Since for s -polarization the field is parallel to the surface there is no need to distinguish the upward or downward direction of propagation as it is needed for the p -polarized fields. Also, $\tilde{\omega} = \omega/c$, and $\hat{\mathbf{s}}$ and $\hat{\mathbf{p}}_{\beta\pm}$ are the unitary vectors for the s and p polarization of the radiated field, respectively. The \pm notation refers to upward (+) or downward (-) direction of propagation within medium β , as shown in Fig. 3.1. Thus,

$$\hat{\mathbf{p}}_{\beta\pm}(\omega) = \frac{\kappa(\omega) \hat{\mathbf{z}} \mp \tilde{w}_\beta(\omega) \hat{\kappa}}{\tilde{w}_\beta n_\beta(\omega)} = \frac{\sin \theta_0 \hat{\mathbf{z}} \mp w_\beta(\omega) \hat{\kappa}}{n_\beta(\omega)}, \quad (\text{C.5}) \quad [\text{r4}]$$

where $\kappa(\omega) = |\kappa(\omega)| = \tilde{\omega} \sin \theta_0$, $n_\beta(\omega) = \sqrt{\epsilon_\beta(\omega)}$ is the index of refraction of medium β , and z is the direction perpendicular to the surface that points towards the vacuum. Lastly, $\tilde{w}_\beta(\omega) = \tilde{\omega} w_\beta$, where

$$w_\beta(\omega) = (\epsilon_\beta(\omega) - \sin^2 \theta_0)^{1/2}, \quad (\text{C.6}) \quad [\text{r3}]$$

with θ_0 the angle of incidence of $\mathbf{E}_v(\omega)$. We choose the plane of incidence along the κz plane, so

$$\hat{\kappa} = \cos \phi \hat{\mathbf{x}} + \sin \phi \hat{\mathbf{y}}, \quad (\text{C.7}) \quad [\text{eqapp:mc1}]$$

and

$$\hat{\mathbf{s}} = -\sin \phi \hat{\mathbf{x}} + \cos \phi \hat{\mathbf{y}}, \quad (\text{C.8}) \quad [\text{eqapp:mmc2}]$$

where ϕ is the azimuthal angle with respect to the x axis.

In the three layer model, the nonlinear polarization responsible for the SHG is immersed in the thin $\beta = \ell$ layer, and is given by

$$\mathcal{P}_{\ell,i}(2\omega) = \begin{cases} \chi_{ijk}(-2\omega; \omega, \omega) E_{\ell,j}(\omega) E_{\ell,k}(\omega) & (\text{cgs units}) \\ \epsilon_0 \chi_{ijk}(-2\omega; \omega, \omega) E_{\ell,j}(\omega) E_{\ell,k}(\omega) & (\text{MKS units}) \end{cases}, \quad (\text{C.9}) \quad [\text{tres}]$$

where the tensor $\chi(-2\omega; \omega, \omega)$ is the surface nonlinear dipolar susceptibility and the Cartesian indices i, j, k are summed over if repeated. We remark that the thickness of the layer ℓ is considered to be much smaller than the wavelength of the fundamental field, thus multiple reflections of both the fundamental and the SH can be neglected. Also, $\chi_{ijk}(-2\omega; \omega, \omega) = \chi_{ikj}(-2\omega; \omega, \omega)$ is the

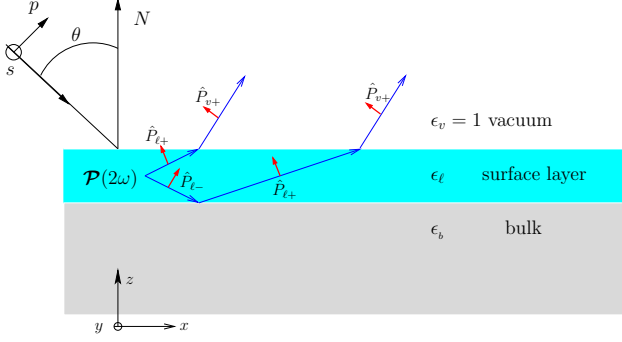


Figure C.1: Sketch of the three layer model for SHG. Vacuum is on top with $\epsilon_v = 1$, the layer with nonlinear polarization $\mathcal{P}(2\omega)$ is characterized with $\epsilon_\ell(\omega)$ and the bulk with $\epsilon_b(\omega)$. In the dipolar approximation the bulk does not radiate SHG. The thin arrows are along the direction of propagation, and the unit vectors for p -polarization are denoted with thick arrows (capital letters denote SH components). The unit vector for s -polarization points along $-y$ (out of the page).

`fig:3layer`

intrinsic permutation symmetry due to the fact that SHG is degenerate in $E_{\ell,j}(\omega)$ and $E_{\ell,k}(\omega)$. For ease of notation, we drop the frequency argument from $\chi(-2\omega; \omega, \omega)$ and we simply write χ from now on. As it was done in Ref. [26], in presenting the results Eq. (C.4)-(C.8) we have taken the polarization sheet (Eq. (C.3)) to be oscillating at some frequency ω . However, in the following we find it convenient to use ω exclusively to denote the fundamental frequency and κ to denote the component of the incident wave vector parallel to the surface. Then the nonlinear generated polarization is oscillating at $\Omega = 2\omega$ and will be characterized by a wave vector parallel to the surface $\mathbf{K} = 2\kappa$. We can carry over Eqs. (C.3)-(C.8) simply by replacing the lowercase symbols $(\omega, \tilde{\omega}, \kappa, n_\beta, \tilde{w}_\beta, w_\beta, \hat{\mathbf{p}}_{\beta\pm}, \hat{\mathbf{s}})$ with uppercase symbols $(\Omega, \tilde{\Omega}, \mathbf{K}, N_\beta, \tilde{W}_\beta, W_\beta, \hat{\mathbf{P}}_{\beta\pm}, \hat{\mathbf{S}})$, all evaluated at 2ω . We always have that $\hat{\mathbf{S}} = \hat{\mathbf{s}}$.

To describe the propagation of the SH field, we see from Fig. C.1, that it is refracted at the layer-vacuum interface (ℓv), and reflected from the layer-bulk (ℓb) and layer-vacuum (ℓv) interfaces, thus we define

$$\mathbf{T}^{\ell v} = \hat{\mathbf{s}} T_s^{\ell v} \hat{\mathbf{s}} + \hat{\mathbf{P}}_{v+} T_p^{\ell v} \hat{\mathbf{P}}_{\ell+}, \quad (\text{C.10}) \quad [\text{r5}]$$

as the tensor for transmission from the ℓv interface,

$$\mathbf{R}^{\ell b} = \hat{\mathbf{s}} R_s^{\ell b} \hat{\mathbf{s}} + \hat{\mathbf{P}}_{\ell+} R_p^{\ell b} \hat{\mathbf{P}}_{\ell-}, \quad (\text{C.11}) \quad [\text{r6}]$$

as the tensor of reflection from the ℓb interface, and

$$\mathbf{R}^{\ell v} = \hat{\mathbf{s}} R_s^{\ell v} \hat{\mathbf{s}} + \hat{\mathbf{P}}_{\ell-} R_p^{\ell v} \hat{\mathbf{P}}_{\ell+}, \quad (\text{C.12}) \quad [\text{r6b}]$$

as that from the ℓv interface. The Fresnel factors in uppercase letters, $T_{s,p}^{ij}$ and $R_{s,p}^{ij}$, are evaluated

at 2ω from the following well known formulas,^{[\[mizrahiJOSA88\]](#)}^{[\[26\]](#)}

$$t_s^{ij}(\omega) = \frac{2w_i(\omega)}{w_i(\omega) + w_j(\omega)}, \quad (\text{C.13})$$

$$t_p^{ij}(\omega) = \frac{2w_i(\omega)\sqrt{\epsilon_i(\omega)\epsilon_j(\omega)}}{w_i(\omega)\epsilon_j(\omega) + w_j(\omega)\epsilon_i(\omega)}, \quad (\text{C.14})$$

$$r_s^{ij}(\omega) = \frac{w_i(\omega) - w_j(\omega)}{w_i(\omega) + w_j(\omega)}, \quad (\text{C.15})$$

$$r_p^{ij}(\omega) = \frac{w_i(\omega)\epsilon_j(\omega) - w_j(\omega)\epsilon_i(\omega)}{w_i(\omega)\epsilon_j(\omega) + w_j(\omega)\epsilon_i(\omega)}. \quad (\text{C.16})$$

From these expressions one can show that,

$$\begin{aligned} 1 + r_s^{\ell b} &= t_s^{\ell b} \\ 1 + r_p^{\ell b} &= \frac{n_b}{n_\ell} t_p^{\ell b} \\ 1 - r_p^{\ell b} &= \frac{n_\ell}{n_b} \frac{w_b}{w_\ell} t_p^{\ell b} \\ t_{s,p}^{\ell v} &= \frac{w_\ell}{w_v} t_{s,p}^{v\ell}. \end{aligned} \quad (\text{C.17}) \quad [\text{mf}]$$

C.1.1 SSHG Yield

sec:yield We obtain the total 2ω radiated field by using Eqs. ([C.10](#)), ([C.11](#)), and ([C.12](#)),

$$\mathbf{E}(2\omega) = E_s(2\omega) \left(\mathbf{T}^{\ell v} + \mathbf{T}^{\ell v} \cdot \mathbf{R}^{\ell b} \right) \cdot \hat{\mathbf{s}} + E_{p+}(2\omega) \mathbf{T}^{\ell v} \cdot \hat{\mathbf{P}}_{\ell+} + E_{p-}(2\omega) \mathbf{T}^{\ell v} \cdot \mathbf{R}^{\ell b} \cdot \hat{\mathbf{P}}_{\ell-}.$$

The first term is the transmitted s -polarized field, the second one is the reflected and then transmitted s -polarized field and the third and fourth terms are the equivalent fields for p -polarization. The transmission is from the layer into vacuum, and the reflection between the layer and the bulk. After some simple algebra, we obtain

$$\mathbf{E}_\ell(2\omega) = \frac{\gamma i \tilde{\Omega}}{W_\ell} \mathbf{H}_\ell \cdot \mathcal{P}_\ell(2\omega), \quad (\text{C.18}) \quad [\text{r8}]$$

where,

$$\mathbf{H}_\ell = \hat{\mathbf{s}} T_s^{\ell v} \left(1 + R_s^{\ell b} \right) \hat{\mathbf{s}} + \hat{\mathbf{P}}_{v+} T_p^{\ell v} \left(\hat{\mathbf{P}}_{\ell+} + R_p^{\ell b} \hat{\mathbf{P}}_{\ell-} \right). \quad (\text{C.19}) \quad [\text{r9}]$$

The magnitude of the radiated SH field is given by $E(2\omega) = \hat{\mathbf{e}}^F \cdot \mathbf{E}_\ell(2\omega)$, where $\hat{\mathbf{e}}^F$ is the unit vector of the final polarization, with $F = S, P$, and then, $\hat{\mathbf{e}}^S = \hat{\mathbf{s}}$ and $\hat{\mathbf{e}}^P = \hat{\mathbf{P}}_{v+}$. We expand the second term in parenthesis of Eq. ([C.19](#)) as

$$\begin{aligned} \hat{\mathbf{P}}_{\ell+} + R_p^{\ell b} \hat{\mathbf{P}}_{\ell-} &= \frac{\sin \theta_0 \hat{\mathbf{z}} - W_\ell \hat{\boldsymbol{\kappa}}}{N_\ell} + R_p^{\ell b} \frac{\sin \theta_0 \hat{\mathbf{z}} + W_\ell \hat{\boldsymbol{\kappa}}}{N_\ell} \\ &= \frac{1}{N_\ell} \left(\sin \theta_0 (1 + R_p^{\ell b}) \hat{\mathbf{z}} - W_\ell (1 - R_p^{\ell b}) \hat{\boldsymbol{\kappa}} \right) \\ &= \frac{T_p^{\ell b}}{N_\ell^2 N_b} \left(N_b^2 \sin \theta_0 \hat{\mathbf{z}} - N_\ell^2 W_b \hat{\boldsymbol{\kappa}} \right), \end{aligned}$$

and rewrite Eq. (C.18) as

$$E(2\omega) = \frac{2\gamma i\omega}{cW_\ell} \hat{\mathbf{e}}^F \cdot \mathbf{H}_\ell \cdot \mathcal{P}_\ell(2\omega) = \frac{2\gamma i\omega}{cW_v} \mathbf{e}_\ell^{2\omega,F} \cdot \mathcal{P}_\ell(2\omega), \quad (\text{C.20}) \quad [\text{r10}]$$

where

$$\mathbf{e}_\ell^{2\omega,F} = \hat{\mathbf{e}}^F \cdot \left[\hat{\mathbf{s}} T_s^{v\ell} T_s^{\ell b} \hat{\mathbf{s}} + \hat{\mathbf{P}}_{v+} \frac{T_p^{v\ell} T_p^{\ell b}}{N_\ell^2 N_b} (N_b^2 \sin \theta_0 \hat{\mathbf{z}} - N_\ell^2 W_b \hat{\boldsymbol{\kappa}}) \right]. \quad (\text{C.21}) \quad [\text{r12mm}]$$

In the three layer model the nonlinear polarization is located in layer ℓ , thus, we evaluate the fundamental field required in Eq. (C.9) in this layer as well. We write

$$\mathbf{E}_\ell(\omega) = E_0 \left(\hat{\mathbf{s}} t_s^{v\ell} (1 + r_s^{\ell b}) \hat{\mathbf{s}} + \hat{\mathbf{p}}_{\ell-} t_p^{v\ell} \hat{\mathbf{p}}_{v-} + \hat{\mathbf{p}}_{\ell+} t_p^{v\ell} r_p^{\ell b} \hat{\mathbf{p}}_{v-} \right) \cdot \hat{\mathbf{e}}^{\text{in}} = E_0 \mathbf{e}_\ell^\omega, \quad (\text{C.22}) \quad [\text{m2}]$$

and following the steps that lead to Eq. (C.21), we find that

$$\mathbf{e}_\ell^{\omega,i} = \left[\hat{\mathbf{s}} t_s^{v\ell} t_s^{\ell b} \hat{\mathbf{s}} + \frac{t_p^{v\ell} t_p^{\ell b}}{n_\ell^2 n_b} (n_b^2 \sin \theta_0 \hat{\mathbf{z}} + n_\ell^2 w_b \hat{\boldsymbol{\kappa}}) \hat{\mathbf{p}}_{v-} \right] \cdot \hat{\mathbf{e}}^i. \quad (\text{C.23}) \quad [\text{m12}]$$

We pause here to reduce this result to the case where the nonlinear polarization $\mathbf{P}(2\omega)$ radiates from vacuum instead from the layer ℓ . For such case we simply take $\epsilon_\ell(2\omega) = 1$ and $\ell = v$ ($T_{s,p}^{\ell v} = 1$), to get

$$\mathbf{e}_v^{2\omega} = \hat{\mathbf{e}}^F \cdot \left[\hat{\mathbf{s}} T_s^{vb} \hat{\mathbf{s}} + \hat{\mathbf{P}}_{v+} \frac{T_p^{vb}}{\sqrt{\epsilon_b(2\omega)}} (\epsilon_b(2\omega) \sin \theta_0 \hat{\mathbf{z}} - W_b \hat{\boldsymbol{\kappa}}) \right], \quad (\text{C.24}) \quad [\text{eq:r13}]$$

which agrees with Eq. (3.10) of Ref. [26].

In the 3-layer model the SH polarization $\mathcal{P}(2\omega)$ is located in layer ℓ , where we evaluate the fundamental field required in Eq. (C.9). We write

$$\begin{aligned} \mathbf{E}_\ell(\omega) &= E_0 \left(\hat{\mathbf{s}} t_s^{v\ell} (1 + r_s^{\ell b}) \hat{\mathbf{s}} + \hat{\mathbf{p}}_{\ell-} t_p^{v\ell} \hat{\mathbf{p}}_{v-} + \hat{\mathbf{p}}_{\ell+} t_p^{v\ell} r_p^{\ell b} \hat{\mathbf{p}}_{v-} \right) \cdot \hat{\mathbf{e}}^i \\ &= E_0 \mathbf{e}_\ell^\omega, \end{aligned} \quad (\text{C.25}) \quad [\text{eq:m2}]$$

where $\hat{\mathbf{e}}^i$ is the s ($\hat{\mathbf{s}}$) or p ($\hat{\mathbf{p}}_{v-}$) incoming polarization of the fundamental electric field. This field is composed of the transmitted field and its first reflection from the ℓb interface for s and p polarizations. The fundamental field, once inside the layer ℓ will be reflected multiple times at the ℓv and ℓb interfaces. However, each reflection will diminish the intensity of the fundamental field. As the SSHG yield scales with the square of this field, the contribution of the subsequent reflections after the one considered in Eq. (C.25) can be safely neglected. From Eq. (2.14) we find that

$$\mathbf{e}_\ell^\omega = \left[\hat{\mathbf{s}} t_s^{v\ell} t_s^{\ell b} \hat{\mathbf{s}} + \frac{t_p^{v\ell} t_p^{\ell b}}{n_\ell^2 n_b} (n_b^2 \sin \theta_0 \hat{\mathbf{z}} + n_\ell^2 w_b \hat{\boldsymbol{\kappa}}) \hat{\mathbf{p}}_{v-} \right] \cdot \hat{\mathbf{e}}^{\text{in}}. \quad (\text{C.26}) \quad [\text{eq:m12}]$$

To connect with the work in Ref. [26], we evaluate the fields in the bulk instead of the layer ℓ and simply take $n_\ell = n_b$ ($t_{s,p}^{\ell b} = 1$), to obtain

$$\mathbf{e}_b^\omega = \left[\hat{\mathbf{s}} T_s^{vb} \hat{\mathbf{s}} + \frac{t_p^{vb}}{n_b} (\sin \theta_0 \hat{\mathbf{z}} + w_b \hat{\boldsymbol{\kappa}}) \hat{\mathbf{p}}_{v-} \right] \cdot \hat{\mathbf{e}}^{\text{in}}, \quad (\text{C.27}) \quad [\text{eq:m13}]$$

that is in agreement with Eq. (3.5) of Ref. [26].

Replacing $\mathbf{E}(\omega) \rightarrow E_0 \mathbf{e}_\ell^{\omega,i}$, in Eq. (C.9), we obtain that

$$\mathcal{P}_\ell(2\omega) = \begin{cases} E_0^2 \chi : \mathbf{e}_\ell^{\omega,i} \mathbf{e}_\ell^{\omega,i} & (\text{cgs units}) \\ \epsilon_0 E_0^2 \chi : \mathbf{e}_\ell^{\omega,i} \mathbf{e}_\ell^{\omega,i} & (\text{MKS units}) \end{cases}, \quad (\text{C.28}) \quad [\text{m4}]$$

where $\mathbf{e}_\ell^{\omega,i}$ is given by Eq. (C.23), and thus Eq. (C.20) reduces to ($W_v = \cos \theta_0$)

$$E(2\omega) = \frac{2\eta i\omega}{c \cos \theta_0} \mathbf{e}_\ell^{2\omega,F} \cdot \chi : \mathbf{e}_\ell^{\omega,i} \mathbf{e}_\ell^{\omega,i}, \quad (\text{C.29}) \quad [\text{mr10}]$$

where $\eta = 2\pi$ for cgs units and $\eta = 1/2$ for MKS units. For ease of notation, we define

$$\Upsilon_{iF} \equiv \mathbf{e}_\ell^{2\omega,F} \cdot \chi : \mathbf{e}_\ell^{\omega,i} \mathbf{e}_\ell^{\omega,i}. \quad (\text{C.30}) \quad [\text{mc0}]$$

From Eqs. (C.1), (C.2), and (C.29) we obtain that

$$\mathcal{R}_{iF} = \frac{\eta \omega^2}{c^3 \cos^2 \theta_0} \left| \frac{1}{n_\ell} \Upsilon_{iF} \right|^2, \quad (\text{C.31}) \quad [\text{mc6}]$$

as the SSHG yield, where $\eta = 32\pi^3$ for cgs units and $\eta = 1/(2\epsilon_0)$ in MKS units. Since χ is a surface second order nonlinear susceptibility, in the MKS unit system is given in m^2/V , and thus \mathcal{R}_{iF} is given in m^2/W .

It is worth mentioning that we can easily recover the results from Ref. [26], which are in turn equivalent to those in Ref. [29]. We simply take $\mathbf{e}_\ell^{2\omega} \rightarrow \mathbf{e}_v^{2\omega}$, $\mathbf{e}_\ell^\omega \rightarrow \mathbf{e}_b^\omega$, and we have

$$\mathcal{R}_{iF}(2\omega) = \frac{\eta \omega^2}{c^3 \cos^2 \theta_0} \left| \mathbf{e}_v^{2\omega} \cdot \chi : \mathbf{e}_b^\omega \mathbf{e}_b^\omega \right|^2. \quad (\text{C.32}) \quad [\text{eq:mc6}]$$

This is the SSHG yield of a nonlinear polarization sheet radiating from the vacuum region above the surface, with the fundamental field evaluated below the surface in the bulk of the material characterized by $\epsilon_b(\omega)$.

Appendix D

Some limiting cases of interest

miting_cases

Outline

D.1	The two layer model	83
D.2	Taking $\mathcal{P}(2\omega)$ and the fundamental fields in the bulk	84
D.3	Taking $\mathcal{P}(2\omega)$ and the fundamental fields in the vacuum	86
D.4	Taking $\mathcal{P}(2\omega)$ in ℓ and the fundamental fields in the bulk	88

In this section, we derive the expressions for \mathcal{R}_{pP} for different limiting cases. We evaluate $\mathcal{P}(2\omega)$ and the fundamental fields in different regions. It is worth noting that the first case, the three layer model, can be reduced to any of the other cases by simply considering where we want to evaluate the 1ω and 2ω terms.

D.1 The two layer model

In order to reduce above result to that of Ref. [26] and [29], we now consider that $\mathcal{P}(2\omega)$ is evaluated in the vacuum region, while the fundamental fields are evaluated in the bulk region. To do this, we take the 2ω radiations factors for vacuum by taking $\ell = v$, thus $\epsilon_\ell(2\omega) = 1$, $T_p^{\ell v} = 1$, $T_p^{\ell b} = T_p^{vb}$, and the fundamental field inside medium b by taking $\ell = b$, thus $\epsilon_\ell(\omega) = \epsilon_b(\omega)$, $t_p^{v\ell} = t_p^{vb}$, and $t_p^{\ell b} = 1$. With these choices

$$\mathbf{e}_v^{2\omega} \cdot \boldsymbol{\chi} : \mathbf{e}_b^\omega \mathbf{e}_b^\omega \equiv \Gamma_{pP}^{vb} r_{pP}^{vb},$$

where,

$$\begin{aligned} r_{pP}^{vb} &= \epsilon_b(2\omega) \sin \theta_0 \left(\sin^2 \theta_0 \chi_{zzz} + k_b^2 \chi_{zxx} \right) \\ &\quad - k_b K_b \left(2 \sin \theta_0 \chi_{xxz} + k_b \chi_{xxx} \cos(3\phi) \right), \end{aligned}$$

and

$$\Gamma_{pP}^{vb} = \frac{T_p^{vb} (t_p^{vb})^2}{\epsilon_b(\omega) \sqrt{\epsilon_b(2\omega)}}.$$

D.2 Taking $\mathcal{P}(2\omega)$ and the fundamental fields in the bulk

To consider the 2ω fields in the bulk, we start with Eq. (C.19) but substitute $\ell \rightarrow b$, thus

$$\mathbf{H}_b = \hat{\mathbf{s}} T_s^{bv} \left(1 + R_s^{bb} \right) \hat{\mathbf{s}} + \hat{\mathbf{P}}_{v+} T_p^{bv} \left(\hat{\mathbf{P}}_{b+} + R_p^{bb} \hat{\mathbf{P}}_{b-} \right).$$

R_p^{bb} and R_s^{bb} are zero, so we are left with

$$\begin{aligned} \mathbf{H}_b &= \hat{\mathbf{s}} T_s^{bv} \hat{\mathbf{s}} + \hat{\mathbf{P}}_{v+} T_p^{bv} \hat{\mathbf{P}}_{b+} \\ &= \frac{K_b}{K_v} \left(\hat{\mathbf{s}} T_s^{vb} \hat{\mathbf{s}} + \hat{\mathbf{P}}_{v+} T_p^{vb} \hat{\mathbf{P}}_{b+} \right) \\ &= \frac{K_b}{K_v} \left[\hat{\mathbf{s}} T_s^{vb} \hat{\mathbf{s}} + \hat{\mathbf{P}}_{v+} \frac{T_p^{vb}}{\sqrt{\epsilon_b(2\omega)}} (\sin \theta_0 \hat{\mathbf{z}} - K_b \cos \phi \hat{\mathbf{x}} - K_b \sin \phi \hat{\mathbf{y}}) \right], \end{aligned}$$

and we define

$$\mathbf{e}_b^{2\omega} = \frac{K_b}{K_v} \hat{\mathbf{e}}^{\text{out}} \cdot \left[\hat{\mathbf{s}} T_s^{vb} \hat{\mathbf{s}} + \hat{\mathbf{P}}_{v+} \frac{T_p^{vb}}{\sqrt{\epsilon_b(2\omega)}} (\sin \theta_0 \hat{\mathbf{z}} - K_b \cos \phi \hat{\mathbf{x}} - K_b \sin \phi \hat{\mathbf{y}}) \right].$$

For \mathcal{R}_{pP} , we require $\hat{\mathbf{e}}^{\text{out}} = \hat{\mathbf{P}}_{v+}$, so we have that

$$\mathbf{e}_b^{2\omega} = \frac{K_b}{K_v} \frac{T_p^{vb}}{\sqrt{\epsilon_b(2\omega)}} (\sin \theta_0 \hat{\mathbf{z}} - K_b \cos \phi \hat{\mathbf{x}} - K_b \sin \phi \hat{\mathbf{y}}).$$

The 1ω fields will still be evaluated inside the bulk, so we have

$$\mathbf{e}_b^\omega = \left[\hat{\mathbf{s}} t_s^{vb} \hat{\mathbf{s}} + \frac{t_p^{vb}}{\sqrt{\epsilon_b(\omega)}} (\sin \theta_0 \hat{\mathbf{z}} + k_b \cos \phi \hat{\mathbf{x}} + k_b \sin \phi \hat{\mathbf{y}}) \hat{\mathbf{p}}_{v-} \right] \cdot \hat{\mathbf{e}}^{\text{in}},$$

and for our particular case of $\hat{\mathbf{e}}^{\text{in}} = \hat{\mathbf{p}}_{v-}$,

$$\mathbf{e}_b^\omega = \frac{t_p^{vb}}{\sqrt{\epsilon_b(\omega)}} (\sin \theta_0 \hat{\mathbf{z}} + k_b \cos \phi \hat{\mathbf{x}} + k_b \sin \phi \hat{\mathbf{y}}),$$

and

$$\begin{aligned} \mathbf{e}_b^\omega \mathbf{e}_b^\omega &= \frac{(t_p^{vb})^2}{\epsilon_b(\omega)} (\sin \theta_0 \hat{\mathbf{z}} + k_b \cos \phi \hat{\mathbf{x}} + k_b \sin \phi \hat{\mathbf{y}})^2 \\ &= \frac{(t_p^{vb})^2}{\epsilon_b(\omega)} \left(\sin^2 \theta_0 \hat{\mathbf{z}} \hat{\mathbf{z}} + k_b^2 \cos^2 \phi \hat{\mathbf{x}} \hat{\mathbf{x}} + k_b^2 \sin^2 \phi \hat{\mathbf{y}} \hat{\mathbf{y}} \right. \\ &\quad \left. + 2k_b \sin \theta_0 \cos \phi \hat{\mathbf{z}} \hat{\mathbf{x}} + 2k_b \sin \theta_0 \sin \phi \hat{\mathbf{z}} \hat{\mathbf{y}} + 2k_b^2 \sin \phi \cos \phi \hat{\mathbf{x}} \hat{\mathbf{y}} \right) \end{aligned}$$

So lastly, we have that

$$\begin{aligned}
\mathbf{e}_b^{2\omega} \cdot \boldsymbol{\chi} : \mathbf{e}_b^\omega \mathbf{e}_b^\omega &= \frac{K_b}{K_v} \frac{T_p^{vb} (t_p^{vb})^2}{\epsilon_b(\omega) \sqrt{\epsilon_b(2\omega)}} \left(\sin^3 \theta_0 \chi_{zzz} \right. \\
&\quad + k_b^2 \sin \theta_0 \cos^2 \phi \chi_{zxx} \\
&\quad + k_b^2 \sin \theta_0 \sin^2 \phi \chi_{zyy} \\
&\quad + 2k_b \sin^2 \theta_0 \cos \phi \chi_{zzx} \\
&\quad + 2k_b \sin^2 \theta_0 \sin \phi \chi_{zzy} \\
&\quad + 2k_b^2 \sin \theta_0 \sin \phi \cos \phi \chi_{zxy} \\
&\quad - K_b \sin^2 \theta_0 \cos \phi \chi_{xzz} \\
&\quad - k_b^2 K_b \cos^3 \phi \chi_{xxx} \\
&\quad - k_b^2 K_b \sin^2 \phi \cos \phi \chi_{xyy} \\
&\quad - 2k_b K_b \sin \theta_0 \cos^2 \phi \chi_{xzx} \\
&\quad - 2k_b K_b \sin \theta_0 \sin \phi \cos \phi \chi_{xzy} \\
&\quad - 2k_b^2 K_b \sin \phi \cos^2 \phi \chi_{xxy} \\
&\quad - K_b \sin^2 \theta_0 \sin \phi \chi_{yzz} \\
&\quad - k_b^2 K_b \sin \phi \cos^2 \phi \chi_{yxx} \\
&\quad - k_b^2 K_b \sin^3 \phi \chi_{yyy} \\
&\quad - 2k_b K_b \sin \theta_0 \sin \phi \cos \phi \chi_{yzx} \\
&\quad - 2k_b K_b \sin \theta_0 \sin^2 \phi \chi_{yzy} \\
&\quad \left. - 2k_b^2 K_b \sin^2 \phi \cos \phi \chi_{yxy} \right),
\end{aligned}$$

and we can eliminate many terms since $\chi_{zzx} = \chi_{zzy} = \chi_{zxy} = \chi_{xzz} = \chi_{xzy} = \chi_{xxy} = \chi_{yzz} = \chi_{yxx} = \chi_{yyy} = \chi_{yzx} = 0$, and substituting the equivalent components of $\boldsymbol{\chi}$,

$$\begin{aligned}
&= \frac{K_b}{K_v} \Gamma_{pP}^b \left(\sin^3 \theta_0 \chi_{zzz} \right. \\
&\quad + k_b^2 \sin \theta_0 \cos^2 \phi \chi_{zxx} \\
&\quad + k_b^2 \sin \theta_0 \sin^2 \phi \chi_{zxx} \\
&\quad - 2k_b K_b \sin \theta_0 \cos^2 \phi \chi_{xxz} \\
&\quad - 2k_b K_b \sin \theta_0 \sin^2 \phi \chi_{xxz} \\
&\quad - k_b^2 K_b \cos^3 \phi \chi_{xxx} \\
&\quad + k_b^2 K_b \sin^2 \phi \cos \phi \chi_{xxx} \\
&\quad \left. + 2k_b^2 K_b \sin^2 \phi \cos \phi \chi_{xxx} \right),
\end{aligned}$$

and reducing,

$$\begin{aligned}
&= \frac{K_b}{K_v} \Gamma_{pP}^b (\sin^3 \theta_0 \chi_{zzz} \\
&\quad + k_b^2 \sin \theta_0 (\sin^2 \phi + \cos^2 \phi) \chi_{zxx} \\
&\quad - 2k_b K_b \sin \theta_0 (\sin^2 \phi + \cos^2 \phi) \chi_{xxz} \\
&\quad + k_b^2 K_b (3 \sin^2 \phi \cos \phi - \cos^3 \phi) \chi_{xxx}) \\
&= \frac{K_b}{K_v} \Gamma_{pP}^b (\sin^3 \theta_0 \chi_{zzz} + k_b^2 \sin \theta_0 \chi_{zxx} - 2k_b K_b \sin \theta_0 \chi_{xxz} - k_b^2 K_b \chi_{xxx} \cos 3\phi),
\end{aligned}$$

where,

$$\Gamma_{pP}^b = \frac{T_p^{vb} (t_p^{vb})^2}{\epsilon_b(\omega) \sqrt{\epsilon_b(2\omega)}}.$$

We find the equivalent expression for \mathcal{R} evaluated inside the bulk as

$$R(2\omega) = \frac{32\pi^3 \omega^2}{c^3 K_b^2} |\mathbf{e}_b^{2\omega} \cdot \boldsymbol{\chi} : \mathbf{e}_b^\omega \mathbf{e}_b^\omega|^2,$$

and we can remove the K_b/K_v factor completely and reduce to the standard form of

$$R(2\omega) = \frac{32\pi^3 \omega^2}{c^3 \cos^2 \theta_0} |\mathbf{e}_b^{2\omega} \cdot \boldsymbol{\chi} : \mathbf{e}_b^\omega \mathbf{e}_b^\omega|^2.$$

D.3 Taking $\mathcal{P}(2\omega)$ and the fundamental fields in the vacuum

To consider the 1ω fields in the vacuum, we start with Eq. (C.22) but substitute $\ell \rightarrow v$, thus

$$\mathbf{E}_v(\omega) = E_0 \left[\hat{\mathbf{s}} t_s^{vv} (1 + r_s^{vb}) \hat{\mathbf{s}} + \hat{\mathbf{p}}_v - t_p^{vv} \hat{\mathbf{p}}_{v-} + \hat{\mathbf{p}}_v + t_p^{vv} r_p^{vb} \hat{\mathbf{p}}_{v-} \right] \cdot \hat{\mathbf{e}}^{\text{in}},$$

t_p^{vv} and t_s^{vv} are one, so we are left with

$$\begin{aligned}
\mathbf{e}_v^\omega &= \left[\hat{\mathbf{s}} (1 + r_s^{vb}) \hat{\mathbf{s}} + \hat{\mathbf{p}}_v - \hat{\mathbf{p}}_{v-} + \hat{\mathbf{p}}_v + r_p^{vb} \hat{\mathbf{p}}_{v-} \right] \cdot \hat{\mathbf{e}}^{\text{in}} \\
&= \left[\hat{\mathbf{s}} (t_s^{vb}) \hat{\mathbf{s}} + (\hat{\mathbf{p}}_{v-} + \hat{\mathbf{p}}_v + r_p^{vb}) \hat{\mathbf{p}}_{v-} \right] \cdot \hat{\mathbf{e}}^{\text{in}} \\
&= \left[\hat{\mathbf{s}} (t_s^{vb}) \hat{\mathbf{s}} + \frac{1}{\sqrt{\epsilon_v(\omega)}} (k_v (1 - r_p^{vb}) \hat{\boldsymbol{\kappa}} + \sin \theta_0 (1 + r_p^{vb}) \hat{\mathbf{z}}) \hat{\mathbf{p}}_{v-} \right] \\
&= \left[\hat{\mathbf{s}} (t_s^{vb}) \hat{\mathbf{s}} + \left(\frac{k_b}{\sqrt{\epsilon_b(\omega)}} t_p^{vb} \hat{\boldsymbol{\kappa}} + \sqrt{\epsilon_b(\omega)} \sin \theta_0 t_p^{vb} \hat{\mathbf{z}} \right) \hat{\mathbf{p}}_{v-} \right] \cdot \hat{\mathbf{e}}^{\text{in}} \\
&= \left[\hat{\mathbf{s}} (t_s^{vb}) \hat{\mathbf{s}} + \frac{t_p^{vb}}{\sqrt{\epsilon_b(\omega)}} (k_b \cos \phi \hat{\mathbf{x}} + k_b \sin \phi \hat{\mathbf{y}} + \epsilon_b(\omega) \sin \theta_0 \hat{\mathbf{z}}) \hat{\mathbf{p}}_{v-} \right] \cdot \hat{\mathbf{e}}^{\text{in}}.
\end{aligned}$$

For \mathcal{R}_{pP} we require that $\hat{\mathbf{e}}^{\text{in}} = \hat{\mathbf{p}}_{v-}$, so

$$\mathbf{e}_v^\omega = \frac{t_p^{vb}}{\sqrt{\epsilon_b(\omega)}} (k_b \cos \phi \hat{\mathbf{x}} + k_b \sin \phi \hat{\mathbf{y}} + \epsilon_b(\omega) \sin \theta_0 \hat{\mathbf{z}}),$$

and

$$\begin{aligned}\mathbf{e}_v^\omega \mathbf{e}_v^\omega = & \left(\frac{t_p^{vb}}{\sqrt{\epsilon_b(\omega)}} \right)^2 [k_b^2 \cos^2 \phi \hat{\mathbf{x}} \hat{\mathbf{x}} \\ & + k_b^2 \sin^2 \phi \hat{\mathbf{y}} \hat{\mathbf{y}} \\ & + \epsilon_b^2(\omega) \sin^2 \theta_0 \hat{\mathbf{z}} \hat{\mathbf{z}} \\ & + 2k_b^2 \sin \phi \cos \phi \hat{\mathbf{x}} \hat{\mathbf{y}} \\ & + 2\epsilon_b(\omega) k_b \sin \theta_0 \sin \phi \hat{\mathbf{y}} \hat{\mathbf{z}} \\ & + 2\epsilon_b(\omega) k_b \sin \theta_0 \cos \phi \hat{\mathbf{x}} \hat{\mathbf{z}}].\end{aligned}$$

We also require the 2ω fields evaluated in the vacuum, so

$$\mathbf{e}_v^{2\omega} = \hat{\mathbf{e}}^{\text{out}} \cdot \left[\hat{\mathbf{s}} T_s^{vb} \hat{\mathbf{s}} + \hat{\mathbf{P}}_{v+} \frac{T_p^{vb}}{\sqrt{\epsilon_b(2\omega)}} (\epsilon_b(2\omega) \sin \theta_0 \hat{\mathbf{z}} - K_b \hat{\mathbf{k}}) \right], \quad (\text{D.1})$$

and with $\hat{\mathbf{e}}^{\text{out}} = \hat{\mathbf{P}}_{v+}$ we have

$$\mathbf{e}_v^{2\omega} = \frac{T_p^{vb}}{\sqrt{\epsilon_b(2\omega)}} (\epsilon_b(2\omega) \sin \theta_0 \hat{\mathbf{z}} - K_b \cos \phi \hat{\mathbf{x}} - K_b \sin \phi \hat{\mathbf{y}}). \quad (\text{D.2})$$

So lastly, we have that

$$\begin{aligned}\mathbf{e}_v^{2\omega} \cdot \boldsymbol{\chi} : \mathbf{e}_v^\omega \mathbf{e}_v^\omega = & \frac{T_p^{vb}}{\sqrt{\epsilon_b(2\omega)}} \left(\frac{t_p^{vb}}{\sqrt{\epsilon_b(\omega)}} \right)^2 [\epsilon_b(2\omega) k_b^2 \sin \theta_0 \cos^2 \phi \chi_{zxx} \\ & + \epsilon_b(2\omega) k_b^2 \sin \theta_0 \sin^2 \phi \chi_{zyy} \\ & + \epsilon_b^2(\omega) \epsilon_b(2\omega) \sin^3 \theta_0 \chi_{zzz} \\ & + 2\epsilon_b(2\omega) k_b^2 \sin \theta_0 \sin \phi \cos \phi \chi_{zxy} \\ & + 2\epsilon_b(\omega) \epsilon_b(2\omega) k_b \sin^2 \theta_0 \sin \phi \chi_{zyz} \\ & + 2\epsilon_b(\omega) \epsilon_b(2\omega) k_b \sin^2 \theta_0 \cos \phi \chi_{zxz} \\ & - k_b^2 K_b \cos^3 \phi \chi_{xxx} \\ & - k_b^2 K_b \sin^2 \phi \cos \phi \chi_{xyy} \\ & - \epsilon_b^2(\omega) K_b \sin^2 \theta_0 \cos \phi \chi_{xzz} \\ & - 2k_b^2 K_b \sin \phi \cos^2 \phi \chi_{xxy} \\ & - 2\epsilon_b(\omega) k_b K_b \sin \theta_0 \sin \phi \cos \phi \chi_{xyz} \\ & - 2\epsilon_b(\omega) k_b K_b \sin \theta_0 \cos^2 \phi \chi_{xxz} \\ & - k_b^2 K_b \sin \phi \cos^2 \phi \chi_{yxx} \\ & - k_b^2 K_b \sin^3 \phi \chi_{yyy} \\ & - \epsilon_b^2(\omega) K_b \sin^2 \theta_0 \sin \phi \chi_{yzz} \\ & - 2k_b^2 K_b \sin^2 \phi \cos \phi \chi_{yxy} \\ & - 2\epsilon_b(\omega) k_b K_b \sin \theta_0 \sin^2 \phi \chi_{yyz} \\ & - 2\epsilon_b(\omega) k_b K_b \sin \theta_0 \sin \phi \cos \phi \chi_{yxz}],\end{aligned}$$

and after eliminating components,

$$\begin{aligned}
&= \Gamma_{pP}^v [\epsilon_b^2(\omega) \epsilon_b(2\omega) \sin^3 \theta_0 \chi_{zzz} \\
&\quad + \epsilon_b(2\omega) k_b^2 \sin \theta_0 \cos^2 \phi \chi_{zxx} \\
&\quad + \epsilon_b(2\omega) k_b^2 \sin \theta_0 \sin^2 \phi \chi_{zxz} \\
&\quad - 2\epsilon_b(\omega) k_b K_b \sin \theta_0 \cos^2 \phi \chi_{xxz} \\
&\quad - 2\epsilon_b(\omega) k_b K_b \sin \theta_0 \sin^2 \phi \chi_{xxz} \\
&\quad + 3k_b^2 K_b \sin^2 \phi \cos \phi \chi_{xxx} \\
&\quad - k_b^2 K_b \cos^3 \phi \chi_{xxx}] \\
&= \Gamma_{pP}^v [\epsilon_b^2(\omega) \epsilon_b(2\omega) \sin^3 \theta_0 \chi_{zzz} + \epsilon_b(2\omega) k_b^2 \sin \theta_0 \chi_{zxz} \\
&\quad - 2\epsilon_b(\omega) k_b K_b \sin \theta_0 \chi_{xxz} - k_b^2 K_b \chi_{xxx} \cos 3\phi],
\end{aligned}$$

where

$$\Gamma_{pP}^v = \frac{T_p^{vb} (t_p^{vb})^2}{\epsilon_b(\omega) \sqrt{\epsilon_b(2\omega)}}.$$

D.4 Taking $\mathcal{P}(2\omega)$ in ℓ and the fundamental fields in the bulk

For this scenario with $\hat{\mathbf{e}}^{\text{in}} = \hat{\mathbf{p}}_{v-}$ and $\hat{\mathbf{e}}^{\text{out}} = \hat{\mathbf{P}}_{v+}$ we have,

$$\mathbf{e}_\ell^{2\omega} = \frac{T_p^{v\ell} T_p^{\ell b}}{\epsilon_\ell(2\omega) \sqrt{\epsilon_b(2\omega)}} (\epsilon_b(2\omega) \sin \theta_0 \hat{\mathbf{z}} - \epsilon_\ell(2\omega) K_b \cos \phi \hat{\mathbf{x}} - \epsilon_\ell(2\omega) K_b \sin \phi \hat{\mathbf{y}}),$$

and

$$\begin{aligned}
\mathbf{e}_b^\omega \mathbf{e}_b^\omega &= \frac{(t_p^{vb})^2}{\epsilon_b(\omega)} (\sin^2 \theta_0 \hat{\mathbf{z}} \hat{\mathbf{z}} + k_b^2 \cos^2 \phi \hat{\mathbf{x}} \hat{\mathbf{x}} + k_b^2 \sin^2 \phi \hat{\mathbf{y}} \hat{\mathbf{y}} \\
&\quad + 2k_b \sin \theta_0 \cos \phi \hat{\mathbf{z}} \hat{\mathbf{x}} + 2k_b \sin \theta_0 \sin \phi \hat{\mathbf{z}} \hat{\mathbf{y}} + 2k_b^2 \sin \phi \cos \phi \hat{\mathbf{x}} \hat{\mathbf{y}}).
\end{aligned}$$

Thus,

$$\mathbf{e}_\ell^{2\omega} \cdot \boldsymbol{\chi} : \mathbf{e}_b^\omega \mathbf{e}_b^\omega = \frac{T_p^{v\ell} T_p^{\ell b} (t_p^{vb})^2}{\epsilon_\ell(2\omega) \epsilon_b(\omega) \sqrt{\epsilon_b(2\omega)}} \left[+ \epsilon_b(2\omega) \sin^3 \theta_0 \chi_{zzz} \right.$$

$$+ \epsilon_b(2\omega) k_b^2 \sin \theta_0 \cos^2 \phi \chi_{zxx}$$

$$+ \epsilon_b(2\omega) k_b^2 \sin \theta_0 \sin^2 \phi \chi_{zyy}$$

$$+ 2\epsilon_b(2\omega) k_b \sin^2 \theta_0 \cos \phi \chi_{zzx}$$

$$+ 2\epsilon_b(2\omega) k_b \sin^2 \theta_0 \sin \phi \chi_{zzy}$$

$$+ 2\epsilon_b(2\omega) k_b^2 \sin \theta_0 \sin \phi \cos \phi \chi_{zxy}$$

$$- \epsilon_\ell(2\omega) \sin^2 \theta_0 K_b \cos \phi \chi_{xzz}$$

$$- \epsilon_\ell(2\omega) k_b^2 K_b \cos^3 \phi \chi_{xxx}$$

$$- \epsilon_\ell(2\omega) k_b^2 K_b \sin^2 \phi \cos \phi \chi_{xyy}$$

$$- 2\epsilon_\ell(2\omega) k_b K_b \sin \theta_0 \cos^2 \phi \chi_{xzx}$$

$$- 2\epsilon_\ell(2\omega) k_b K_b \sin \theta_0 \sin \phi \cos \phi \chi_{xzy}$$

$$- 2\epsilon_\ell(2\omega) k_b^2 K_b \sin \phi \cos^2 \phi \chi_{xxy}$$

$$- \epsilon_\ell(2\omega) K_b \sin^2 \theta_0 \sin \phi \chi_{yzz}$$

$$- \epsilon_\ell(2\omega) k_b^2 K_b \cos^2 \phi \sin \phi \chi_{yxx}$$

$$- \epsilon_\ell(2\omega) k_b^2 K_b \sin^3 \phi \chi_{yyy}$$

$$- 2\epsilon_\ell(2\omega) k_b K_b \sin \theta_0 \cos \phi \sin \phi \chi_{yzx}$$

$$- 2\epsilon_\ell(2\omega) k_b K_b \sin \theta_0 \sin^2 \phi \chi_{yzy}$$

$$\left. - 2\epsilon_\ell(2\omega) k_b^2 K_b \sin^2 \phi \cos \phi \chi_{yxy} \right].$$

We eliminate and replace components,

$$\mathbf{e}_\ell^{2\omega} \cdot \boldsymbol{\chi} : \mathbf{e}_b^\omega \mathbf{e}_b^\omega = \Gamma_{pP}^{\ell b} \left[+ \epsilon_b(2\omega) \sin^3 \theta_0 \chi_{zzz} \right.$$

$$+ \epsilon_b(2\omega) k_b^2 \sin \theta_0 \cos^2 \phi \chi_{zxx}$$

$$+ \epsilon_b(2\omega) k_b^2 \sin \theta_0 \sin^2 \phi \chi_{zxx}$$

$$- 2\epsilon_\ell(2\omega) k_b K_b \sin \theta_0 \cos^2 \phi \chi_{xxz}$$

$$- 2\epsilon_\ell(2\omega) k_b K_b \sin \theta_0 \sin^2 \phi \chi_{xxz}$$

$$- \epsilon_\ell(2\omega) k_b^2 K_b \cos^3 \phi \chi_{xxx}$$

$$+ \epsilon_\ell(2\omega) k_b^2 K_b \sin^2 \phi \cos \phi \chi_{xxx}$$

$$\left. + 2\epsilon_\ell(2\omega) k_b^2 K_b \sin^2 \phi \cos \phi \chi_{xxx} \right],$$

so lastly

$$\mathbf{e}_\ell^{2\omega} \cdot \boldsymbol{\chi} : \mathbf{e}_b^\omega \mathbf{e}_b^\omega = \Gamma_{pP}^{\ell b} \left[\epsilon_b(2\omega) \sin^3 \theta_0 \chi_{zzz} + \epsilon_b(2\omega) k_b^2 \sin \theta_0 \chi_{zxx} \right.$$

$$\left. - 2\epsilon_\ell(2\omega) k_b K_b \sin \theta_0 \chi_{xxz} - \epsilon_\ell(2\omega) k_b^2 K_b \chi_{xxx} \cos 3\phi \right],$$

where

$$\Gamma_{pP}^{\ell b} = \frac{T_p^{v\ell} T_p^{\ell b} (t_p^{vb})^2}{\epsilon_\ell(2\omega) \epsilon_b(\omega) \sqrt{\epsilon_b(2\omega)}}.$$

Appendix E

The two layer model for SHG radiation from Sipe, Moss, and van Driel

`oss_vandriel`

Outline

E.1	\mathcal{R}_{pP}	92
E.2	\mathcal{R}_{pS}	94
E.3	\mathcal{R}_{sP}	95
E.4	Summary	96

In this treatment we follow the work of Ref. [29]. They define the following for all polarizations;

$$\begin{aligned} f_s &= \frac{\kappa}{n\tilde{\omega}} = \frac{\kappa}{\sqrt{\epsilon(\omega)}\tilde{\omega}}, \\ f_c &= \frac{w}{n\tilde{\omega}} = \frac{w}{\sqrt{\epsilon(\omega)}\tilde{\omega}}, \\ f_s^2 + f_c^2 &= 1, \end{aligned} \tag{E.1} \quad \boxed{\text{fcfs}}$$

where

$$\kappa = \tilde{\omega} \sin \theta, \tag{E.2} \quad \boxed{\text{wzero}}$$

$$w_0 = \sqrt{\tilde{\omega} - \kappa^2} = \tilde{\omega} \cos \theta, \tag{E.3} \quad \boxed{\text{w}}$$

From this point on, all capital letters and symbols indicate evaluation at 2ω . Common to all three polarization cases studied here, we require the nonzero components for the (111) face for crystals

with C_{3v} symmetry,

$$\begin{aligned}\delta_{11} &= \chi^{xxx} = -\chi^{xyy} = -\chi^{yyx}, \\ \delta_{15} &= \chi^{xxz} = \chi^{yyz}, \\ \delta_{31} &= \chi^{zxx} = \chi^{zyy}, \\ \delta_{33} &= \chi^{zzz}.\end{aligned}\tag{E.4} \quad \boxed{\text{deltas}}$$

Lastly, the remaining quantities that will be needed for all three cases are

$$\begin{aligned}A_p &= \frac{4\pi\tilde{\Omega}\sqrt{\epsilon(2\omega)}}{W_0\epsilon(2\omega) + W}, \\ A_s &= \frac{4\pi\tilde{\Omega}}{W_0 + W}.\end{aligned}\tag{E.5} \quad \boxed{\text{apas}}$$

E.1 \mathcal{R}_{pP}

For the (111) face ($m = 3$), we have

$$\frac{E^{(2\omega)}(\parallel, \parallel)}{E_p^2 A_p} = a_{\parallel, \parallel} + c_{\parallel, \parallel}^{(3)} \cos 3\phi.\tag{E.6} \quad \boxed{\text{totalshgpp}}$$

We extract these coefficients from Table V, noting that $\Gamma = \gamma = 0$ as we are only interested in the surface contribution,

$$\begin{aligned}a_{\parallel, \parallel} &= i\tilde{\Omega}F_s\epsilon(2\omega)\delta_{31} + i\tilde{\Omega}\epsilon(2\omega)F_sf_s^2(\delta_{33} - \delta_{31}) - 2i\tilde{\Omega}f_sf_cF_c\delta_{15}, \\ c_{\parallel, \parallel}^{(3)} &= -i\tilde{\Omega}F_cf_c^2\delta_{11}.\end{aligned}$$

We substitute these in Eq. (E.6),

$$\begin{aligned}\frac{E^{(2\omega)}(\parallel, \parallel)}{E_p^2 A_p} &= i\tilde{\Omega}F_s\epsilon(2\omega)\delta_{31} + i\tilde{\Omega}\epsilon(2\omega)F_sf_s^2(\delta_{33} - \delta_{31}) \\ &\quad - 2i\tilde{\Omega}f_sf_cF_c\delta_{15} - i\tilde{\Omega}F_cf_c^2\delta_{11} \cos 3\phi\end{aligned}$$

and reduce (omitting the (\parallel, \parallel) notation),

$$\begin{aligned}\frac{E^{(2\omega)}}{E_p^2} &= A_p i\tilde{\Omega} [F_s\epsilon(2\omega)(\delta_{31} + f_s^2(\delta_{33} - \delta_{31})) - f_cF_c(2f_s\delta_{15} + f_c\delta_{11} \cos 3\phi)] \\ &= A_p i\tilde{\Omega} [F_s\epsilon(2\omega)(f_s^2\delta_{33} + (1 - f_s^2)\delta_{31}) - f_cF_c(2f_s\delta_{15} + f_c\delta_{11} \cos 3\phi)] \\ &= A_p i\tilde{\Omega} [F_s\epsilon(2\omega)(f_s^2\delta_{33} + f_c^2\delta_{31}) - f_cF_c(2f_s\delta_{15} + f_c\delta_{11} \cos 3\phi)].\end{aligned}$$

As every term has an $f_i^2 F_i$, we can factor out the common

$$\frac{1}{\tilde{\omega}^2 \tilde{\Omega} \epsilon(\omega) \sqrt{\epsilon(2\omega)}}$$

factor after substituting the appropriate terms from Eq. (E.1),

$$\begin{aligned}
\frac{E^{(2\omega)}}{E_p^2} &= \frac{A_p i}{\epsilon(\omega) \sqrt{\epsilon(2\omega)} \tilde{\omega}^2} [K\epsilon(2\omega)(\kappa^2 \delta_{33} + w^2 \delta_{31}) - wW(2\kappa \delta_{15} + w \delta_{11} \cos 3\phi)] \\
&= \frac{A_p i \tilde{\Omega}}{\epsilon(\omega) \sqrt{\epsilon(2\omega)}} [\sin \theta \epsilon(2\omega) (\sin^2 \theta \delta_{33} + k_z^2(\omega) \delta_{31}) \\
&\quad - k_z(\omega) k_z(2\omega) (2 \sin \theta \delta_{15} + k_z(\omega) \delta_{11} \cos 3\phi)] \\
&= \frac{A_p i \tilde{\Omega}}{\epsilon(\omega) \sqrt{\epsilon(2\omega)}} [\sin \theta \epsilon(2\omega) (\sin^2 \theta \chi^{zzz} + k_z^2(\omega) \chi^{xxx}) \\
&\quad - k_z(\omega) k_z(2\omega) (2 \sin \theta \chi^{xxz} + k_z(\omega) \chi^{xxx} \cos 3\phi)].
\end{aligned}$$

We substitute Eq. (E.5) to complete the expression,

$$\begin{aligned}
\frac{E^{(2\omega)}}{E_p^2} &= \frac{4i\pi\tilde{\Omega}^2}{\epsilon(\omega)(W_0\epsilon(2\omega) + W)} [\dots] \\
&= \frac{4i\pi\tilde{\Omega}}{\epsilon(\omega)(\epsilon(2\omega) \cos \theta + k_z(2\omega))} [\dots] \\
&= \frac{4i\pi\tilde{\omega}}{\cos \theta} \frac{1}{\epsilon(\omega)} \frac{2 \cos \theta}{\epsilon(2\omega) \cos \theta + k_z(2\omega)} [\dots].
\end{aligned}$$

However, our interest lies in \mathcal{R}_{pP} which is calculated as

$$\mathcal{R}_{pP} = \frac{I_p(2\omega)}{I_p^2(\omega)} = \frac{2\pi}{c} \left| \frac{E^{(2\omega)}(\parallel, \parallel)}{E_p^2} \right|^2,$$

and we can finally complete the expression,

$$\begin{aligned}
\mathcal{R}_{pP} &= \frac{2\pi}{c} \left| \frac{4i\pi\tilde{\omega}}{\cos \theta} \frac{1}{\epsilon(\omega)} \frac{2 \cos \theta}{\epsilon(2\omega) \cos \theta + k_z(2\omega)} r_{pP} \right|^2 \\
&= \frac{32\pi^3 \tilde{\omega}^2}{c \cos^2 \theta} |t_p(\omega) T_p(2\omega) r_{pP}|^2 \\
&= \frac{32\pi^3 \omega^2}{c^3 \cos^2 \theta} |t_p(\omega) T_p(2\omega) r_{pP}|^2,
\end{aligned} \tag{E.7} \boxed{\text{RPP}}$$

where

$$\begin{aligned}
t_p(\omega) &= \frac{1}{\epsilon(\omega)}, \\
T_p(2\omega) &= \frac{2 \cos \theta}{\epsilon(2\omega) \cos \theta + k_z(2\omega)}, \\
r_{pP} &= \sin \theta \epsilon(2\omega) (\sin^2 \theta \chi^{zzz} + k_z^2(\omega) \chi^{xxx}) \\
&\quad - k_z(\omega) k_z(2\omega) (2 \sin \theta \chi^{xxz} + k_z(\omega) \chi^{xxx} \cos 3\phi).
\end{aligned}$$

E.2 \mathcal{R}_{pS}

We follow the same procedure as above. For the (111) face ($m = 3$),

$$\frac{E^{(2\omega)}(\parallel, \perp)}{E_p^2 A_s} = b_{\parallel, \perp}^{(3)} \sin 3\phi, \quad (\text{E.8}) \quad [\text{totalshgps}]$$

and we extract the relevant coefficient from Table V with $\Gamma = \gamma = 0$,

$$b_{\parallel, \perp}^{(3)} = i\tilde{\Omega} f_c^2 \delta_{11}.$$

Substituting this coefficient and Eq. (E.5) into Eq. (E.8),

$$\begin{aligned} \frac{E^{(2\omega)}(\parallel, \perp)}{E_p^2} &= A_s i\tilde{\Omega} f_c^2 \delta_{11} \sin 3\phi \\ &= \frac{A_s i\tilde{\Omega}}{\tilde{\omega}^2 \epsilon(\omega)} w^2 \delta_{11} \sin 3\phi \\ &= \frac{A_s i\tilde{\Omega}}{\epsilon(\omega)} k_z^2(\omega) \delta_{11} \sin 3\phi \\ &= \frac{A_s i\tilde{\Omega}}{\epsilon(\omega)} k_z^2(\omega) \chi^{xxx} \sin 3\phi \\ &= \frac{4i\pi\tilde{\Omega}^2}{W_0 + W} \frac{1}{\epsilon(\omega)} k_z^2(\omega) \chi^{xxx} \sin 3\phi \\ &= 4i\pi\tilde{\Omega} \frac{1}{\epsilon(\omega) \cos \theta + k_z(2\omega)} k_z^2(\omega) \chi^{xxx} \sin 3\phi \\ &= \frac{4i\pi\omega}{c \cos \theta} \frac{1}{\epsilon(\omega) \cos \theta + k_z(2\omega)} k_z^2(\omega) \chi^{xxx} \sin 3\phi \end{aligned}$$

As before, we must calculate

$$\mathcal{R}_{pS} = \frac{2\pi}{c} \left| \frac{E^{(2\omega)}(\parallel, \perp)}{E_s^2} \right|^2,$$

to obtain the final expression,

$$\begin{aligned} \mathcal{R}_{pS} &= \frac{2\pi}{c} \left| \frac{4i\pi\omega}{c \cos \theta} \frac{1}{\epsilon(\omega) \cos \theta + k_z(2\omega)} k_z^2(\omega) \chi^{xxx} \sin 3\phi \right|^2 \\ &= \frac{32\pi^3 \omega^2}{c^3 \cos^2 \theta} \left| \frac{1}{\epsilon(\omega) \cos \theta + k_z(2\omega)} k_z^2(\omega) \chi^{xxx} \sin 3\phi \right|^2 \\ &= \frac{32\pi^3 \omega^2}{c^3 \cos^2 \theta} |t_p(\omega) T_s(2\omega) k_z^2(\omega) r_{pS}|^2, \end{aligned} \quad (\text{E.9}) \quad [\text{RpS}]$$

where

$$\begin{aligned} t_p(\omega) &= \frac{1}{\epsilon(\omega)}, \\ T_s(2\omega) &= \frac{2 \cos \theta}{\cos \theta + k_z(2\omega)}, \\ r_{pS} &= k_z^2(\omega) \chi^{xxx} \sin 3\phi. \end{aligned}$$

E.3 \mathcal{R}_{sP}

We follow the same procedure as above for the final polarization case. For the (111) face ($m = 3$),

$$\frac{E^{(2\omega)}(\perp, \parallel)}{E_s^2 A_p} = a_{\perp, \parallel} + c_{\perp, \parallel}^{(3)} \cos 3\phi, \quad (\text{E.10}) \quad [\text{totalshgsp}]$$

and we extract the relevant coefficients from Table V with $\Gamma = \gamma = 0$,

$$\begin{aligned} a_{\perp, \parallel} &= i\tilde{\Omega}F_s\epsilon(2\omega)\delta_{31}, \\ c_{\perp, \parallel}^{(3)} &= i\tilde{\Omega}F_c\delta_{11}. \end{aligned}$$

Substituting this coefficient and Eq. (E.5) into Eq. (E.10),

$$\begin{aligned} \frac{E^{(2\omega)}(\perp, \parallel)}{E_s^2} &= A_p(i\tilde{\Omega}F_s\epsilon(2\omega)\delta_{31} + i\tilde{\Omega}F_c\delta_{11}\cos 3\phi) \\ &= A_p i\tilde{\Omega}(F_s\epsilon(2\omega)\delta_{31} + F_c\delta_{11}\cos 3\phi) \\ &= \frac{A_p i\tilde{\Omega}}{\sqrt{\epsilon(2\omega)}}(\sin\theta\epsilon(2\omega)\delta_{31} + k_z(2\omega)\delta_{11}\cos 3\phi) \\ &= \frac{A_p i\tilde{\Omega}}{\sqrt{\epsilon(2\omega)}}(\sin\theta\epsilon(2\omega)\chi^{zxx} + k_z(2\omega)\chi^{xxx}\cos 3\phi) \\ &= \frac{4i\pi\tilde{\Omega}^2}{W_0\epsilon(2\omega) + W}(\sin\theta\epsilon(2\omega)\chi^{zxx} + k_z(2\omega)\chi^{xxx}\cos 3\phi) \\ &= \frac{4i\pi\tilde{\Omega}}{\epsilon(2\omega)\cos\theta + k_z(2\omega)}(\sin\theta\epsilon(2\omega)\chi^{zxx} + k_z(2\omega)\chi^{xxx}\cos 3\phi) \\ &= \frac{4i\pi\omega}{c\cos\theta} \frac{2\cos\theta}{\epsilon(2\omega)\cos\theta + k_z(2\omega)}(\sin\theta\epsilon(2\omega)\chi^{zxx} + k_z(2\omega)\chi^{xxx}\cos 3\phi). \end{aligned}$$

And we finally obtain \mathcal{R}_{sP} ,

$$\begin{aligned} \mathcal{R}_{sP} &= \frac{2\pi}{c} \left| \frac{E^{(2\omega)}(\perp, \parallel)}{E_s^2} \right|^2 \\ &= \frac{2\pi}{c} \left| \frac{4i\pi\omega}{c\cos\theta} \frac{2\cos\theta}{\epsilon(2\omega)\cos\theta + k_z(2\omega)}(\sin\theta\epsilon(2\omega)\chi^{zxx} + k_z(2\omega)\chi^{xxx}\cos 3\phi) \right|^2 \\ &= \frac{32\pi^3\omega^2}{c^3\cos^2\theta} \left| \frac{2\cos\theta}{\epsilon(2\omega)\cos\theta + k_z(2\omega)}(\sin\theta\epsilon(2\omega)\chi^{zxx} + k_z(2\omega)\chi^{xxx}\cos 3\phi) \right|^2 \\ &= \frac{32\pi^3\omega^2}{c^3\cos^2\theta} |t_s(\omega)T_p(2\omega)r_{sP}|^2, \end{aligned} \quad (\text{E.11}) \quad [\text{RsP}]$$

where

$$\begin{aligned} t_s(\omega) &= 1, \\ T_p(2\omega) &= \frac{2\cos\theta}{\epsilon(2\omega)\cos\theta + k_z(2\omega)}, \\ r_{sP} &= \sin\theta\epsilon(2\omega)\chi^{zxx} + k_z(2\omega)\chi^{xxx}\cos 3\phi. \end{aligned}$$

iF	$t_i(\omega)$	$T_F(2\omega)$	r_{iF}
pP	$\frac{1}{\epsilon(\omega)}$	$\frac{2 \cos \theta}{\epsilon(2\omega) \cos \theta + k_z(2\omega)}$	$\sin \theta \epsilon(2\omega) (\sin^2 \theta \chi^{zzz} + k_z^2(\omega) \chi^{zxx})$ $-k_z(\omega) k_z(2\omega) (2 \sin \theta \chi^{xxz}$ $+ k_z(\omega) \chi^{xxx} \cos 3\phi)$ $+$
pS	$\frac{1}{\epsilon(\omega)}$	$\frac{2 \cos \theta}{\cos \theta + k_z(2\omega)}$	$k_z^2(\omega) \chi^{xxx} \sin 3\phi$
sP	1	$\frac{2 \cos \theta}{\epsilon(2\omega) \cos \theta + k_z(2\omega)}$	$\sin \theta \epsilon(2\omega) \chi^{zxx} + k_z(2\omega) \chi^{xxx} \cos 3\phi$

`tabsize`

Table E.1: The necessary factors for Eq. (E.12) for each polarization case.

E.4 Summary

We unify the final expressions for the SHG yield, Eqs. (E.7), (E.9), and (E.11), as

$$\mathcal{R}_{iF} = \frac{32\pi^3 \omega^2}{c^3 \cos^2 \theta} |t_i(\omega) T_F(2\omega) r_{iF}|^2. \quad (\text{E.12}) \quad \boxed{\text{Rsipe}}$$

The necessary factors are summarized in Table E.1.

Bibliography

- [1] J. D. Jackson. *Classical Electrodynamics, 3rd Edition.* Wiley-VCH, 3rd edition edition, July 1998.
- [2] M. C. Downer, B. S. Mendoza, and V. I. Gavrilenko. Optical second harmonic spectroscopy of semiconductor surfaces: advances in microscopic understanding. *Surf. Interface Anal.*, 31(10):966–986, 2001.
- [3] C. Aversa and J. E. Sipe. Nonlinear optical susceptibilities of semiconductors: Results with a length-gauge analysis. *Phys. Rev. B*, 52(20):14636–14645, 1995.
- [4] J. E. Sipe and A. I. Shkrebtii. Second-order optical response in semiconductors. *Phys. Rev. B*, 61(8):5337, 2000.
- [5] E. N. Adams. The crystal momentum as a quantum mechanical operator. *J. Chem. Phys.*, 21(11):2013–2017, November 1953.
- [6] E. I. Blount, F. Seitz, and D. Turnbull. Formalisms of band theory. *Solid State Phys.*, 13:305, 1962.
- [7] S. Ismail-Beigi, E. K. Chang, and S. G. Louie. Coupling of nonlocal potentials to electromagnetic fields. *Phys. Rev. Lett.*, 87(8):087402, August 2001.
- [8] C. Motta, M. Giantomassi, M. Cazzaniga, K. Gaál-Nagy, and X. Gonze. Implementation of techniques for computing optical properties in 0-3 dimensions, including a real-space cutoff, in ABINIT. *Comput. Mater. Sci.*, 50(2):698–703, 2010.
- [9] L. Kleinman and D. M. Bylander. Efficacious form for model pseudopotentials. *Phys. Rev. Lett.*, 48(20):1425–1428, 1982.
- [10] B. Adolph, V. I. Gavrilenko, K. Tenelsen, F. Bechstedt, and R. Del Sole. Nonlocality and many-body effects in the optical properties of semiconductors. *Phys. Rev. B*, 53(15):9797–9808, 1996.
- [11] L. Reining, R. Del Sole, M. Cini, and J. G. Ping. Microscopic calculation of second-harmonic generation at semiconductor surfaces: As/Si(111) as a test case. *Phys. Rev. B*, 50(12):8411–8422, 1994.
- [12] B. S. Mendoza, A. Gaggiotti, and R. Del Sole. Microscopic theory of second harmonic generation at si (100) surfaces. *Phys. Rev. Lett.*, 81(17):3781–3784, 1998.

- [13] B. S. Mendoza, M. Palummo, G. Onida, and R. Del Sole. Ab initio calculation of second-harmonic-generation at the si(100) surface. *Phys. Rev. B*, 63(20):205406, 2001.
- [14] H. Sano, G. Mizutani, W. Wolf, and R. Podloucky. Ab initio study of linear and nonlinear optical responses of si(111) surfaces. *Phys. Rev. B*, 66(19):195338, November 2002.
- [15] J. E. Mejía, B. S. Mendoza, and C. Salazar. Layer-by-layer analysis of second harmonic generation at a simple surface. *Revista Mexicana de Física*, 50(2):134–139, 2004.
- [16] C. Hogan, R. Del Sole, and G. Onida. Optical properties of real surfaces from microscopic calculations of the dielectric function of finite atomic slabs. *Phys. Rev. B*, 68(3):035405, 2003.
- [17] C. Castillo, B. S. Mendoza, W. G. Schmidt, P. H. Hahn, and F. Bechstedt. Layer-by-layer analysis of surface reflectance anisotropy in semiconductors. *Phys. Rev. B*, 68(4):041310, 2003.
- [18] B. S. Mendoza, F. Nastos, N. Arzate, and J. Sipe. Layer-by-layer analysis of the linear optical response of clean and hydrogenated si(100) surfaces. *Phys. Rev. B*, 74(7):075318, 2006.
- [19] Nicolas Tancogne-Dejean private communication. Indeed, one can compute the layered contribution of the non-local contribution to \mathbf{v} with an analytic expression. However, one needs to compute this within the DP code.
- [20] S. N. Rashkeev, W. R. L. Lambrecht, and B. Segall. Efficient ab initio method for the calculation of frequency-dependent second-order optical response in semiconductors. *Phys. Rev. B*, 57(7):3905–3919, 1998.
- [21] Valérie Véniard, E. Luppi, and H. Hübener. unpublished.
- [22] N. W. Ashcroft and N. D. Mermin. *Solid State Physics*. Brooks Cole, Saunders College, Philadelphia, 1976.
- [23] Robert W. Boyd. *Nonlinear Optics*. AP, New York, 2007.
- [24] Richard L. Sutherland. *Handbook of Nonlinear Optics*. CRC Press, April 2003.
- [25] Michele Cini. Simple model of electric-dipole second-harmonic generation from interfaces. *Phys. Rev. B*, 43(6):4792–4802, February 1991.
- [26] V. Mizrahi and J. E. Sipe. Phenomenological treatment of surface second-harmonic generation. *J. Opt. Soc. Am. B*, 5(3):660–667, 1988.
- [27] J. E. Sipe. New Green-function formalism for surface optics. *Journal of the Optical Society of America B*, 4(4):481–489, 1987.
- [28] N. Tancogne-Dejean, C. Giorgetti, and V. Véniard. Optical properties of surfaces with supercell *ab initio* calculations: Local-field effects. *Phys. Rev. B*, 92(24):245308, July 2015.
- [29] J. E. Sipe, D. J. Moss, and H. M. van Driel. Phenomenological theory of optical second- and third-harmonic generation from cubic centrosymmetric crystals. *Phys. Rev. B*, 35(3):1129–1141, January 1987.

- [30] S. V. Popov, Y. P. Svirko, and N. I. Zheludev. *Susceptibility tensors for nonlinear optics*. CRC Press, 1995.
- [31] U. Höfer. Nonlinear optical investigations of the dynamics of hydrogen interaction with silicon surfaces. *Appl. Phys. A*, 63(6):533–547, December 1996.
- [32] S. Bergfeld, B. Braunschweig, and W. Daum. Nonlinear Optical Spectroscopy of Suboxides at Oxidized Si(111) Interfaces. *Phys. Rev. Lett.*, 93(9):097402, August 2004.
- [33] J. E. Mejía, B. S. Mendoza, M. Palummo, G. Onida, R. Del Sole, S. Bergfeld, and W. Daum. Surface second-harmonic generation from si (111)(1x1) h: Theory versus experiment. *Phys. Rev. B*, 66(19):195329, 2002.
- [34] S. A. Mitchell, M. Mehendale, D. M. Villeneuve, and R. Boukherroub. Second harmonic generation spectroscopy of chemically modified Si(1 1 1) surfaces. *Surf. Sci.*, 488(3):367–378, August 2001.
- [35] X. Gonze, B. Amadon, P. . M. Anglade, J. . M. Beuken, F. Bottin, P. Boulanger, F. Bruneval, D. Caliste, R. Caracas, M. Cote, T. Deutsch, L. Genovese, Ph. Ghosez, M. Giantomassi, S. Goedecker, D. R. Hamann, P. Hermet, F. Jollet, G. Jomard, S. Leroux, M. Mancini, S. Mazevet, M. J. T. Oliveira, G. Onida, Y. Pouillon, T. Rangel, G. . M. Rignanese, D. Sangalli, R. Shaltaf, M. Torrent, M. J. Verstraete, G. Zerah, and J. W. Zwanziger. ABINIT: First-principles approach to material and nanosystem properties. *Comput. Phys. Commun.*, 180(12):2582–2615, December 2009.
- [36] The ABINIT code is a common project of the Université Catholique de Louvain, Corning Incorporated, and other contributors (URL <http://www.abinit.org>).
- [37] N. Troullier and J. L. Martins. Efficient pseudopotentials for plane-wave calculations. *Phys. Rev. B*, 43(3):1993–2006, January 1991.
- [38] V. Olevano, L. Reining, and F. Sottile. <http://dp-code.org>.
- [39] L. Caramella, C. Hogan, G. Onida, and R. Del Sole. High-resolution electron energy loss spectra of reconstructed si(100) surfaces: First-principles study. *Phys. Rev. B*, 79:155447, Apr 2009.
- [40] For bulk calculations schemes of the SH susceptibility tensor beyond the independent particle approximation, see Refs. [50, 49, 48, 66, 67, 68, 69, 70].
- [41] F. Nastos, B. Olejnik, K. Schwarz, and J. E. Sipe. Scissors implementation within length-gauge formulations of the frequency-dependent nonlinear optical response of semiconductors. *Phys. Rev. B*, 72(4):045223, 2005.
- [42] The half-slab layer extends to the middle of the vacuum region between consecutive (front-back or back-front) surfaces of the repeated super cell scheme.
- [43] M. Rohlfing, P. Krüger, and J. Pollmann. Efficient scheme for GW quasiparticle band-structure calculations with applications to bulk si and to the si(001)-(2x1) surface. *Phys. Rev. B*, 52(3):1905–1917, July 1995.

- [44] P. García-González and R. W. Godby. GW self-energy calculations for surfaces and interfaces. *Comput. Phys. Commun.*, 137(1):108–122, June 2001.
- [45] Eleonora Luppi, Hans-Christian Weissker, Sandro Bottaro, Sottile Francesco, Valérie Véniard, Lucia Reining, and Giovanni Onida. Accuracy of the pseudopotential approximation in *ab initio* theoretical spectroscopies. *Phys. Rev. B*, 78:245124, 2008.
- [46] R. Asahi, W. Mannstadt, and A. J. Freeman. Screened-exchange lda methods for films and superlattices with applications to the si(100)2x1 surface and inasinsb superlattices. *Phys. Rev. B*, 62:2552, 2000.
- [47] J. Cabellos, B. Mendoza, M. Escobar, F. Nastos, and J. Sipe. Effects of nonlocality on second-harmonic generation in bulk semiconductors. *Phys. Rev. B*, 80(15):155205, 2009.
- [48] E. Luppi, H. Hübener, and V. Véniard. Ab initio second-order nonlinear optics in solids: Second-harmonic generation spectroscopy from time-dependent density-functional theory. *Phys. Rev. B*, 82:235201, 2010.
- [49] R. Leitsmann, W. Schmidt, P. Hahn, and F. Bechstedt. Second-harmonic polarizability including electron-hole attraction from band-structure theory. *Phys. Rev. B*, 71(19):195209, 2005.
- [50] B. Adolph and F. Bechstedt. Influence of crystal structure and quasiparticle effects on second-harmonic generation: Silicon carbide polytypes. *Phys. Rev. B*, 62:1706, 2000.
- [51] S. M. Anderson, N. Tancogne-Dejean, B. S. Mendoza, and V. Véniard. Theory of surface second-harmonic generation for semiconductors including effects of nonlocal operators. *Phys. Rev. B*, 91(7):075302, February 2015.
- [52] Nicolas Tancogne-Dejean. *Ab initio description of second-harmonic generation from crystal surfaces*. PhD thesis, Ecole polytechnique, September 2015.
- [53] J. R. Power, J. D. O’Mahony, S. Chandola, and J. F. McGilp. Resonant optical second harmonic generation at the steps of vicinal si(001). *Phys. Rev. Lett.*, 75(6):1138–1141, August 1995.
- [54] E. Kaxiras and J. D. Joannopoulos. Hydrogenation of semiconductor surfaces: Si and Ge (111). *Phys. Rev. B*, 37(15):8842–8848, May 1988.
- [55] F. Jona, W. A. Thompson, and P. M. Marcus. Experimental determination of the atomic structure of a H-terminated Si111 surface. *Phys. Rev. B*, 52(11):8226–8230, September 1995.
- [56] D. R. Alfonso, C. Noguez, D. A. Drabold, and S. E. Ulloa. First-principles studies of hydrogenated Si(111)-7x7. *Phys. Rev. B*, 54(11):8028–8032, September 1996.
- [57] F. Cargnoni, C. Gatti, E. May, and D. Narducci. Geometrical reconstructions and electronic relaxations of silicon surfaces. I. An electron density topological study of H-covered and clean Si(111)(1×1) surfaces. *J. Chem. Phys.*, 112(2):887–899, January 2000.
- [58] R. C. Weast, M. J. Astle, and W. H. Beyer. *CRC handbook of chemistry and physics*, volume 69. CRC press Boca Raton, FL, 1988.

- [59] Y. Li and G. Galli. Electronic and spectroscopic properties of the hydrogen-terminated Si(111) surface from ab initio calculations. *Phys. Rev. B*, 82(4):045321, July 2010.
- [60] P. Yu and M. Cardona. *Fundamentals of Semiconductors: Physics and Materials Properties*. Springer Science & Business Media, third edition, March 2005.
- [61] S. M. Anderson, N. Tancogne-Dejean, B. S. Mendoza, and V. Véniard. Improved *ab initio* calculation of surface second-harmonic generation from si(111)(1×1)h. *Physical Review B*, May 2016. *Submitted*.
- [62] J. I. Dadap, Z. Xu, X. F. Hu, M. C. Downer, N. M. Russell, J. G. Ekerdt, and O. A. Aktsipetrov. Second-harmonic spectroscopy of a Si (001) surface during calibrated variations in temperature and hydrogen coverage. *Phys. Rev. B*, 56(20):13367, 1997.
- [63] M. Palummo, G. Onida, R. Del Sole, and B. S. Mendoza. Ab initio optical properties of Si(100). *Phys. Rev. B*, 60(4):2522–2527, July 1999.
- [64] K. Gaál-Nagy, A. Incze, G. Onida, Y. Borensztein, N. Witkowski, O. Pluchery, F. Fuchs, F. Bechstedt, and R. Del Sole. Optical spectra and microscopic structure of the oxidized Si(100) surface: Combined *in situ* optical experiments and first principles calculations. *Phys. Rev. B*, 79(4):045312, January 2009.
- [65] The size of the excitonic Hamiltonian scales as $(N_k^3 \times N_v \times N_c)^2$, where N_k is the total number of \mathbf{k} -points, and N_v and N_c are the number of valence and conduction states, respectively. For these values, the size of the Hamiltonian for the Si(111)(1×1):H surface of this article would be over 1 petabyte, which far exceeds conventional computing capabilities.
- [66] E. Luppi, H. Hübener, and V. Véniard. Communications: Ab initio second-order nonlinear optics in solids. *J. Chem. Phys.*, 132(24):241104, 2010.
- [67] H. Hübener, E. Luppi, and V. Véniard. Ab initio calculation of many-body effects on the second-harmonic generation spectra of hexagonal sic polytypes. *Phys. Rev. B*, 83:115205, 2011.
- [68] Mads L. Trolle, Gotthard Seifert, and Thomas G. Pedersen. Theory of excitonic second-harmonic generation in monolayer MoS₂. *Phys. Rev. B*, 89(23):235410, June 2014.
- [69] C. Attaccalite and M. Grüning. Nonlinear optics from an ab initio approach by means of the dynamical berry phase: Application to second- and third-harmonic generation in semiconductors. *Phys. Rev. B*, 88:235113, 2013.
- [70] M. Grüning and C. Attaccalite. Second harmonic generation in *h*-bn and mos₂ monolayers: Role of electron-hole interaction. *Phys. Rev. B*, 89:081102, 2014.